Development of Novel Satellite Attitude Determination and Control Algorithms Based on Telemetry Data From An Earth Satellite

Narendra Gollu

A Thesis

in

The Department

of

Mechanical and Industrial Engineering

Presented in Partial Fulfillment of the Requirements

for the Degree of Doctor of Philosophy at

Concordia University

Montréal, Québec, Canada

August 2008

Canada

ABSTRACT

Development of Novel Satellite Attitude Determination and Control Algorithms Based on Telemetry Data From An Earth Satellite

Narendra Gollu, Ph.D.

Concordia Unviersity, 2008

All spacecraft missions require accurate knowledge of attitude, which is derived from on-board sensors using attitude determination algorithms. The increasing demands for attitude accuracy, high performance and low cost spacecraft are driving designers to change from available attitude determination methods to those that are more robust and accurate. However, the cost, the processor workload and the time-constraints in spacecraft development and deployment projects curtail the opportunity for developing new on-board attitude determination methods, especially with regards to the development of more precise sensors. Therefore, it is always desired to achieve the required attitude accuracy with the existing set of on-board sensors, but using effective attitude determination methods and sensor fusion algorithms. Developing such algorithms starts on the ground and is subject to verification and tuning with real experimental data from telemetry. Moreover, the on-ground mission control center has to evaluate the attitude accuracy, calibrate sensors and performance. Motivated by these needs, the main objective of this thesis is to develop novel attitude determination algorithms combining several sensors and attitude estimation methods for Ground-Based Attitude Estimation (GBAE) with telemetry data. The GBAE formulation will be based on a guaranteed ellipsoidal state estimation for acquisition mode and a modified Kalman filter for pointing mode, to provide optimal attitude estimates of the spacecraft. The GBAE has to be evaluated both in the simulation environment and in the flight environment. In the simulation environment, the evaluation of the GBAE rests on the availability of an accurate dynamical model for the spacecraft. However, spacecraft dynamics are complex with multiple modes of operation. Moreover, the nonlinearities in the actual system make the spacecraft dynamics

more complex. This motivates the use of switching between a global nonlinear controller for acquisition mode and a local linear controller for pointing mode, which can guarantee performance and is less computationally intensive for implementation in an on-board microprocessor. In this thesis, novel attitude determination and control algorithms are evaluated in the flight environment for a case study in collaboration with the Canadian Space Agency for the SCISAT-1 satellite.

Dedicated to my parents and my late supervisor Dr. Jaroslav Svoboda(1946-2004).

ACKNOWLEDGEMENTS

TABLE OF CONTENTS

List of Figures

xi

List of Tables

List of Symbols and Abbreviations

ABBREVIATIONS

ADCS	Attitude Determination and Control Systems
ACS	Attitude Control Systems
GBAE	Ground Based Attitude Estimator
TRIAD	TRI Attitude Determination
QUEST	QUaternion ESTimator
FOAM	Fast Optimal Attitude Matrix
SVD	Singular Value Decomposition
SKF	Standard Kalman Filter
MKF	Modified Kalman Filter
EKF	Extended Kalman Filter
GPS	Global Positioning System
ESMF	Extended Set Membership Filter
LTI	Linear Time-Invariant
TLM	Telemetry
km	kilometer
GEO	Geostationary Orbit
LEO	Low Earth Orbit
deg	degrees
rad	radians
MRP	Modified Rodrigues Parameters
Nms	Newton meter second
nT	Nano Tesla
SOS	Sum of Squares
$\mathcal{NP}$	Nondeterministic Polynomial-time
LQR	Linear Quadratic Regulator
JD	Julian Date

$\{\hat{i}_x, \hat{i}_y, \hat{i}_z\}$	the three unit base vectors in inertial frame	[-]
$\{\hat{o}_x, \hat{o}_y, \hat{o}_z\}$	the three unit base vectors in orbital frame	[-]
$\{\hat{b}_x, \hat{b}_y, \hat{b}_z\}$	the three unit base vectors in body frame	[-]
$\{\hat{s}_x, \hat{s}_y, \hat{s}_z\}$	the three unit base vectors in Sun frame	[-]
$\mathbf{F}_i$	inertial frame	[-]
$\mathbf{F}_0$	orbital frame	[-]
$\mathbf{F}_b$	body frame	[-]
$\mathbf{F}_s$	Sun frame	[-]
$\mathbf{R}$	rotation matrix	[-]
$\mathbf{R}_b^a$	rotation matrix from $\mathbf{F}_b$ to $\mathbf{F}_a$	[-]
ϕ	roll angle	[deg]
θ	pitch angle	[deg]
ψ	yaw angle	[deg]
$c\psi$	$\cos\psi$	[deg]
$s\phi$	$\sin\phi$	[deg]
$\boldsymbol{\omega}$	angular velocity	[rad/s]
$\omega_x, \omega_y, \omega_z$	angular velocity	[rad/s]
ω_{es}	angular velocity of the Sun frame	[rad/s]
q_1, q_2, q_3, q_4	quaternions	[-]
$\mathbf{q}$	q_1, q_2, q_3	[-]
$\hat{e}$	principal axis	[-]
Φ	principal angle	[deg]
$\mathbb{R}^4$	four dimensional real space	[-]
$\sigma_1, \sigma_2, \sigma_3$	modified Rodrigues parameter	[-]
$\mathbf{H}$	angular momentum	[N.m.s]
$\mathbf{H}_s$	satellite angular momentum	[N.m.s]
$\mathbf{H}_\omega$	momentum of momentum exchange devices	[N.m.s]
$\mathbf{T}$	Torque	[N.m]
I_x, I_y, I_z	inertia	$[kg.m^2]$

T_x, T_y, T_z	torque	[N.m]
T_c	control torque	[N.m]
T_d	disturbance torque	[N.m]
w_{Td}	white noise	[-]
k_p	proportional gain	[-]
k_d	derivative gain	[-]
k_i	integral gain	[-]
Ω	control bandwidth	[rad/s]
d	damping coefficient	[-]
τ	time constant	s
σ	variance	[-]
Φ	state transition matrix	[-]
Γ	transition matrix	[-]
Q	covariance matrix	[-]
R	covariance matrix	[-]
P	covariance matrix	[-]
C	covariance matrix	[-]
$E(x_c, P_0)$	ellipsoid with center x_c	[-]
P_0	positive definite matrix	[-]
K_i	Kalman gain	[-]
$\hat{\mathbf{s}}$	sun vector	[-]
$\hat{\mathbf{m}}$	magnetic field vector	[-]
$\mathbf{m}_r$	magnetic field vector in reference frame	[-]
$\mathbf{m}_b$	magnetic field vector in body frame	[-]
$\mathbf{s}_r$	sun vector in reference frame	[-]
$\mathbf{s}_b$	sun vector in body frame	[-]
$\mathbb{R}$	real space	[-]
$\mathbf{A(x)}$	state matrix of a state space system	[-]
$\mathbf{A}_l$	linearized state matrix of a state space system	[-]
$\mathbf{B}$	input matrix of a state space system	[-]

$\mathbf{k}_l$	optimal feedback gain matrix of LQR	[-]
$\mathbf{K(x)}$	optimal feedback gain matrix of SOS	[-]
$\mathbf{x}$	state variable	[-]
$\mathbf{Q}$	positive definite matrix	[-]
$\mathbf{V}$	Lyapunov function	[-]
Ω_α	invariant set	[-]
α^*	upper boundary	[-]

Chapter 1

INTRODUCTION

1.1 Motivation

Future space missions call for very high levels of pointing accuracy and reliability, thereby increasing the demands on Attitude Determination and Control Systems (ADCS). The ADCS, as shown in Figure 1.1, stabilizes a satellite and maneuvers it in any direction during a mission using the actuators (reaction wheel and magnetic torque rods) despite the presence of external disturbance torques. Attitude determination using attitude sensors, (Sun sensor, magnetometer and startracker), is a key component of most missions and improvements in its accuracy and reliability contribute directly to the success of the mission [74].
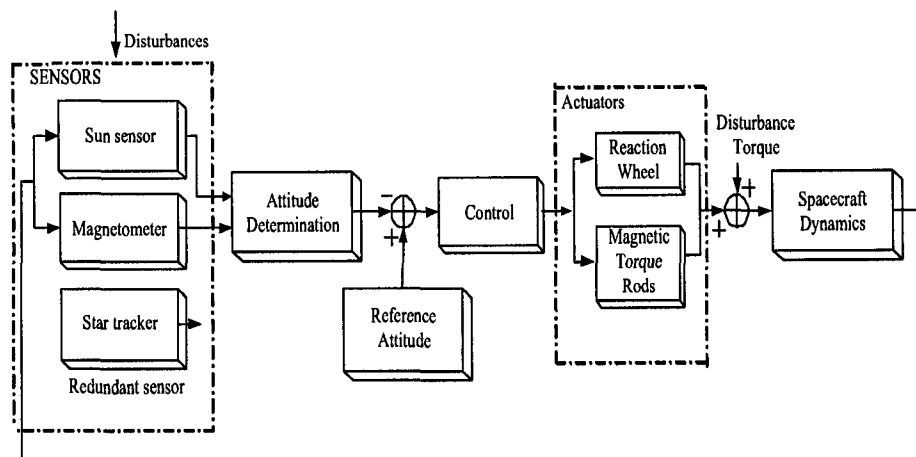
Figure 1.1: Attitude determination and control block diagram

Space missions in general have three distinct phases: *launch, acquisition* and *mission operations* [36]. The *launch* phase consists of the activities performed from lift-off until the satellite separates from the rocket in a preliminary Earth orbit. The *acquisition* phase consists of orbit maneuvers, attitude maneuvers and hardware checkout. The *mission operations* consist of carrying out the normal activities for which the satellite is intended. The primary subsystem on any space mission is its payload. In most cases, the payload must be pointed at its intended target with a certain level of accuracy. The accuracy is a significant parameter to be determined during design, manufacturing, testing and verification, and during all the operation phases. Attitude accuracy requirements for the spacecraft payload are very diverse, but are often more stringent, than the engineering requirements, which are dictated by solar panel lighting, thermal and other conditions. In fact, some payload requirements, such as antenna pointing and Earth observations, demand an accuracy down to a fraction of an arc-second. The ability to achieve such high attitude precision significantly depends on efforts from the mission control center on the ground. The ground personnel in the mission control center provide appropriate fine-tuning and sensor calibration via radio communication to the on-board satellite attitude control system. In most cases, this intervention is inevitable because of many technological and design factors that, can only be adequately evaluated when a satellite is in

space. Because of the cost, the processor workload and the time constraints in space-craft development and deployment projects, the opportunity for developing powerful estimation algorithms for on-board use is difficult presently. Improvements to the attitude determination accuracy can be accomplished beyond that of the on-board ADCS by using sophisticated estimation algorithms on the ground. Hence, some means of on-ground attitude estimation are required to evaluate satellite attitude control system performance.

Motivated by the need described above, one of the objectives of this thesis is to develop a multipurpose Ground Based Attitude Estimator (GBAE) for the evaluation of attitude estimation and accuracy. Developing the estimator is a complicated scientific-engineering problem that requires accurate system modelling and adequate assumptions enabling the application of novel estimation theory results. If appropriately designed, the GBAE is a powerful tool that can be used for satellite attitude control system performance evaluation during the commissioning period, performing periodical sensor calibration, and the adjustment of controller gains. Moreover, the developed attitude estimator can be considered as an on-ground prototyping for newly developed optimal attitude estimation methods and algorithms for future on-board implementation. Furthermore, a ground-based attitude estimator can be a platform for scientific research to develop new attitude sensor fusion methods, and for identifying attitude perturbations and sensor errors, thus making it possible for satellites to benefit from cutting edge technology.

Based on the above considerations, this thesis addresses the general development of novel attitude determination and control algorithms to improve attitude estimation accuracy. The next section reviews the previous work done on the relevant topics for the thesis.

1.2 Literature Review

This section presents a review of the relevant literature on satellite attitude determination, estimation and control.

1.2.1 Attitude Determination

The attitude of a spacecraft is its orientation in space with respect to a global reference frame. Three axis deterministic methods that utilize only two vector measurements from two different sensors obtained at a single time point to determine the attitude of the spacecraft are widely used. The well-known TRIaxial Attitude Determination (TRIAD) algorithm [41], also known as the algebraic method, is based on the computation of vector products of measured vectors that create an auxiliary orthogonal vector triad.

Remark 1.1. *The word "TRIAD" can be thought of as the word "triad", or an acronym for TRIaxial Attitude Determination.*

Because the algorithm is very simple and very transparent, it has become the most popular method for determining three-axis attitude for spacecraft. Numerous other deterministic methods have been developed based on minimizing the Wahba loss function. Wahba [73] was the first to choose a least square criterion to find the attitude of a spacecraft. Davenport introduced a new method, called the q-method, which provides a quaternion-based solution for the Wahba problem. Shuster and Oh [63] developed the QUEST (QUaternion ESTimator) algorithm, which is faster and avoids solving the eigenvalue problem explicitly. Markley proposed a method based on Singular Value Decomposition (SVD) [44] that computes the attitude matrix directly. Another alternative solution was by Markley, called Fast Optimal Attitude Matrix(FOAM) method, provides an iterated solution to find the attitude matrix. The efficiency of QUEST and FOAM are compared in the work [43].

Limitations: The greatest drawback of these deterministic methods is that they can only be used when two vector measurements are simultaneously available and the angle between the vectors is larger than certain critical value.

1.2.2 Attitude Estimation

Estimation algorithms use a dynamic and/or a kinematic model of the spacecraft's motion to determine its attitude. Consequently, such methods can estimate the attitude of the spacecraft using only one set of vector measurements. In this subsection two different types of estimation techniques are discussed. One is based on stochastic theory and the other on ellipsoidal estimation theory.

Kalman Filtering

In 1960, Kalman proposed a new approach to linear filtering [28]. Since then, the Kalman filter has become one of the most well-known stochastic estimation algorithms and has been extensively used in several areas of research [26,68]. Although proposed in 1960, Kalman filtering has only been used in spacecraft attitude determination since 1982 [37]. The essential feature of Kalman filtering is the use of a state space formulation for the system model. Errors in the dynamic model are treated as 'process noise', since system models are not usually improved or updated during the estimation process. There are three main assumptions in Kalman filtering:

1. The model error (process noise) is a zero-mean Gaussian stochastic process with known covariance. However, in practice, the determination of the process noise covariance is usually obtained by an ad hoc or heuristic approach.

2. The system model is linear. However, most practical systems are, in general, nonlinear.

3. The correlation between the model noise and the measurement noise is zero. However, in situations where feedback is involved, e.g., in control problems where the output is used to modify the state equation, it is useful to consider models in which there is a correlation between these two sources of noise [9,27].

The Extended Kalman Filter (EKF) [19, 26, 27] is an attempt to address the limitations caused by assumption 2 of Kalman filtering discussed above. It has the advantage that it is computationally inexpensive, and fairly robust with respect to

model errors. Unfortunately, the EKF can exhibit sensitivity to the initial attitude estimate because it relies on linearizations of the spacecraft's nonlinear measurement and dynamic models. In some situations this sensitivity can cause the EKF to diverge. The algorithm described in [14] is based on predictive filtering. Furthermore, the algorithm is not limited to the Gaussian noise characteristics for the model error. Essentially, this algorithm combines the good qualities of both the Kalman filter and minimum model error algorithm [12]. Some simulation results comparing predictive filtering and extended Kalman filtering for a particular case study are given in [54]. In [13] a new and efficient algorithm is developed for attitude determination using Global Positioning System (GPS) signals. The advantages of this algorithm over previously developed methods are that it guarantees convergence (even for poor initial conditions) and is computational efficiency. However, the failure of GPS could be disastrous if it is the primary sensor for attitude estimation without backup sensors. Other approaches for attitude estimation are discussed in references [15,38,41].

Limitations: The attitude estimation algorithms using stochastic theory presented above are based on the statistical information of the system, which is often not available. Moreover, all the existing approaches assume that the correlation between the process noise and the measurement noise is zero. In the next paragraph, the first limitation is addressed by using ellipsoidal estimation theory.

Guaranteed Ellipsoidal Estimation

A confidence region for a state estimate consists of a set that is determined from the system dynamics, the bounds on the noise, and observations. Numerous algorithms have been developed based on the idea of determining a set of possible states in the last four decades [4, 10, 35, 42, 58, 60, 61]. Exact computation of sets is not generally possible, so approximation techniques are needed instead. The choice of the set representation determines the efficiency of such techniques. On the other hand, the more complex the representation is, the more costly is the storage of the sets and the more elaborate are the computations. On the other hand, more complex representations result in better approximations of the reachability set. Choosing the set

6

representation is a compromise between these factors. Representations of these sets can be approximated either by polyhedral [10], parallelotopes [11], zonotopes [1] or ellipsoids [10]. However, polyhedral, zonotopes and parallelotopes need a lot of computations for large dimensions of the state space when compared to ellipsoids [10]. Ellipsoidal approximations are popular because they depend only on a limited number of parameters and are therefore chosen for the guaranteed state estimation of dynamic systems. Schweppe [60] lays the foundations for the work on set membership state estimation using ellipsoids. However, optimization of the ellipsoids was not addressed in this pioneering work. These developments were continued by Bertsekas [5] and Chernousko [10]. Using some of Schweppe's development, bounding of constant parameters was considered by Fogel *et al.* [18, 35]. In the context of linear programming, an algorithm was developed to obtain a minimal volume ellipsoid containing the intersection of an ellipsoid with a half-space or a region limited by two parallel hyperplanes [6, 8]. Maksarov and Norton further explored this approach in [42], where they propose a function whose single root in the range of interest gives the minimum volume ellipsoid inside a linear convex combination of two ellipsoids. Recently, Polyak *et al.* [50] extended linear set estimation to uncertain linear systems. Their technique is based on the fact that the matrix uncertainty is combined with the uncertainty due to state perturbations and measurement noise by ellipsoidal constraints. However, they only studied set estimation for uncertain linear systems. The biggest limitation of the above mentioned approaches is that they are primarily derived for linear systems. Extensions to nonlinear systems have been made by Shamma and Jaulin [25, 61]. The most recent work on state estimation using set estimation for nonlinear systems is given by Scholte and Campbell [59], in which their design is called an Extended Set Membership Filter (ESMF). The most recent work on satellite attitude estimation using guaranteed ellipsoidal estimation is given by Sanyal *et.al.* [55]. In Sanyal's work, Lie algebra theory is used to describe the attitude kinematics.

Limitations: The guaranteed ellipsoidal estimation algorithms for linear systems seek to approximate the feasibility set from the outside. However, by finding the set

first, the computational load is high. For nonlinear systems, the set estimation algorithms deal with the cases when the linearization error about the current estimate is bounded using interval mathematics [47].

The work carried out in this section is included in the development of new approaches to the attitude control, which is discussed in the next subsection.

1.2.3   Attitude Control

Attitude control consists of two steps: attitude stabilization and attitude maneuvering. Attitude stabilization is the process of maintaining an existing orientation, while attitude maneuvering is the process of controlling the reorientation of the spacecraft from one attitude to another. These processes are executed by actuators, such as gyro wheels, magnetic torque rods and/or momentum wheels. The attitude control system uses a number of operating modes to accomplish the stabilization and maneuver control of the various phases of a mission, from launch vehicle separation all the way to the science operation. The primary attitude control modes of a satellite are:

- Wait mode - provides no control torques to the spacecraft. The ADCS actuators are normally powered off.

- Attitude acquisition mode - uses torque rods to damp nutation, capture the desired body rate and acquire the pointing attitude.

- Pointing mode - is the nominal operating mode in which the satellite is precisely stabilized with respect to a desired reference frame.

- Safe mode - when the Attitude Control System (ACS) is shut down and/or maintains a certain solar array orientation with respect to the Sun.

Switching between these modes is necessary during any mission. Note, in particular, that during the acquisition mode, the attitude control system may be required to perform large-angle maneuvers, which are highly nonlinear. Similarly, the pointing mode usually only requires small attitude adjustments, which could accurately be described using a linearized model.

8

Crouch [17] extended the work of Meyer [45] and provided necessary and sufficient conditions for the controllability of a rigid body in the case of one, two or three independent torques. Wie and Barba [75] derived nonlinear feedback control schemes using quaternions and angular velocity feedback and proved asymptotic stability using Lyapunov functions. Tsiotras [69–71] extended these results using a Lyapunov function that involved the sum of a quadratic term in the angular velocities and a logarithmic term in the kinematic parameters, leading to the design of linear controllers. Singh and Bossart [66] derived a feedback control law for prescribed pitch attitude tracking based on dynamic feedback linearization for spacecraft using a control moment gyro. Singh and Iyer [67] used sliding modes for attitude control of an orbiting spacecraft using reaction jets in the presence of uncertainty. A nonlinear H_∞ control methodology has been developed by Kang [29] to control rigid spacecraft with three torques in the presence of disturbances. This methodology involves the solution of the Hamilton-Jacobi-Isaacs inequalities. Crassidis *et al.*. [16] were the first to consider the problem of controlling a spacecraft without full state feedback. The controller is designed by minimizing the norm-squared local errors between the predicted and desired quantities. A Lyapunov-based adaptive controller that estimates external torques has been developed by Schaub *et al.*. [57]. Lim [39] developed a linear parameter-varying controller, in which a single quadratic Lyapunov function for each frozen Linear Time-Invariant (LTI) system was used in a parameter variation set. Raymond and Johan [53] used integrator backstepping design for satellite attitude control based on quaternions. In the authors previous work [20], a two step integrated and systematic approach for modelling and control of large angle attitude maneuvers of a rigid body was developed. Notice however that the cost, the processor workload and the time-constraints in spacecraft development and deployment projects curtail the opportunity for implementing nonlinear control laws during entire missions. For example in a pointing mission the satellite is always required to point toward either the Sun or the Zenith. In such a mission, nonlinear control is only needed during the acquisition mode . This motivates the use of switching between a global nonlinear controller for acquisition mode and a local linear controller

for pointing mode that can guarantee performance and that uses less computational operations to be implemented in a microprocessor.

Limitations: While the problem of attitude control and stabilization has been the subject of much research, the problem of switching between a global controller and a local controller has not been explicitly considered for spacecraft.

1.3 Problem Formulation

Based on the state of the art and the limitations of the existing methods discussed in the previous section, this section formulates the main objectives of the thesis.

1.3.1 Thesis Objective

The main objective of this thesis is to develop novel attitude determination and control algorithms. Verification of these algorithms is performed by on-ground prototyping using telemetry data available from the on-board equipment of an orbiting satellite. Moreover, the on-ground mission control center has to evaluate the attitude accuracy, calibrate sensors and provide analytical attitude estimates from the telemetry data sent by the satellite. Hence, significant development of novel sensor fusion algorithms has to be carried out on the ground for potential future implementation on satellites. The GBAE formulation will be based on the guaranteed ellipsoidal state estimation for the acquisition mode and a modified Kalman filter for the pointing mode, thus enabling optimal estimates of the spacecraft attitude. A modified Kalman filter assumes that there exists a correlation between the measurement noise and the process noise. This is proposed because when the sensors are in closed-loop, the measurement noise and the process noise are correlated. The guaranteed ellipsoidal state estimation method does not need the statistical information of the uncertainties and uses only the bounds on the uncertain factors. In the simulation environment, the ground-based attitude estimator obtains the data from the spacecraft dynamical model. Spacecraft dynamics are complex with multiple modes of operation. This motivates the use of switching between a global nonlinear controller for acquisition mode

and a local linear controller for pointing mode, which can guarantee performance and is less computationally intensive for implementation in an on-board microprocessor. In this thesis, the novel attitude determination and control algorithms are evaluated in the flight environment for a case study in collaboration with the Canadian Space Agency (CSA) for the SCISAT-1 satellite.

1.3.2 Case Study

SCISAT-1 was launched aboard the Pegasus XL rocket on August 12, 2003. SCISAT-1 was placed in a highly inclined orbit with an altitude of 670 km and is currently performing its mission in space successfully. The purpose of this mission is to measure and understand the chemical process that controls the distribution of ozone in the Earth's atmosphere, especially at high latitudes. The attitude determination and control system provides on-orbit attitude control through all mission phases. This is performed with the aid of on-board attitude sensors and actuators. The attitude sensors and actuators on SCISAT-1 are as follows: six coarse Sun sensors and fine Sun sensors, a star tracker, a three-axis magnetometer, a momentum wheel, and three magnetic torque rods. The present attitude and body rate determination algorithm used in the SCISAT-1 is a deterministic approach, based on the "small angles" assumption.

The next subsection summarizes the main contributions and provides an outline of this thesis.

1.3.3 Original Contributions

The main contributions of this thesis are the following:

1. A novel attitude determination algorithm, called the dyad method, is proposed to avoid the discarding information when using the TRIAD method. This method is based on the inherent informational redundancy of a pair of vector measurements and allows the independent use of each of two vector measurements to determine two Euler angles and combine this information to derive

the third angle.

2. The implementation of the modified Kalman filter for the linearized spacecraft dynamical model in the pointing mode when the process and measurement noise are correlated. The correlation between the measurement noise and the process noise is motivated by the fact that attitude sensors are involved in the attitude feedback control loop.

3. An attitude estimation algorithm using the guaranteed ellipsoidal state estimation method for acquisition mode is proposed. This method is being proposed because the guaranteed ellipsoidal state estimation does not need statistical information of the uncertainties, which is often not available, and uses only the bounds on the uncertain factors.

4. A switched controller for a satellite attitude problem in which a switching strategy is developed using a global controller in the acquisition mode and a local controller during the pointing mode. When the rigid body is close to its desired attitude set point, which usually corresponds to the pointing mode, the control switches to a linear controller that can guarantee performance. Linear controllers are also usually less computationally intensive, making them better for implementation in on-board microprocessors.

1.3.4 Thesis Outline

The outline of the thesis is given below.

Chapter 1: The introduction, contributions and thesis outline are presented in this chapter.

Chapter 2: In this chapter, mathematical preliminaries which will be used in this thesis are discussed. The reference frames relevant to the estimation problem are described, as well as the different ways to represent the attitude of a spacecraft. Further, a brief explanation of the dynamic equations of a spacecraft is provided.

Chapter 3: A novel deterministic attitude determination algorithm, called the

12

dyad method, is proposed to avoid the question of discarded information when using the TRIAD method. This method is based on the inherent informational redundancy of a pair of vector measurements and allows the independent use of each of two vector measurements to determine two Euler angles and combine this information to derive the third angle. Application of the dyad method is demonstrated by on-ground processing of the TELEMETRY (TLM) data from the Canadian scientific satellite, SCISAT-1.

Chapter 4: This chapter addresses the problem of satellite attitude estimation using modified Kalman filter and set theory. A modified Kalman filter is proposed for processing the satellite telemetry data, which takes into account correlations between the process and measurement noise. Moreover, a guaranteed ellipsoidal state estimation method is proposed in this chapter for acquisition mode where the dynamic model is nonlinear. This is accomplished by finding the minimum volume ellipsoid using quadratic constraints on the model uncertainty and then applying a set membership filter. This filter recursively estimates an ellipsoid set in which the true state lies. The center of the ellipsoidal set provides state estimates and the size of the ellipsoid measures the accuracy of these estimates.

Chapter 5: In this chapter, a switched controller for a satellite attitude problem in which a switching strategy between global and local controllers is developed. The global controller is used during the acquisition mode, while the local controller is used during the pointing mode. When the rigid body is close to its desired attitude set point, which usually corresponds to the pointing mode, the control switches to a linear controller that can guarantee performance. Linear controllers are also usually less computationally intensive, making them better for implementation in on-board microprocessors.

Chapter 6: This chapter concludes the thesis and makes some recommendations for future work.

1.4 Publications

The following publications were written during the course of the present research.

1. N. Gollu, Y. V. Kim and A. Ng, "Ground based satellite attitude estimator," *15th AAS/AIAA Space Flight Mechanics,*Copper mountain,Colorado, 2005.

2. Y. V. Kim, N. Gollu, and A. Ng, "On inherent informational redundancy in vector measuring attitude determination methods," *56th International Astronautical Congress Conference*, Fukuoka, Japan, 2005.

3. L. Rodrigues and N. Gollu, "Analysis and state feedback control for piecewise affine systems with additive noise," in *Proceedings of American Control Conference*, pp. 5438-5443, Minneapolis, U.S.A, 2006.

4. N. Gollu and L. Rodrigues, "Control of large angle attitude maneuvers for rigid bodies using sum of squares," in *Proceedings of American Control Conference*, pp. 3156-3161, New York, U.S.A, 2007.

5. N. Gollu "Switched control for attitude maneuvers of rigid bodies using sum of squares," in *Proceedings American Control Conference*,pp. 2987-2992, Seattle, U.S.A, 2008.

1.5 Chapter Summary

In this chapter, the thesis objectives and the state of the art were discussed. The next chapter will discuss the mathematical preliminaries required for the development of novel attitude determination and control algorithms.

Chapter 2

BACKGROUND

In the previous chapter, an introduction to the Attitude Determination and Control System (ADCS) was given and the problem formulation was discussed. This chapter first presents background information on the coordinate systems and the reference frames used in the development of attitude determination and control methods for satellites. Then, the satellite kinematic and dynamic equations are presented.

2.1   Attitude Determination

The objective of spacecraft attitude determination is to determine the orientation of the spacecraft relative to either an inertial reference frame or some specific object of interest such as the Earth. The attitude determination system commonly uses Sun sensors, horizon sensors, star trackers, magnetometers and gyroscopes. These sensors will now be explained briefly.

Sun Sensors

The objective of a Sun sensor is to provide a measurement of a unit vector that points from the satellite to the Sun. Sun sensors are one of the most widely used attitude determination sensors because the Sun is easy to detect. In addition, the angular radius of the Sun is sufficiently small that for most applications a point-source approximation is valid. However, the Sun is not always visible. An example

15

of a situation where the Sun is not visible is during eclipse periods.

Magnetometer

The objective of a magnetometer is to measure the strength and direction of the Earth's magnetic field to determine the orientation of a spacecraft with respect to the local magnetic field. Magnetometers are reliable, lightweight, and have low power requirements. Furthermore, they operate over a wide temperature range and has no moving part. However, they are not accurate inertial attitude sensors because the Earth's magnetic field is only partially known. In addition, because the Earth's magnetic field strength decreases with distance from the Earth, residual spacecraft magnetic biases eventually dominate the total magnetic field measurement, generally limiting the use of magnetometers to spacecraft missions below 1000 km.

Horizon Sensors

Horizon sensors are the principal means for directly determining the orientation of the spacecraft with respect to the Earth. However, the location of the horizon is poorly defined for a body possessing an atmosphere because of the gradual decrease in radiated intensity away from the true or hard horizon of the solid surface.

Star Trackers

Star trackers measure star coordinates in the spacecraft frame and provide attitude information when these observed coordinates are compared with known star directions obtained from a star catalog. Star trackers are the most accurate attitude sensors. However, star sensors are often heavy, complex and expensive. Searching the library of constellations is also time-consuming and requires extensive computer software programs. Typically, for high accuracy and rapid response, star trackers are used along with gyroscopes.

Gyroscopes

Gyroscopes determine the attitude directly or by measuring the rate of rotation of the spacecraft. Gyroscopes have a high accuracy for limited time intervals. They must be used along with other attitude sensors to prevent increase of attitude errors with time as they are prone to drift with time.

Table 2.1: Sensor accuracy ranges (adapted from [36])

Sensor	Accuracy	Pros	Cons
Magnetometers	0.5 - 1°	low cost, continuous coverage	low altitude
Sun sensor	0.01 - 4°	low cost, simple, reliable	intermittent use
Horizon sensor	0.1°	accurate	no yaw
Star tracker	2 arc-sec	very accurate	expensive heavy,complex
Gyros	drift rate 0.01 °/hr	high bandwidth	expensive, drifts with time

Based on the pros and the cons of each of the attitude sensors discussed above, any attitude determination method should use the information from all the appropriate sensors available to increase accuracy. Most often, the attitude determination system cannot rely on a single sensor to provide sufficient information. For example, gyroscopes are used to measure three attitude angles but they suffer from a drift error problem. The drift error is compensated by using the horizon sensors. Since horizon sensors can only measure pitch and roll angles, the yaw angle is left uncompensated. Therefore Sun sensors are used for further compensation. However, Sun sensors are not functional during eclipse periods, therefore magnetometers are used. Star trackers are commonly used together with gyroscopes to estimate and compensate drift error. Some general attitude sensor characteristics are presented in Table 2.1.

2.2 Attitude Kinematics

2.2.1 Reference Frames

A reference frame, or coordinate system, is generally taken to be a set of three unit vectors that are mutually orthogonal, forming a right-handed triad. Reference frames are important in attitude dynamics because describing the orientation of a rigid body is completely equivalent to describing the orientation of a frame attached to the body. The most common reference frames used for describing the attitude of a spacecraft are the inertial frame, the orbital frame, and the Sun frame.

Inertial Frame

An inertial frame for spacecraft attitude determination is defined as follows: the $\hat{i}_x$ axis points from the focus of the orbit to the vernal equinox [74], and the $\hat{i}_z$ axis is aligned with the Earth's rotation axis and perpendicular to the equatorial plane, the $\hat{i}_y$ axis is in the equatorial plane and completes a right-handed triad. The inertial frame is denoted by $\{\hat{i}_x, \hat{i}_y, \hat{i}_z\}$ or $\mathbf{F}_i$ and is shown in Figure 2.1. The hats are used to denote unit vectors.
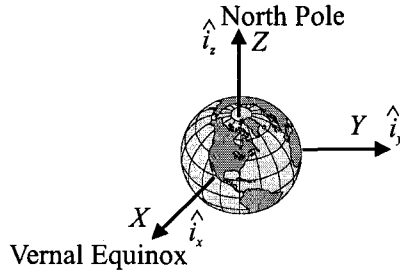
Figure 2.1: Inertial frame

Orbital Frame

The orbital frame is attached to the center of mass of the spacecraft. The motion of the frame depends only on the orbit and is not effected by body rotations. This frame is non-inertial because of the orbital acceleration and the rotation of the frame. The $\hat{o}_z$ axis points from the spacecraft to the Earth (nadir direction), $\hat{o}_y$ points in

18

the direction opposite to the orbit normal, and $\hat{o}_x$ is in the direction of the flight and completes the right-handed triad. The orbital frame is denoted by $\{\hat{o}_x, \hat{o}_y, \hat{o}_z\}$ or $\mathbf{F}_o$ and is shown in Figure 2.2.

Orbit
Normal

Flight
Direction
$\hat{O}_x$

$\hat{O}_z$ Nadir

$\hat{O}_y$
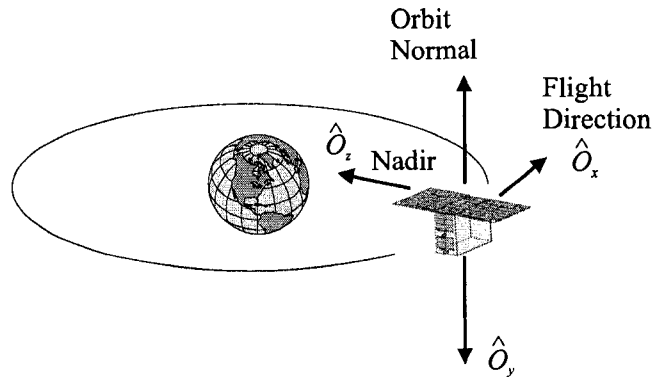
Figure 2.2: Orbital frame

Body Frame

As with the orbital frame, the body frame has its origin at the center of mass of the spacecraft. This frame is fixed to the satellite body and therefore is non-inertial. The relative orientation between the orbital and body frames describes the attitude of the spacecraft. The body frame is represented by $\{\hat{b}_x, \hat{b}_y, \hat{b}_z\}$ or $\mathbf{F}_b$.

Sun Frame

The Sun pointing frame is used to define the satellite attitude with respect to the Sun. The $\hat{s}_x$ is along the line joining the spacecraft center of mass and the Sun, and point towards the Sun. The $\hat{s}_z$ is normal to the ecliptic plane and point towards north. The $\hat{s}_y$ completes a right handed triad. The Sun frame is represented by $\{\hat{s}_x, \hat{s}_y, \hat{s}_z\}$ or $\mathbf{F}_s$

2.2.2 Rotations

A rotation matrix is a 3×3 orthonormal matrix describing the orientation of a frame $\mathbf{F}_b$ relative to a frame $\mathbf{F}_a$ and is represented by

$$\mathbf{R}_b^a = [[i]^a [j]^a [k]^a], \tag{2.1}$$

19

where $[[i]^a[j]^a[k]^a]$ represent the coordinates relative to $\mathbf{F}_a$ of the directional vectors of $\mathbf{F}_b$. $\mathbf{R}_b^a$ is a matrix of direction cosines and is hence frequently referred to as the direction cosine matrix. Applied to a free vector v expressed in frame $\mathbf{F}_b$, $\mathbf{R}_b^a v^b$ gives the same vector expressed in frame $\mathbf{F}_a$, that is, $v_a = \mathbf{R}_b^a v^b$.

2.2.3 Attitude Representations

There are numerous ways to describe the attitude of a rigid body, and a brief overview of the three commonly used representations in spacecraft attitude control is discussed here. The kinematic differential equations associated with each representation has also been addressed to describe their time rate of change. A more detailed description of these, and other attitude representations, is provided by Shuster [62].

Euler angles

Euler angles make it possible to represent arbitrary rotations as a composition of three successive principal rotations. Let us consider the $x - y - z$ rotation sequence. These angles are called roll (x rotation), pitch (y rotation) and yaw (z rotation), respectively. The orientation of a body frame $\mathbf{F}_b$ relative to a fixed inertial frame $\mathbf{F}_i$. The three rotations are shown in Figure 2.3. A positive rotation ϕ about the X_1 axis resulting in X_2, Y_2, Z_2 coordinate systems where $X_2 = X_1$ and then a positive rotation θ about the $Y2-$axis resulting in X_3, Y_3, Z_3 where $Y_3 = Y_2$ and finally the third positive rotation about the Z_3-axis resulting in X_4, Y_4, Z_4 where $Z_4 = Z_3$. The corresponding principal rotation matrices are expressed as
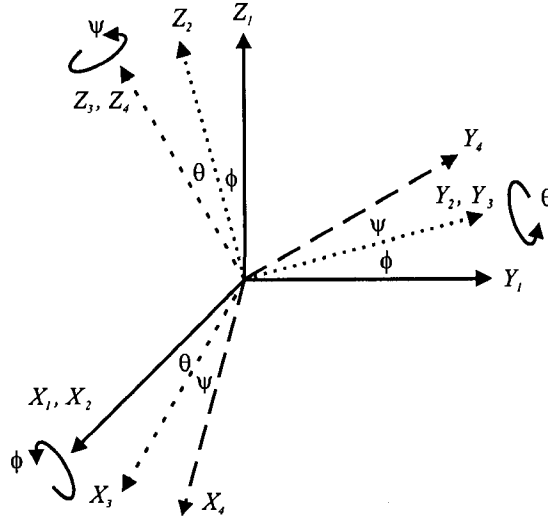
Figure 2.3: Euler axis rotation

The corresponding principal rotation matrices are expressed as

$$
R_x(\phi) = \begin{bmatrix} 1 & 0 & 0 \\ 0 & c\phi & s\phi \\ 0 & -s\phi & c\phi \end{bmatrix}, R_y(\theta) = \begin{bmatrix} c\theta & 0 & -s\theta \\ 0 & 1 & 0 \\ s\theta & 0 & c\theta \end{bmatrix}, R_z(\psi) = \begin{bmatrix} c\psi & s\psi & 0 \\ -s\psi & c\psi & 0 \\ 0 & 0 & 1 \end{bmatrix}, \quad (2.2)
$$

where $c\psi \equiv \cos\psi$, $s\phi \equiv \sin\phi$, and so on. The orientation of frame F_b relative to frame F_i for $x - y - z$ rotation sequence is described by the matrix product

$$
\mathbf{R}_i^b(\phi, \theta, \psi) = R_z(\psi)R_y(\theta)R_x(\phi) \tag{2.3}
$$

or, equivalently,

$$
\mathbf{R}_i^b = \begin{bmatrix} \cos\theta\cos\psi & \sin\phi\sin\theta\cos\psi + \cos\phi\sin\psi & -\cos\phi\sin\theta\cos\psi + \sin\phi\sin\psi \\ -\cos\theta\sin\psi & -\sin\phi\sin\theta\sin\psi + \cos\phi\cos\psi & \cos\phi\sin\theta\sin\psi + \sin\phi\cos\psi \\ \sin\theta & -\sin\phi\cos\theta & \cos\phi\cos\theta \end{bmatrix} .
$$
$$\tag{2.4}$$

This parameterization is not ideal and the spacecraft can have all possible orientations

[74]. The formulae for Euler angles can be derived from (2.4) as

$$\phi = -\tan^{-1}\left(\frac{\mathbf{R}^b_{i_{32}}}{\mathbf{R}^b_{i_{33}}}\right) \tag{2.5}$$

$$\theta = \sin^{-1}\left(\mathbf{R}^b_{i_{31}}\right)$$

$$\psi = -\tan^{-1}\left(\frac{\mathbf{R}^b_{i_{21}}}{\mathbf{R}^b_{i_{11}}}\right).$$

The kinematic differential equation for the roll-pitch-yaw derivatives is given by [74]

$$\begin{bmatrix} \dot{\phi} \\ \dot{\theta} \\ \dot{\psi} \end{bmatrix} = \begin{bmatrix} \cos\psi\sec\theta & -\sin\psi\sec\theta & 0 \\ \sin\psi & \cos\psi & 0 \\ -\cos\psi\tan\theta & \sin\psi\tan\theta & 1 \end{bmatrix} \begin{bmatrix} \omega_x \\ \omega_y \\ \omega_z \end{bmatrix}. \tag{2.6}$$

As an attitude representation, the rotation matrix has nine parameters, of which six are redundant. In addition, it is observed that at $\theta = \pm 90°$ the equation (2.6) becomes singular, making the Euler angles impractical for describing arbitrary, large-angle rotations. It should be noted that these singularities are numerical in nature and are not based on physical limitations. Moreover, the kinematic differential equations arising from the use of Euler angles is nonlinear and requires many computationally intensive trigonometric functions. For these reasons, other attitude representations were developed. The next representation to be described is the quaternion.

Quaternions

Another popular attitude representation is the four-parameter set known as quaternions. Quaternions are a redundant attitude representation well suited to economical computations. They are based on Euler's principal rotation theorem, which states that *any arbitrary rotation can be represented by a single rotation about the principal axis* $\hat{e} = (e_1, e_2, e_3)$ *through a principal angle* Φ [56]. In Figure 2.4, Euler's principal rotation theorem requires the transformation of $\mathbf{F}_b(\hat{b}_1, \hat{b}_2, \hat{b}_3)$ with respect to $\mathbf{F}_a((\hat{a}_1, \hat{a}_2, \hat{a}_3)$ be a rotation about the principal axis.
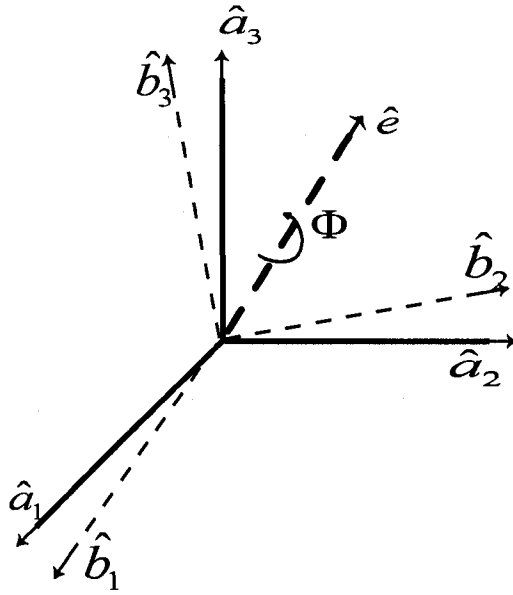
Figure 2.4: Geometry pertaining to Euler's theorem

The quaternion vector $\mathbf{q}$ is defined in terms of the principal rotation elements $(\hat{e}, \Phi)$ as

$$q_1 = e_1 \sin{(\Phi/2)}$$
$$q_2 = e_2 \sin{(\Phi/2)}$$
$$q_3 = e_3 \sin{(\Phi/2)} \qquad (2.7)$$
$$q_4 = \cos{(\Phi/2)}$$

where the first three elements, which indicate the direction of the Euler axis, are usually grouped together and written as $\mathbf{q}_{13} = \hat{e}\sin{(\Phi/2)}$. The fourth element, q_4, is commonly referred to as the scalar component of the quaternion and indicates the principal angle. The kinematic differential equation using quaternions is given by

$$\begin{bmatrix} \dot{q}_1 \\ \dot{q}_2 \\ \dot{q}_3 \\ \dot{q}_4 \end{bmatrix} = \frac{1}{2} \begin{bmatrix} q_4 & -q_3 & q_2 \\ q_3 & q_4 & -q_1 \\ -q_2 & q_1 & q_4 \\ -q_1 & -q_2 & -q_3 \end{bmatrix} \begin{bmatrix} \omega_x \\ \omega_y \\ \omega_z \end{bmatrix}. \qquad (2.8)$$

Additionally, quaternions are characterized by a magnitude constraint:

$$\mathbf{q}^T\mathbf{q} = q_1^2 + q_2^2 + q_3^2 + q_4^2 = 1, \qquad (2.9)$$

23

and therefore represent a unit sphere in $\mathbb{R}^4$. This indicates that the four elements are not all independent, and the fourth element is frequently determined from the other three based on this constraint. However, this constraint often causes problems in numerical computations due to computer rounding errors. Due to these numerical problems, and the need for four parameters to describe an attitude using quaternions, other methods were developed. The modified Rodrigues parameters are described next.

Modified Rodrigues Parameters

The modified Rodrigues parameters (MRP) are a recent addition to the family of attitude representations and are particularly well suited for describing very large attitudes [56]. The MRP are able to describe any arbitrary orientation with only three parameters, instead of the four required by quaternions. The MRP vector $\boldsymbol{\sigma}$ can be expressed in terms of the principal rotation elements $(\hat{\mathbf{e}}, \Phi)$ as

$$\boldsymbol{\sigma} = \hat{\mathbf{e}} \tan \frac{\Phi}{4} \tag{2.10}$$

or in terms of the four quaternion elements (q_1, q_2, q_3, q_4) as

$$\boldsymbol{\sigma} = \begin{bmatrix} q_1/(1+q_4) \\ q_2/(1+q_4) \\ q_3/(1+q_4) \end{bmatrix}. \tag{2.11}$$

It can be seen from these equations that the MRP representation has a geometric singularity at $\Phi = \pm 360°$, which corresponds to $q_4 = -1$ in (2.11). Thus, any rotation less than a complete revolution can be expressed using these parameters. However, this situation is generally not encountered in most attitude maneuvers. The kinematic differential equation can be written in terms of the MRP [62] as

$$\dot{\boldsymbol{\sigma}} = \Omega(\boldsymbol{\sigma})\boldsymbol{\omega}, \tag{2.12}$$

24

where $\omega = [\omega_x \; \omega_y \; \omega_z]^T$ are the angular velocities of the satellite about each of the principal body axes,

$$\Omega(\boldsymbol{\sigma}) = \frac{1}{4} \begin{bmatrix} 1 - \sigma^2 + 2\sigma_1^2 & 2(\sigma_1\sigma_2 - \sigma_3) & 2(\sigma_1\sigma_3 - \sigma_2) \\ 2(\sigma_2\sigma_1 - \sigma_3) & 1 - \sigma^2 + 2\sigma_2^2 & 2(\sigma_2\sigma_3 - \sigma_1) \\ 2(\sigma_3\sigma_1 - \sigma_2) & 2(\sigma_3\sigma_2 - \sigma_1) & 1 - \sigma^2 + 2\sigma_3^2 \end{bmatrix},$$

and $\sigma^2 = \sigma_1^2 + \sigma_2^2 + \sigma_3^2$.

Now that three different attitude kinematic representations have been described, the next section discusses the dynamics of rigid bodies.

2.3 Rigid Body Dynamics

The angular momentum of a rigid body and the total moment applied to the same body relative to any point O in frame F_i are given by the expressions

$$H_0 = \int (r - r_0) \times (v - v_0) dm \tag{2.13}$$

and

$$M_0 = \int (r - r_0) \times dF, \tag{2.14}$$

where

- $r = [x \; y \; z]^T$ is the position of the elementary mass dm in frame F_i,

- $r = [x_0 \; y_0 \; z_0]^T$ is the position of the point O in frame F_i,

- $v = \dot{r}$ and $v_0 = \dot{r}_0$ are the velocities of the elementary mass dm and the point O, respectively, both measured in F_i,

- dF is the elementary force applied to the elementary mass dm.

The velocity of the elementary mass dm for a rigid body is given as [23]

$$v = v_0 + \omega \times (r - r_0).$$

25

Using this relation, expression (2.13) can be written as a function of the angular velocity ω of the body relative to frame F_i in the form

$$H_0 = \int_v (r - r_0) \times \omega \times (r - r_0)\rho(x,\ y,\ z)dV. \tag{2.15}$$

This expression can in turn be expanded and rewritten as

$$H_0 = I_0\omega, \tag{2.16}$$

where I_0 represents the inertia tensor given by

$$I_0 = \begin{bmatrix} I_x & -I_{xy} & -I_{xz} \\ -I_{yx} & I_y & -I_{yz} \\ -I_{zx} & -I_{zy} & I_z \end{bmatrix}.$$

The entities I_x, I_y and I_z are the moments of inertia about the x, y and z axes, respectively, of the coordinate frame, and $I_{yx} = I_{xy}$, $I_{zx} = I_{xz}$, $I_{zy} = I_{yz}$ are the products of inertia. These quantities are defined as

$$I_x = \int_v (y^2 + z^2)\rho(x,y,z)dV, \quad I_{xy} = \int_v (xy)\rho(x,y,z)dV,$$
$$I_y = \int_v (x^2 + z^2)\rho(x,y,z)dV, \quad I_{xz} = \int_v (xz)\rho(x,y,z)dV,$$
$$I_z = \int_v (x^2 + y^2)\rho(x,y,z)dV, \quad I_{yz} = \int_v (yz)\rho(x,y,z)dV.$$

After this small introduction, it is easy to show by differentiation of (2.13) and taking into account (2.14) and the equality

$$dF = dm \frac{dv}{dt}_{F_i} \tag{2.17}$$

the following differential equation can be derived

$$\frac{dH_0}{dt}_{F_i} = M_0. \tag{2.18}$$

This is called Newton-Euler's moment equation.

Principal axes

A principal axis has its origin at the center of mass and is such that the products of inertia are all zero. Thus, the moment of inertia matrix is diagonal. The diagonal elements are known as the principal moments of inertia and the corresponding new axes are called principal axes. The three principal axes include the axes of maximum and minimum inertia, referred to as the major and minor axes, respectively.

2.4 Attitude Dynamics

The attitude dynamics are given by Newton-Euler's moment equations (2.17) expressed in principal axes as

$$I_x \dot{\omega}_x + (I_z - I_y)\omega_y\omega_z = T_x$$
$$I_y \dot{\omega}_y + (I_x - I_z)\omega_z\omega_x = T_y \qquad (2.19)$$
$$I_z \dot{\omega}_z + (I_y - I_x)\omega_x\omega_y = T_z$$

which can also be written as

$$
\begin{bmatrix} \dot{\omega}_x \\ \dot{\omega}_y \\ \dot{\omega}_z \end{bmatrix} =
\begin{bmatrix} \frac{I_y - I_z}{I_x}\omega_y\omega_z \\ \frac{I_z - I_x}{I_y}\omega_z\omega_x \\ \frac{I_x - I_y}{I_z}\omega_x\omega_y \end{bmatrix} +
\begin{bmatrix} \frac{1}{I_x} & 0 & 0 \\ 0 & \frac{1}{I_y} & 0 \\ 0 & 0 & \frac{1}{I_z} \end{bmatrix}
\begin{bmatrix} T_x \\ T_y \\ T_z \end{bmatrix} \qquad (2.20)
$$

or

$$\dot{\omega} = -\mathbf{I}^{-1}(\omega \times \mathbf{I}\omega) + \mathbf{I}^{-1}\mathbf{u}, \qquad (2.21)$$

where $\mathbf{u} = [T_x\ T_y\ T_z]^T$ are the control torques acting on the satellite, and the principal moments of inertia I_x, I_y and I_z, are the components of the inertia tensor $\mathbf{I}$ given by

$$
\mathbf{I} = \begin{bmatrix} I_x & 0 & 0 \\ 0 & I_y & 0 \\ 0 & 0 & I_z \end{bmatrix}. \qquad (2.22)
$$

The external torque $\mathbf{T}$ is given by the summation of the control torque, T_c, and the disturbance torque, T_d,

$$\mathbf{T} = T_c + T_d. \qquad (2.23)$$

The next subsections describe disturbance torques and the actuators used in control torques more explicitly.

2.4.1 Disturbance Torques

A spacecraft is subject to many disturbance torques from the environment [23]. These torques can include aerodynamic, solar radiation, gravity-gradient torques, etc. The gravity-gradient torque is sometimes used as a passive control and therefore discussed in the the actuators section.

Solar Radiation

The solar radiation pressure has the most effect on light objects with a large surface. The surface area of the satellite which faces the Sun is essential in determination of the resulting acceleration caused by solar radiation.

Aerodynamic Drag

Satellites in low-earth orbits are affected by aerodynamic drag from the atmosphere, resulting in a reduction of speed and loss of altitude. As the satellite's altitude decreases the force due to the atmosphere increases due to the higher air density.

2.4.2 Actuators

Attitude control devices are highly mission dependent, and several types of actuators are available. Passive attitude control makes use of environmental torques, such as the gravity gradient or spin stabilization, to maintain the satellite's orientation. Active control actuators include reaction wheels, magnetic control devices, and thrusters. The decision to use a passive or an active control system or a combination of the two depends on mission pointing and stability requirements, power constraints, weight restrictions and the control system's stability and response time. Advantages to active control include good pointing accuracy, and a non-inertial pointing accuracy. However, the hardware is often expensive, and complicated, leading to higher weight and power requirement as compared to using passive control.

Reaction wheels

By definition, a reaction wheel or a momentum wheel is a flywheel with a body-fixed axis designed to operate at zero bias. The difference in reaction wheel and momentum wheel is primarily attributed to the speed at which they operate. A momentum wheel operates at non-zero nominal speeds while a reaction wheel operates at mean nominal speeds. When the spacecraft is exposed to a perturbation or is accelerated, so are the

wheels mounted inside, and the result is a torque generated from the wheels in the opposite direction.

Magnetic actuators

An active magnetic actuator takes advantage of the magnetic field surrounding the Earth. These devices use electricity carrying coils inside the spacecraft to exploit the Earth's magnetic field to produce torques. The principle can best be explained with the well-known compass needle that attempts to align itself with the local magnetic field. Magnetic actuators offer a cheap, reliable and robust way to control a spacecraft attitude. Unfortunately, they are only effective for Low-Earth orbit (LEO) spacecraft and require a complex model of the geomagnetic field surrounding the Earth.

Thrusters

Thrusters or reaction jets produce torque by expelling mass, and are potentially the largest source of force and torque on a spacecraft. They are highly active sources, and being external they will affect the total momentum. They can be used for both attitude and position control. In fact, they are the only actuators that can increase the altitude of a spacecraft in orbit. When used for attitude control, a pair of thrusters on opposite sides of the spacecraft are activated to create a couple. The main advantage of using thrusters is that they can produce an accurate and well defined torque on demand, as well as being independent of altitude. The main disadvantage is that a spacecraft can only carry a limited amount of propellant.

Spin stabilization

If the satellite rotates around one axis, the gyroscopic effect of this will reduce the influence of fluctuations on the other axes. The spin can be obtained in various ways. If the satellite is colored differently on each other side, the solar pressure will be greater on the lighter surfaces than on the darker ones. This, however, is a very slow method. Spinning could also be obtained by a thruster and maintained by

magnetic torquers. Instead of spinning the entire satellite, a momentum wheel inside the satellite could accomplish the same job.

Gravity-Gradient

Gravity-gradient is the most common passive control that uses the inertial properties of a vehicle to keep it pointed toward the Earth, but the magnitude of torque decreases with the cube of the orbit radius [74]. Gravity-gradient torques stabilize spacecraft such that an amplitude-bounded harmonic angular motion about an average bias value remains. However, passive dampers can dampen out these oscillations.

Table 2.2 shows the obtainable accuracy, as suggested by Wertz and Larson [36], together with some advantages/disadvantages of the different actuators.

Table 2.2: Actuator accuracy ranges (adapted from [36])

Method	Accuracy	Pros	Cons
Spin Stabilization	0.1°-1°	Passive, simple Cheap	Inertially oriented
Gravity Gradient	1°-5°	Passive, simple Cheap	Central body Central body oriented
Magnetic torquers	1°-2°	Cheap	Slow, lightweight, LEO only
Reaction Wheels	0.001°-1°	Expensive, precise, faster slew	Weight

2.5 Chapter Summary

In this chapter, a summary of attitude determination and control methods was presented. The following chapter will focus on developing a novel attitude determination algorithm.

Chapter 3

ATTITUDE DETERMINATION

In the previous chapter, background on attitude determination has been addressed. In this chapter, analysis and application of a novel attitude determination method, called the dyad method is presented. This method is validated using the telemetry data from the Canadian scientific satellite SCISAT. The origins of the dyad method can be traced back to a technical report from the Canadian space agency [32]. In the report an initial problem formulation has been developed. The method, however, has not been verified or studied with regard to conventional attitude determination methods and is the subject of this chapter.

3.1 Introduction

For any spacecraft attitude control design, the choice of an appropriate attitude determination method is very important. Furthermore, attitude should be computed very frequently to meet mission requirements. Attitude can be computed either by deterministic methods or by using optimal estimation methods. Regardless of the mission, deterministic methods play an important role in attitude determination especially during the backup modes, when the computational load should be kept to the minimum. The well-known deterministic TRIAD (TRI Attitude Determination) method [41], also known as the algebraic method, is based on the computation of vector products of measured vectors that create an auxiliary orthogonal vector triad.

31

The main limitation of the TRIAD algorithm is that it can only be used when two vector measurements are simultaneously available and the angle between the vectors is larger than some critical value ("co-linearity event" [74]). In addition, even when there are two observations, some potential accuracy is lost because part of the measured information is discarded.

Motivated by the limitations just mentioned, this chapter concentrates on the problem of inherent informational redundancy of vector measurements by considering a new approach, termed the dyad method, as an alternative to the TRIAD method. Unlike the TRIAD method, where both measured vectors are used to determine all three Euler angles, the dyad method allows for the determination of two Euler angles from only one of the measured vectors and then calculates the third angle using the second measured vector. This phenomenon of obtaining partial Euler angle sequence is vital in cases when only one observation vector is available. For example, a magnetometer vector during the eclipse period, sensor failure or even when a co-linearity event occurs. In real applications, using the dyad method can bring significant advantages. For example, the Canadian SCISAT spacecraft is a sun-pointing satellite that experiences an eclipse event once per orbit that lasts for approximately 2200 seconds. During the eclipse event, Sun sensors are not available, resulting in the failure of the TRIAD method. During the initial stages of the SCISAT mission, the main attitude determination sensor, the star tracker, was not tuned appropriately and only 2-axes Sun sensor and 3-axes magnetometer measurements were available to determine satellite attitude. The attitude determination method implemented in the SCISAT satellite is called the small angle hypothesis method. This method is based on considering small turn angles as a vector. The main limitation of this method was that it is applicable only when the Euler angles are in the range of 5 degrees or less.

Spacecraft attitude is determined by obtaining the rotation matrix describing the orientation of a reference frame fixed to the spacecraft with respect to a known reference frame. Since each measured unit vector provides two pieces of information (direction and magnitude), it takes at least two different measurements to determine the three components of attitude. An attitude determination method might use

32

different attitude sensors depending upon the mission [36]. In this work a Sun unit vector $\hat{\mathbf{s}}$ obtained using a Sun sensor and a magnetic field unit vector $\hat{\mathbf{m}}$ obtained from magnetometers is considered.

A sun sensor measures the components of $\hat{\mathbf{s}}$ in the body frame $\mathbf{F}_b$, while the components in the reference frame $\mathbf{F}_r$ are determined using a mathematical model of the Sun's apparent motion relative to the spacecraft. Similarly, a magnetometer measures the components of $\hat{\mathbf{m}}$ in the body frame $\mathbf{F}_b$, with the components in the reference frame $\mathbf{F}_r$ obtained from a mathematical model of the Earth's magnetic field relative to the spacecraft. An attitude determination algorithm is then used to find a rotation matrix $\mathbf{R}_r^b$ such that

$$\hat{\mathbf{s}}_b = \mathbf{R}_r^b \hat{\mathbf{s}}_r$$

$$\hat{\mathbf{m}}_b = \mathbf{R}_r^b \hat{\mathbf{m}}_r \tag{3.1}$$

Consequently, this results in an over determined problem, since there are three unknowns (3 Euler angles) and six known quantities (measured vector projections).

The next section presents problem statement followed by the small angle hypothesis and TRIAD methods in more detail. Then, the following section describes the dyad method. The last section presents simulation results using the dyad method and compares the TRIAD and dyad methods using telemetry data from SCISAT.

3.2 Problem Statement

Given measured sensor vectors and the reference sensor vectors determine the spacecraft attitude using the novel attitude determination method, dyad. Moreover analyze the method using the telemetry data obtained from the Canadian scientific satellite SCISAT. In addition, find partial Euler angles when only one sensor vector information is available for a short period of time. Based on the problem statement the following section discusses the previous work on attitude determination methods.

3.3 Previous Work

In this section, two attitude determination methods are discussed. The first is the small angle hypothesis method and the second is the TRIAD method.

3.3.1 Small Angle Hypothesis

Due to the presence of trigonometric functions in the rotation matrix, equation (3.1) is not linear with respect to the Euler angles, and hence cannot be solved analytically. However, by assuming that the Euler angles are small, the rotation matrix can be represented as follows

$$\mathbf{R}_r^b \approx I + \delta\mathbf{R}_r^b, \tag{3.2}$$

where I is an identity matrix and $\mathbf{R}_r^b$ is a matrix of small rotation angles defined as follows:

$$\delta\mathbf{R}_r^b = \begin{bmatrix} 0 & \alpha_3 & -\alpha_2 \\ -\alpha_3 & 0 & \alpha_1 \\ \alpha_2 & -\alpha_1 & 0 \end{bmatrix}, \tag{3.3}$$

where α_1 represents a angle, α_2 represents pitch angle, α_3 represents yaw angle. It should be noted that it is a well-known fact that, unlike the original matrix R_r^b, the matrix (3.3) stays the same for any rotation order [65]. Combining (3.2), (3.3) and (3.1), one can derive the following relations

$$\delta\hat{s}_1 = \alpha_3\hat{s}_{r2} - \alpha_2\hat{s}_{r3}$$

$$\delta\hat{s}_2 = -\alpha_3\hat{s}_{r1} + \alpha_1\hat{s}_{r3}$$

$$\delta\hat{s}_3 = \alpha_2\hat{s}_{r1} - \alpha_1\hat{s}_{r2} \tag{3.4}$$

$$\delta\hat{m}_1 = \alpha_3\hat{m}_{r2} - \alpha_2\hat{m}_{r3}$$

$$\delta\hat{m}_2 = -\alpha_3\hat{m}_{r1} + \alpha_1\hat{m}_{r3}$$

$$\delta\hat{m}_3 = \alpha_2\hat{m}_{r1} - \alpha_1\hat{m}_{r2}$$

where $\delta\hat{s}_i = \hat{s}_{bi} - \hat{s}_{ri}$ and $\delta\hat{m}_i = \hat{m}_{bi} - \hat{m}_{ri}$, for $i = 1, 2, 3$. As mentioned above, these equations are evidently over-determined with regards to obtaining the attitude.

34

However, if one takes into consideration only one vector, for example $\hat{\mathbf{s}}$, then the problem is under-determined, which reflects an apparent physical fact that any one sensor cannot measure changes in rotation around the measured vector. These under-determined and over-determined problems can be solved by considering one of the vectors as being coincident with the axes of the reference vector. For example, if

$$\hat{\mathbf{s}}_r = \hat{\mathbf{s}} = \begin{bmatrix} 1 \\ 0 \\ 0 \end{bmatrix}, \tag{3.5}$$

then two of three Euler angles (α_2 and α_3) can be solved from the second and third equations of (3.4) as follows

$$\alpha_2 = \delta\hat{\mathbf{s}}_3$$

$$\alpha_3 = -\delta\hat{\mathbf{s}}_2 \tag{3.6}$$

Then the third angle, α_1, can be determined from the fifth or sixth equations of (3.4) as follows

$$\alpha_1 = \frac{1}{\hat{\mathbf{m}}_{r3}}(\delta\hat{\mathbf{m}}_2 + \alpha_3\hat{\mathbf{m}}_{r1}) \tag{3.7}$$

or

$$\alpha_1 = \frac{1}{\hat{\mathbf{m}}_{r2}}(-\delta\hat{\mathbf{m}}_3 + \alpha_2\hat{\mathbf{m}}_{r1}). \tag{3.8}$$

In the above, either vector $\hat{\mathbf{s}}$ or $\hat{\mathbf{m}}$ can be considered as a master vector that contributes two angles in the problem of attitude determination, and the other vector can be considered as the auxiliary vector to get the third angle. In the general case, when Euler angles are not small, the TRIAD method can be implemented to solve (3.1), which is the discussion of next section.

3.3.2 TRIAD Method

The deterministic TRIAD method [41] is based on constructing two triads of orthonormal unit vectors using the vector information available. The two triads are the components of the same coordinate frame expressed in the body and reference frames.
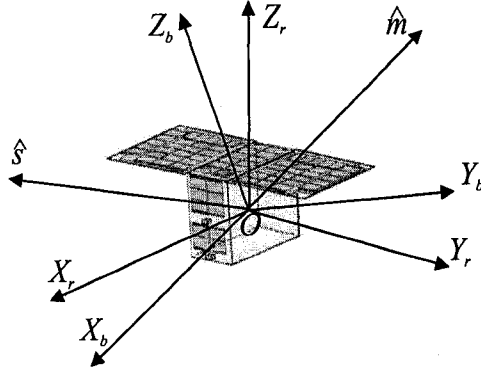
Figure 3.1: Rigid body attitude determination

Let us consider the problem of determining the attitude of the rigid body in Figure 3.1, where F_r is the reference frame and $\mathbf{F}_b$ is the body frame. Consider two position vectors $\hat{\mathbf{s}}$ and $\hat{\mathbf{m}}$. These vectors can be expressed in the body frame $\mathbf{F}_b(X_b, Y_b, Z_b)$ as $\mathbf{s}_b$ and $\mathbf{m}_b$, or they can be expressed in some reference frame $\mathbf{F}_r(X_r, Y_r, Z_r)$ as $\mathbf{s}_r$ and $\mathbf{m}_r$. An orthogonal coordinate system with basis vectors $\hat{\mathbf{q}}$, $\hat{\mathbf{r}}$, $\hat{\mathbf{t}}$ can then be constructed as follows [74]. In what follows, the Sun unit vector $\hat{\mathbf{s}}$ will be chosen as the master vector. The first basis vector, $\hat{\mathbf{q}}$, is chosen to coincide with the master vector as

$$\hat{\mathbf{q}} = \hat{\mathbf{s}} \tag{3.9}$$

$$\hat{\mathbf{q}}_b = \hat{\mathbf{s}}_b$$

$$\hat{\mathbf{q}}_r = \hat{\mathbf{s}}_r$$

The second basis vector, $\hat{\mathbf{r}}$, is then constructed such that it is perpendicular to the two observations $\hat{\mathbf{s}}$ and $\hat{\mathbf{m}}$, and is written as

$$\hat{\mathbf{r}} = \frac{\hat{\mathbf{s}} \times \hat{\mathbf{m}}}{|\hat{\mathbf{s}} \times \hat{\mathbf{m}}|} \tag{3.10}$$

$$\hat{\mathbf{r}}_b = \frac{\hat{\mathbf{s}}_b \times \hat{\mathbf{m}}_b}{|\hat{\mathbf{s}}_b \times \hat{\mathbf{m}}_b|}$$

$$\hat{\mathbf{r}}_r = \frac{\hat{\mathbf{s}}_r \times \hat{\mathbf{m}}_r}{|\hat{\mathbf{s}}_r \times \hat{\mathbf{m}}_r|}$$

36

The third basis vector, $\hat{\mathbf{t}}$, is then chosen to complete the triad:

$$\hat{\mathbf{t}} = \hat{\mathbf{q}} \times \hat{\mathbf{r}} \tag{3.11}$$

$$\hat{\mathbf{t}}_b = \hat{\mathbf{q}}_b \times \hat{\mathbf{r}}_b$$

$$\hat{\mathbf{t}}_r = \hat{\mathbf{q}}_r \times \hat{\mathbf{r}}_r$$

The direction cosine matrix $\mathbf{R}_r^b$ that defines the attitude of the body frame with respect to the reference frame is determined according to

$$\mathbf{R}_r^b = \begin{bmatrix} \hat{\mathbf{q}}_b & \hat{\mathbf{r}}_b & \hat{\mathbf{t}}_b \end{bmatrix} \begin{bmatrix} \hat{\mathbf{q}}_r & \hat{\mathbf{r}}_r & \hat{\mathbf{t}}_r \end{bmatrix}^T . \tag{3.12}$$

Equation (3.12) completes the TRIAD algorithm. However, it is usually desirable to obtain the three Euler angles (roll, pitch and yaw) for a conventional 3-axes attitude control system. Considering a $z - y - x$ rotation sequence as described in [74] then the matrix $\mathbf{R}_r^b$ can be expressed through Euler angles as [65]

$$\mathbf{R}_r^b = \begin{bmatrix} \cos\theta\cos\psi & \sin\phi\sin\theta\cos\psi + \cos\phi\sin\psi & -\cos\phi\sin\theta\cos\psi + \sin\phi\sin\psi \\ -\cos\theta\sin\psi & -\sin\phi\sin\theta\sin\psi + \cos\phi\cos\psi & \cos\phi\sin\theta\sin\psi + \sin\phi\cos\psi \\ \sin\theta & -\sin\phi\cos\theta & \cos\phi\cos\theta \end{bmatrix} , \tag{3.13}$$

where ϕ is the roll angle, θ is the pitch angle and ψ is the yaw angle. Then the Euler angles can be computed with the following formulas:

$$\phi = -\tan^{-1}\left(\frac{\mathbf{R}_{r_{32}}^b}{\mathbf{R}_{r_{33}}^b}\right) \tag{3.14}$$

$$\theta = \sin^{-1}\mathbf{R}_{r_{31}}^b$$

$$\psi = -\tan^{-1}\left(\frac{\mathbf{R}_{r_{21}}^b}{\mathbf{R}_{r_{11}}^b}\right)$$

where $\mathbf{R}_{r_{ij}}^b$, $i, j = 1, 2, 3$, corresponds to the elements in (3.13). It can be seen from (3.13) and (3.14) that when $\theta = 90°$ (*i.e.*, gimbal mechanism folding), two angles ϕ and ψ become uncertain. The problem of using TRIAD algorithm appears when either the master or the auxiliary vector cannot be measured or when they are parallel.

In the first case, the TRIAD method can be used only by assuming $\mathbf{s}_m = \mathbf{s}_r$ (if $\mathbf{s}_m$ is not available) or $\mathbf{m}_m = \mathbf{m}_r$ (if $\mathbf{m}_m$ is not available). It is clear that all three

Euler angles determined with the TRIAD method are dependent on both vectors **s** and **m** (only in the case when **s** and **m** are mutually perpendicular, two angles derived from the master vector **s** are independent of the third one, derived from the auxiliary vector **m**). So if there is any significant change in actual satellite attitude, the hypothesis of equality between measured and referenced vectors will affect all 3 Euler angles.

In the second case, where both vectors are almost parallel to each other, an assumption can be made that the auxiliary vector $\mathbf{m}_m = \mathbf{m}_r$, where $\mathbf{m}_r = 1$ and is perpendicular to $\mathbf{s}_r$. Then two angles determined with the master vector **s** will not be dependent on the third. They can be used and the third can be ignored. The above described cases can be solved directly with the dyad algorithm without the assumption made and is a topic of discussion in the next section. This fact allows one to choose a special reference frame where one of its axes, the first rotation axis, always coincides with one of the reference vectors. This vector can be considered as the master vector that contributes two angles in the problem of attitude determination and another vector can be considered as the auxiliary vector to get the third angle. This procedure can be repeated twice with vector $\hat{\mathbf{s}}$ and with vector $\hat{\mathbf{m}}$. The option of choosing $\hat{\mathbf{s}}$ or $\hat{\mathbf{m}}$ vectors as the master vector can be considered as a vectors dualism problem. Also it can be shown that the vector that is close to the desired frame outperforms the other vector. This approach is used to extend the TRIAD method, taking advantage of its inherent informational redundancy for three Euler angles attitude determination. This is discussed in the next section.

3.4 Dyad Method

The TRIAD method briefly described above presumes that two vectors are available and measured continuously at the same time. However, in practical situations when environmental obstacles occur or in the event of temporary sensor failure, this method cannot be used. This has led to the development of a novel attitude determination method called the dyad method [33]. The method considered in this section can be
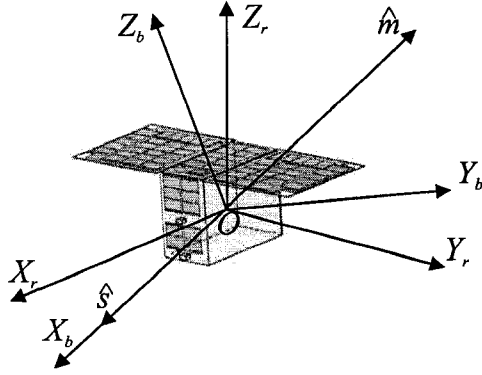
Figure 3.2: Dyad attitude determination

used independently or in combination with the TRIAD method. The advantages of this method are studied in this section and demonstrated with experimental telemetry data from the Canadian scientific satellite SCISAT.

Consider a reference frame $\mathbf{F}_r$, as shown in Figure 3.2, where the vector $\hat{s}$ is aligned with the X_r axis. Vector $\hat{s}$ here is called the master vector. The components of vector $\hat{s}$, resolved in the reference frame, are given by

$$\hat{s}_r = \begin{bmatrix} 1 \\ 0 \\ 0 \end{bmatrix}. \tag{3.15}$$

Using equation (3.13), the projection of $\hat{s}$ onto the body frame can be written as

$$\hat{s}_b = \mathbf{R}_r^b \hat{s}_r, \tag{3.16}$$

which results in

$$\hat{s}_{b_x} = \cos\theta\cos\psi$$

$$\hat{s}_{b_y} = -\cos\theta\sin\psi \tag{3.17}$$

$$\hat{s}_{b_z} = \sin\theta$$

39

From equation (3.17), one can obtain a simple set of trigonometric relations to determine the two Euler angles, the pitch angle θ and the yaw angle ψ, as follows

$$\sin \theta_s = \hat{s}_{b_z}$$

$$\tan \psi_s = -\frac{\hat{s}_{b_y}}{\hat{s}_{b_x}} \tag{3.18}$$

The subscript s on the pitch and yaw angles is used to indicate that these angles have been determined with respect to the reference frame attached to the $\hat{s}$ vector. To determine the roll angle ϕ_{sm} with respect to the reference frame attached to the $\hat{s}$ vector and using the auxiliary vector $\hat{m}$, the following approach is proposed.

Using a $x - y - z$ rotation sequence, described in [74] the relation between the components of vector $\hat{m}$ in the body and reference frames can be written as

$$\hat{m}_b = \mathbf{R}_r^b(\phi_{sm}, \theta_s, \psi_s)\hat{m}_r = R_z(\phi_{sm})R_y(\theta_s)R_x(\psi_s)\hat{m}_r. \tag{3.19}$$

Thus, rearranging this expression yields

$$\hat{m}_{b_s} = R_y^T(\theta_s)R_z^T(\psi_s)\hat{m}_b = R_x(\phi_{sm})\hat{m}_r, \tag{3.20}$$

where principal rotation matrices $R_x(\phi_{sm})$, $R_y(\theta_s)$ and $R_z(\psi_s)$ are defined in [74]. This last expression yields

$$\begin{bmatrix} \hat{m}_{b_{sx}} \\ \hat{m}_{b_{sy}} \\ \hat{m}_{b_{sz}} \end{bmatrix} = \begin{bmatrix} 1 & 0 & 0 \\ 0 & \cos \phi_{sm} & \sin \phi_{sm} \\ 0 & -\sin \phi_{sm} & \cos \phi_{sm} \end{bmatrix} \begin{bmatrix} \hat{m}_{r_x} \\ \hat{m}_{r_y} \\ \hat{m}_{r_z} \end{bmatrix}. \tag{3.21}$$

Expanding the last two lines in the matrix of equation (3.21) yields

$$\hat{m}_{b_y} = \hat{m}_{r_y} \cos \phi_{sm} + \hat{m}_{r_z} \sin \phi_{sm}$$

$$\hat{m}_{b_z} = -\hat{m}_{r_y} \sin \phi_{sm} + \hat{m}_{r_z} \cos \phi_{sm} \tag{3.22}$$

From the first equation of (3.22), $\cos(\phi_{sm})$ is obtained as

$$\cos \phi_{sm} = \frac{\hat{m}_{b_y} - \hat{m}_{r_z} \sin \phi_{sm}}{\hat{m}_{r_y}}. \tag{3.23}$$

Substituting (3.23) into the second equation of (3.22) gives

$$\hat{m}_{b_z} = -\hat{m}_{r_y} \sin \phi_{sm} + \hat{m}_{r_z} \frac{\hat{m}_{b_y} - \hat{m}_{r_z} \sin \phi_{sm}}{\hat{m}_{r_y}}. \tag{3.24}$$

40

Rearranging terms, an expression for $\sin(\phi_{sm})$ is obtained as

$$\sin\phi_{sm} = \frac{\hat{m}_{r_z}\hat{m}_{b_y} - \hat{m}_{b_z}\hat{m}_{r_y}}{\hat{m}_{r_y}^2 + \hat{m}_{r_z}^2}. \tag{3.25}$$

Following the same approach, an equation for $\cos(\phi_{sm})$ follows

$$\cos\phi_{sm} = \frac{\hat{m}_{r_y}\hat{m}_{b_y} + \hat{m}_{b_z}\hat{m}_{r_z}}{\hat{m}_{r_y}^2 + \hat{m}_{r_z}^2}. \tag{3.26}$$

Dividing equation (3.25) by (3.26), $\tan\phi_{sm}$ is

$$\tan\phi_{sm} = \frac{\hat{m}_{r_z}\hat{m}_{b_y} - \hat{m}_{r_y}\hat{m}_{b_z}}{\hat{m}_{b_y}\hat{m}_{r_y} + \hat{m}_{b_z}\hat{m}_{r_z}}. \tag{3.27}$$

In the situation considered above, $\hat{s}$ was used as the master vector and $\hat{m}$ as the auxiliary vector. A similar approach can be applied using $\hat{m}$ as the master vector and $\hat{s}$ as the auxiliary vector. An additional set of Euler angles, denoted by ϕ_{ms}, θ_m and ψ_m, can be found in this way. Note that it is not necessary for the reference frame to coincide with the desired frame of attitude determination. Indeed, if the transformation matrix $\mathbf{R}_r^d$ between the reference frame and the desired attitude determination frame is known, then the matrix $\mathbf{R}_b^d$ between the body frame and the desired frame can be derived by using the formula

$$\mathbf{R}_b^d = \mathbf{R}_r^d \mathbf{R}_b^r \tag{3.28}$$

The dyad method presented here is more flexible in comparison with the TRIAD method. Either $\hat{s}$ or $\hat{m}$ can be chosen as the master vector, and a set of Euler angles can be obtained for each case (i.e., one set using s as the master and another set using m as the master). It can be seen that the dyad method still uses two vector measurements to determine the three Euler angles. However, in the absence of one vector measurement, while the TRIAD method fails completely (i.e., it is unable to determine any Euler angles) the dyad method is able to determine two Euler angles. This represents a significant advantage in many situations. In practice, with two Euler angles determined, spacecraft operators can at least determine the bounds of the third Euler angle using techniques such as gyrocompassing. This technique is beyond the scope of the thesis and will not be discussed. Simulation results from the specially developed simulator and the telemetry data obtained from the Canadian satellite SCISAT-1 are discussed in the next section.

41

3.5 Simulation Results

The dyad method is verified using the attitude determination simulator Appendix C. The simulator allows for simulating a free rigid body rotating in inertial space and to determine its attitude by two vector-measuring devices based on attitude determination methods (TRIAD and Dyad methods). The proposed approach is first evaluated using the mathematical model and then verified using the telemetry data provided by the Canadian scientific satellite SCISAT. In the model it is chosen that the desired frame of attitude determination is Sun reference frame. The two sensors used in the attitude determination method are two-axes Sun sensor and three-axis magnetometer. The vectors of these sensors are simulated on ground and are shown in the following graphs. In Figure 3.3 the magnetic field measured vector can be seen while in Figure 3.4, the magnetic field reference vector is shown. In the x-axis, time is shown and in the y-axis magnetic field vector measured in nano Tesla (nT) is shown. These vectors are obtained from the IGRF model [74] of 10-th order and measured magnetic field vector-by transformation of reference vector into satellite body frame with known directional cosine matrix. The measured Sun vector is shown in Figure 3.5 and the reference Sun vector in Figure 3.6. The Sun reference vector is obtained by knowing the position of the satellite in the orbit. For example, to obtain the direction to the Sun in the inertial frame, current time expressed in Julian date [72] is required. Based on the vector information Figures (3.3,3.4,3.5,3.6), the attitude is determined using the TRIAD and the dyad methods. It is seen from the figure that during the eclipse period, $0 - 1800$ seconds, there is no signal from Sun sensor. Based on this vector information the attitude is determined using the TRIAD and the dyad methods. The Sun sensor is chosen as the master sensor, but the magnetometer can also be chosen.
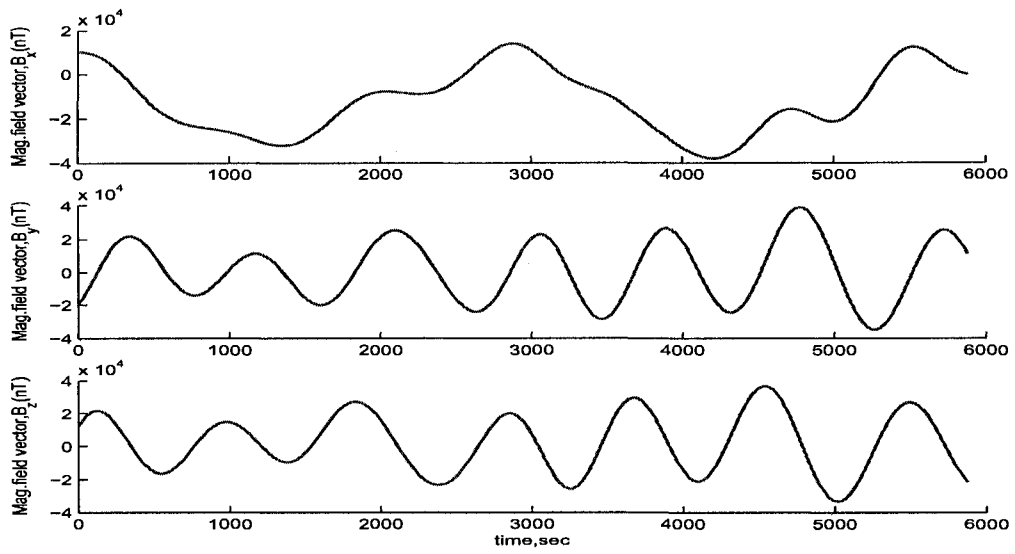
Figure 3.3: Measured magnetic vector
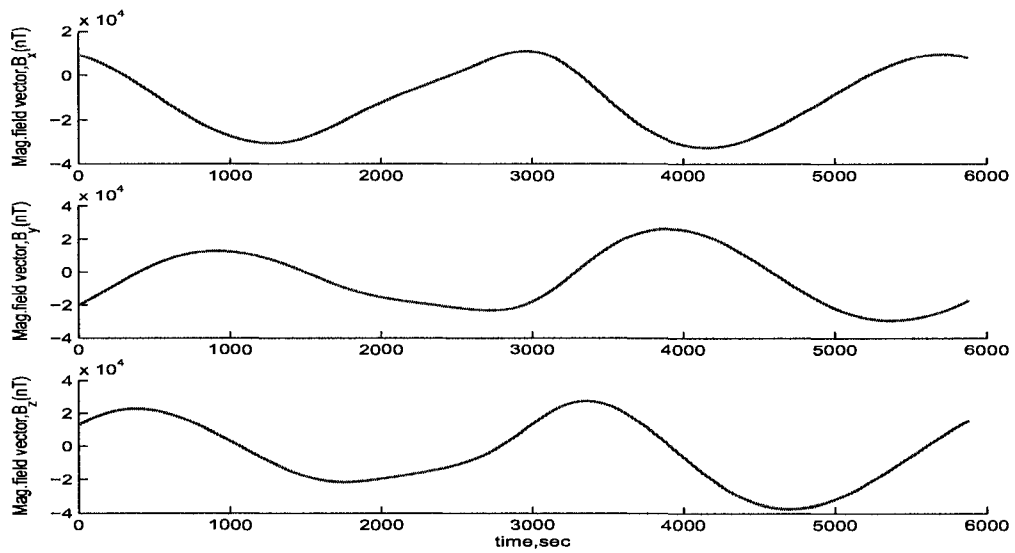
Figure 3.4: Reference magnetic vector

43
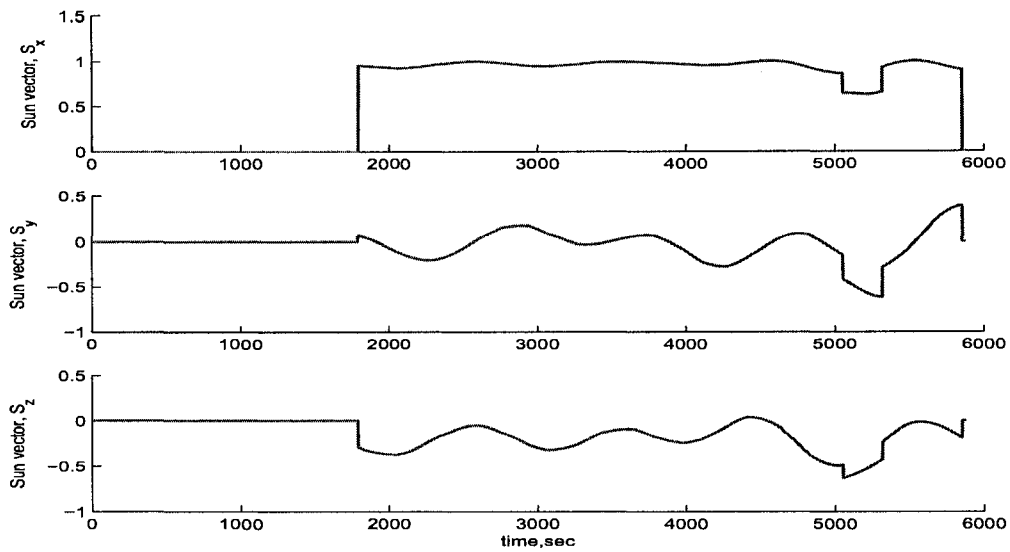
Figure 3.5: Measured Sun vector
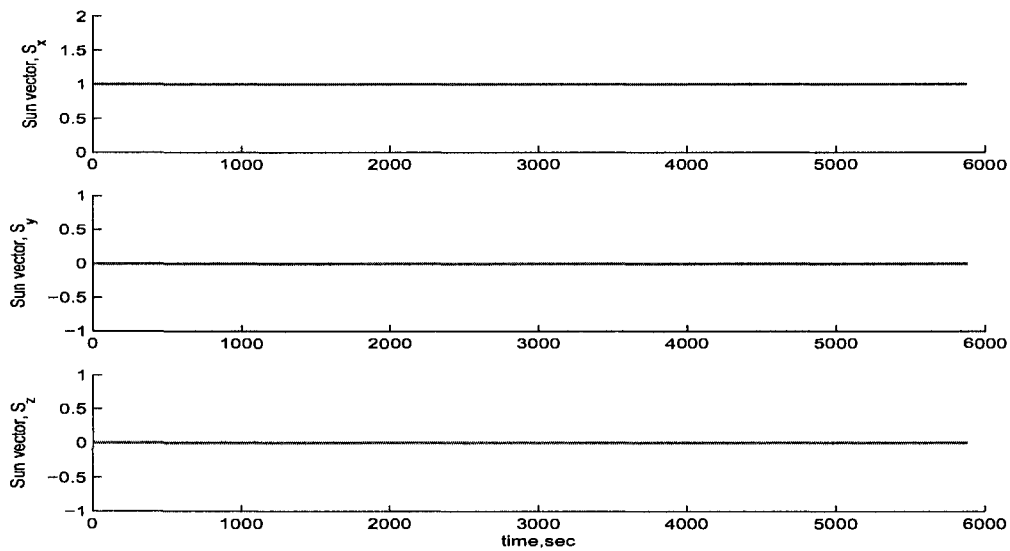
Figure 3.6: Reference Sun vector

In Figure 3.7, the attitude is obtained using the TRIAD algorithm. The x-axis and the y-axis in Figure 3.7 are time and degrees respectively. It is observed that there is no attitude information during the eclipse period and all the angles are equal to zero. However, Figure 3.8 does reveal attitude information about roll angle during the eclipse period. In this figure the attitude is obtained using the dyad method. The

comparison of both methods is shown in Figure 3.9 and clearly the dyad and TRIAD methods perform identically outside the eclipse period while only dyad algorithm outputs roll during the eclipse period. In Figure 3.9, the roll angle error is displayed. The roll angle error is obtained from the roll angle determined using dyad method and the true roll angle.
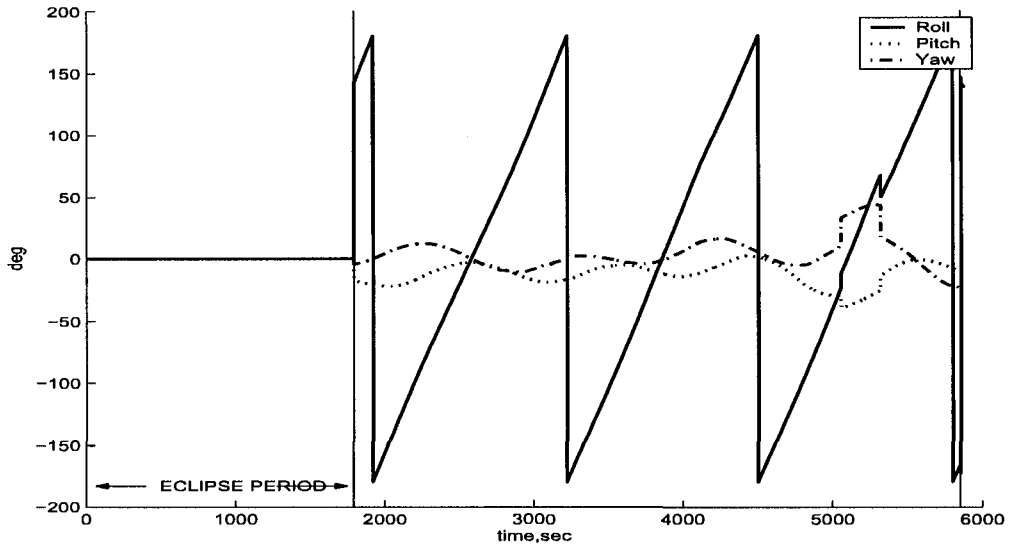
Figure 3.7: Euler angles obtained using TRIAD
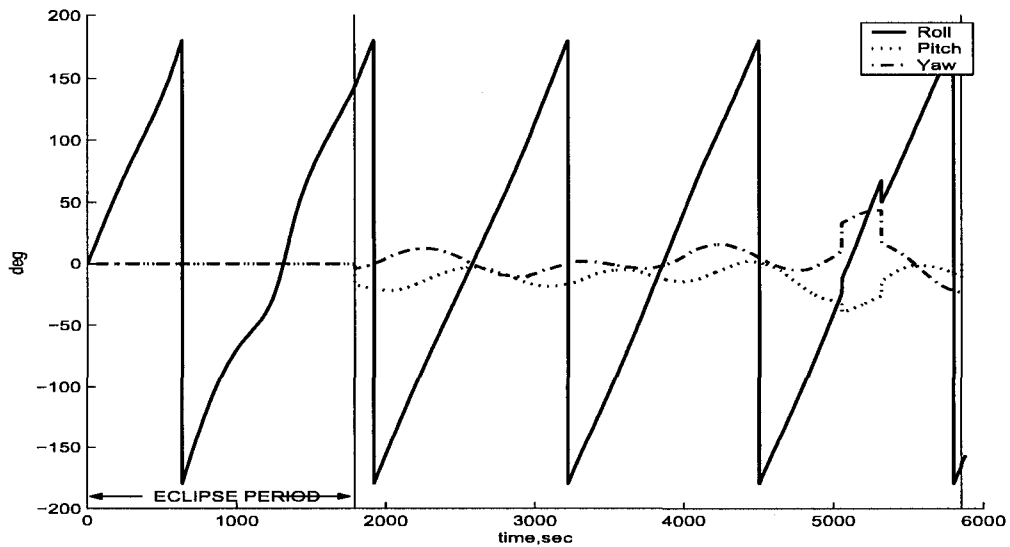
Figure 3.8: Euler angles using dyad

45
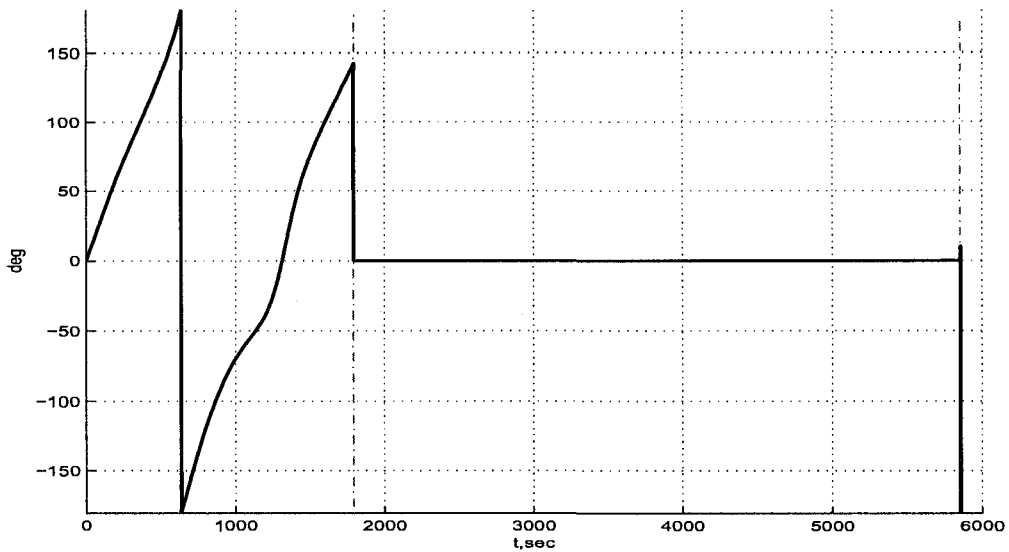
Figure 3.9: Comparison of roll angle error using TRIAD and dyad

It could be possible to switch the vectors and consider $\hat{m}$ vector as the master vector during eclipse with the dyad method, obtaining pitch and yaw angles instead of the roll from the magnetometer. However, SCISAT is not required to have continuous positional control in the pitch and yaw axes. Due to this fact, the satellite is gyro-stabilized in pitch and yaw because the satellite is continuously rotating in roll. Hence, it was preferred to keep continuous control in roll from the magnetometer. Attitude determination also includes the evaluation of the telemetry from various onboard attitude sensors for any sign of physical deterioration, improper configuration, or changes in calibration or alignment. To validate the proposed method and the simulator, telemetry data was used from the Canadian scientific satellite SCISAT. In this scenario, the reference frame is taken to be the Sun frame, and the sensors involved are the magnetometer and the Sun sensors. The measured magnetic vector from the telemetry is shown in Figure 3.10 and the magnetic reference vector is shown in Figure 3.11. The measured sun vector from telemetry is shown in Figure 3.12. The Sun reference vector is assumed to be $[1\ 0\ 0]^T$ and is shown in Figure 3.13. These vectors (Figures 3.10,3.11,3.12,3.13) are processed on the ground to obtain the satellite attitude using the TRIAD and dyad method. The simulations are performed

46

for 4 orbits. Time taken to complete one orbit is 98 minutes.
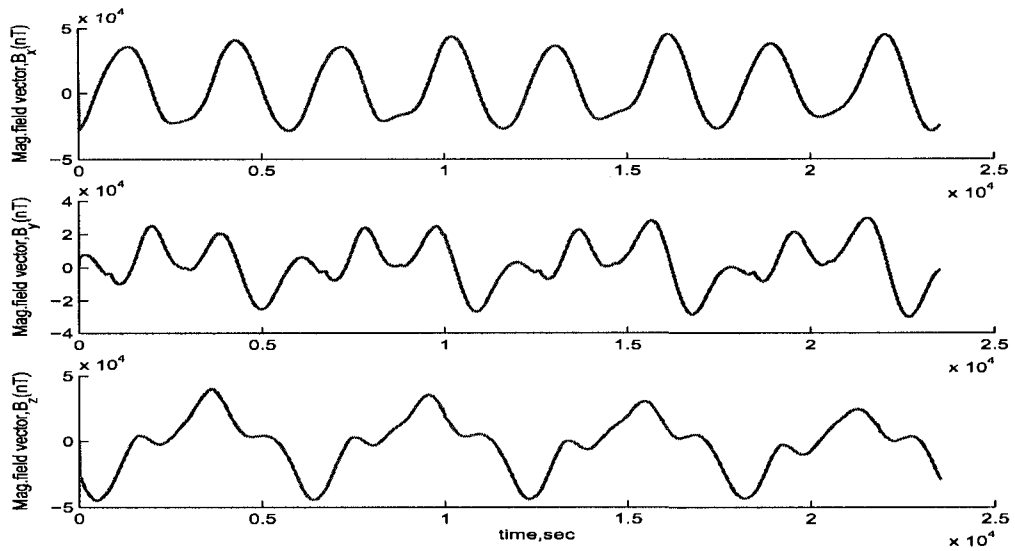
Figure 3.10: Measured magnetic vector from telemetry
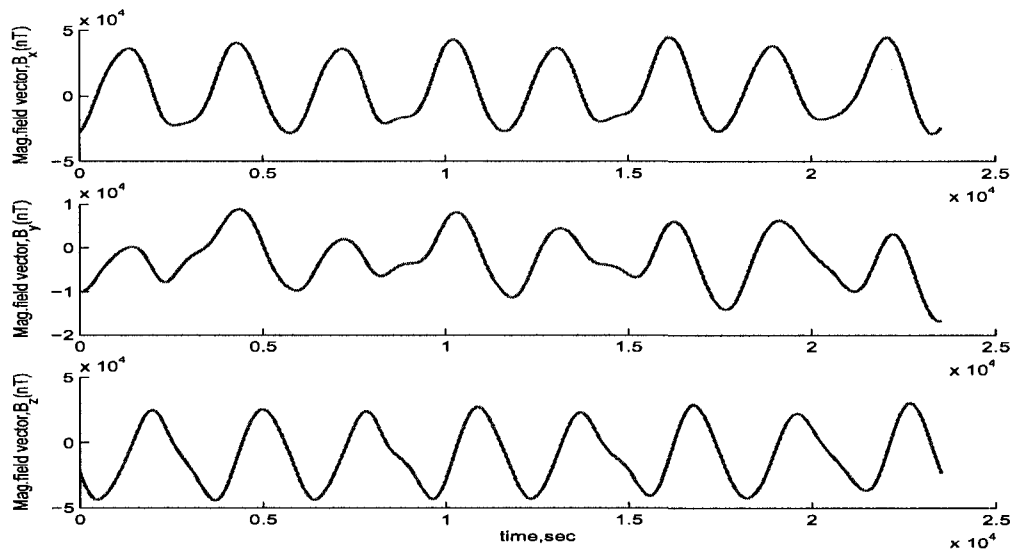
Figure 3.11: Reference magnetic vector from telemetry
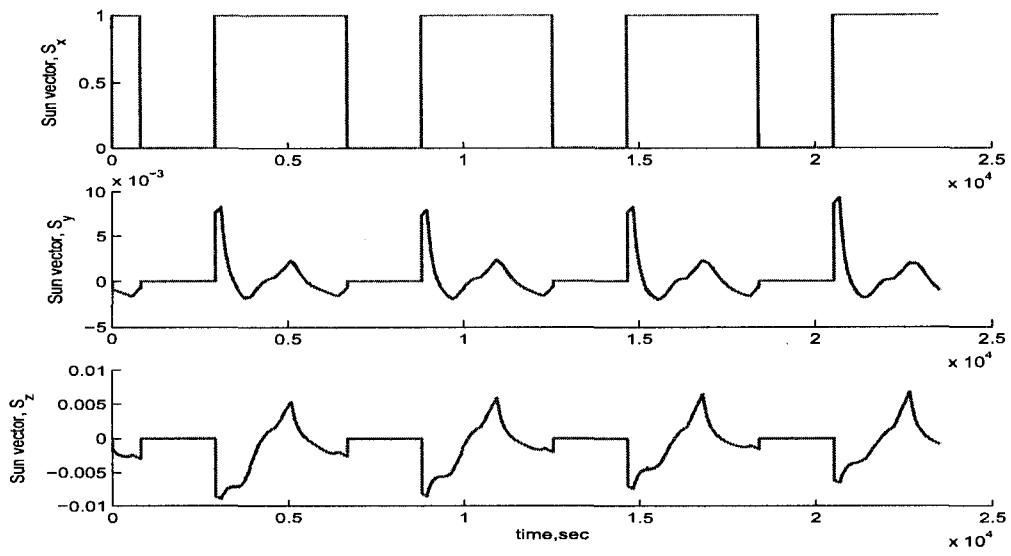
Figure 3.12: Measured Sun vector from telemetry
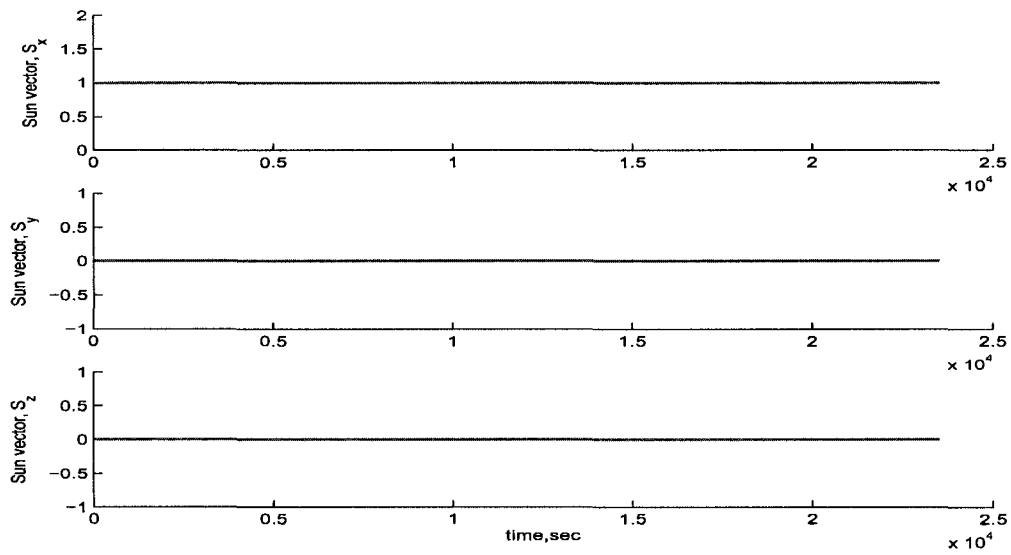
Figure 3.13: Reference Sun vector from telemetry
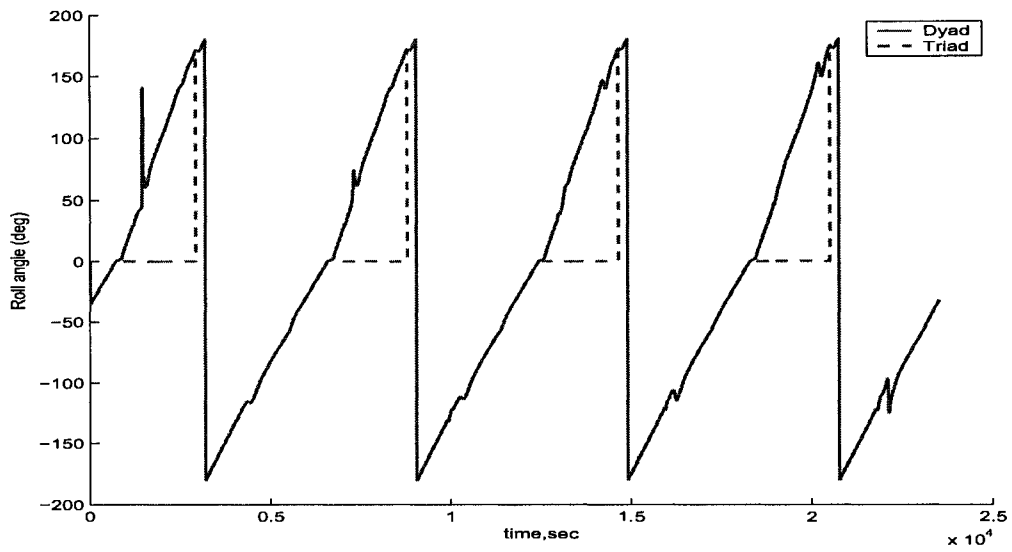
Figure 3.14: Comparison of roll angle using TRIAD and dyad
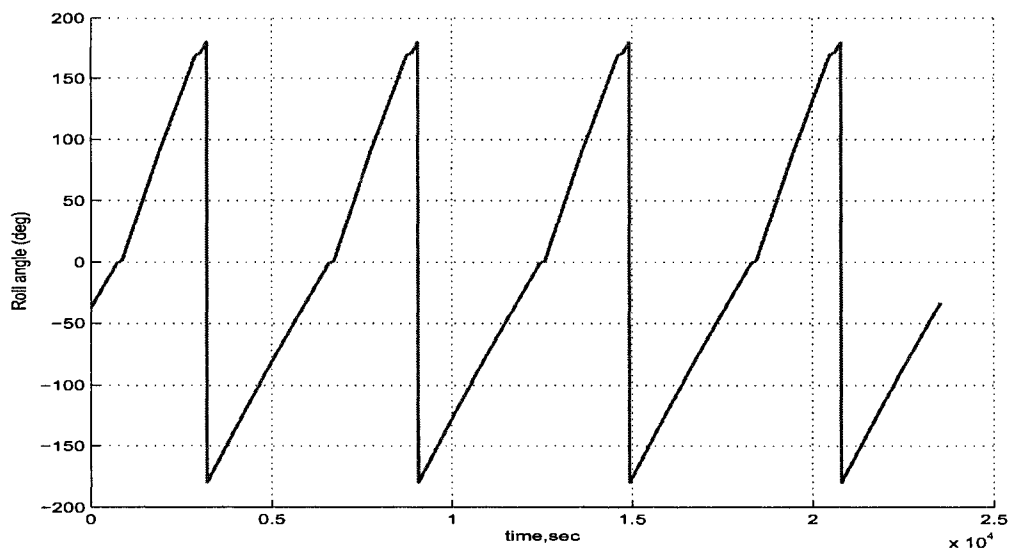
Figure 3.15: Roll angle obtained using startracker
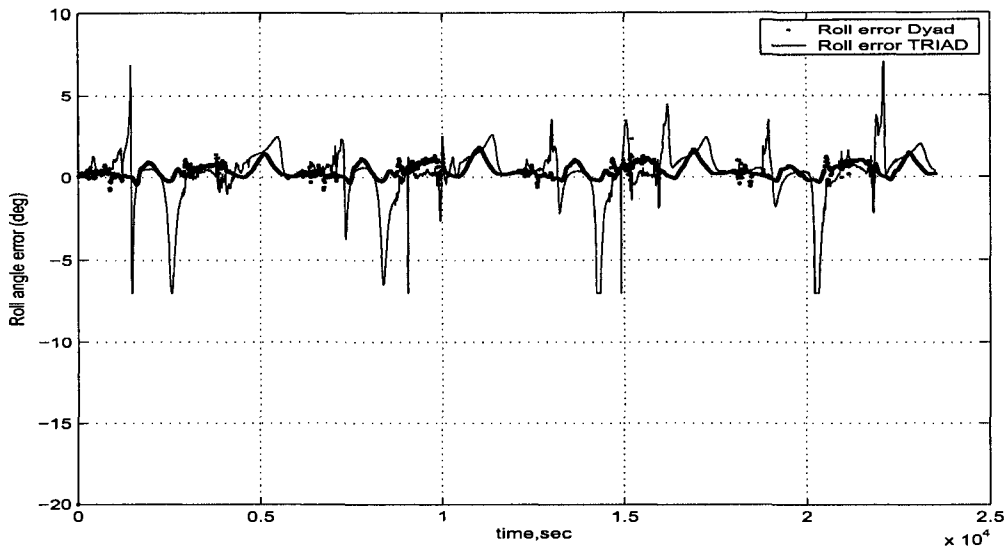
Figure 3.16: Comparison of roll angle error using TRIAD and dyad
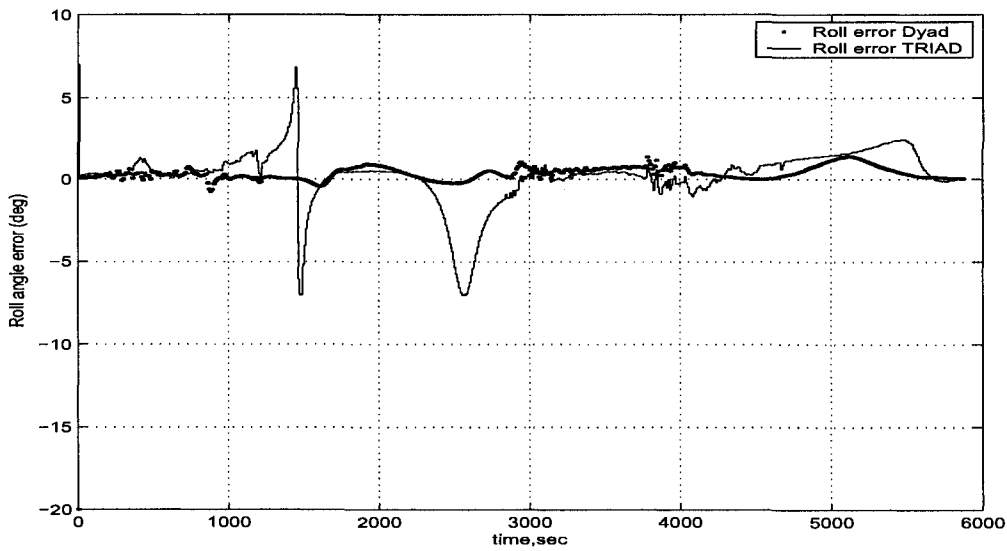
Figure 3.17: Comparison of roll angle error using TRIAD and dyad for one orbit

In Figure 3.14, the comparison of the roll angle using TRIAD and dyad is presented. The dashed line represents the roll angle obtained when the TRIAD method is implemented and the thick line represents the dyad method. It can be viewed from the figure, that during the eclipse period (810-2930 seconds), there is no attitude measurement, when TRIAD method is implemented. In Figure 3.16

50

comparison on roll error using TRIAD and dyad is presented. In this scenario it was assumed that during the eclipse period, when there is no measured Sun vector, the reference sun vector is equal to the measured vector $\hat{s}_r = \hat{s}_m$. By assuming that the Sun reference vector and measured vector are same, the TRIAD method can be implemented. However, when compared to the dyad method with no assumptions, it was observed from Figure 3.16, that the roll error during the eclipse period for the TRIAD method is larger when compared to the dyad method. In Figure 3.17, the simulations are executed for only one orbit to illustrate the error in greater details. The roll error is the difference between the roll obtained using on-board star tracker, Figure 3.15 and the roll obtained using the dyad and TRIAD method. The roll error shown in the figure is only for one orbit which is 98 minutes. From the Figure 3.17 it is observed that the roll error using the TRIAD method is larger, 7 $^\circ$ during the eclipse period, whereas the roll error is less than 1° using the dyad method.

3.6 Chapter Summary

In this chapter, a novel attitude determination method, called the dyad method, was analyzed and verified. It was shown through numerical simulation and verified with experimental data that the dyad method is very effective. During the loss of sensor information the TRIAD method is not valid whereas dyad method at least gives two angles. In practice, with two Euler angles determined, spacecraft operators can at least determine the bounds of the third Euler angle using techniques such as gyrocompassing. The dyad method is therefore recommended for implementation in modern satellite ACS design to determine single-frame (i.e. non-sequential) attitude estimates. For high complexity spacecraft where there is a freedom for more computational power other methods such as stochastic algorithms, should be used which is the topic of next chapter.

51

Chapter 4

ATTITUDE ESTIMATION

In the previous chapter, attitude determination was performed using a deterministic method. This chapter addresses the problem of satellite attitude estimation by developing a multipurpose Ground-Based Attitude Estimator(GBAE). If appropriately designed, such a ground-based attitude estimator is a powerful tool that can be used for satellite attitude control system performance evaluation, as well as for system calibration. In addition, the proposed attitude estimator can be considered as an on-ground prototype for newly developed optimal attitude estimation methods and algorithms for future implementations on board. Developing the attitude estimator is a complicated scientific-engineering problem that requires accurate system modelling and adequate assumptions enabling the application of powerful estimation theory. The main contributions in this chapter are two-fold. First, a modified Kalman filter is applied to satellite attitude estimation in pointing mode. Second, a novel attitude estimation method is developed using guaranteed ellipsoidal estimation theory for acquisition method.

4.1 Attitude Estimation using Modified Kalman Filter

A traditional ground-based attitude estimator used in satellite operation practice for performance evolution solves the estimation problem by processing the telemetry data information in a Kalman filter [37] as shown in Figure 4.1.
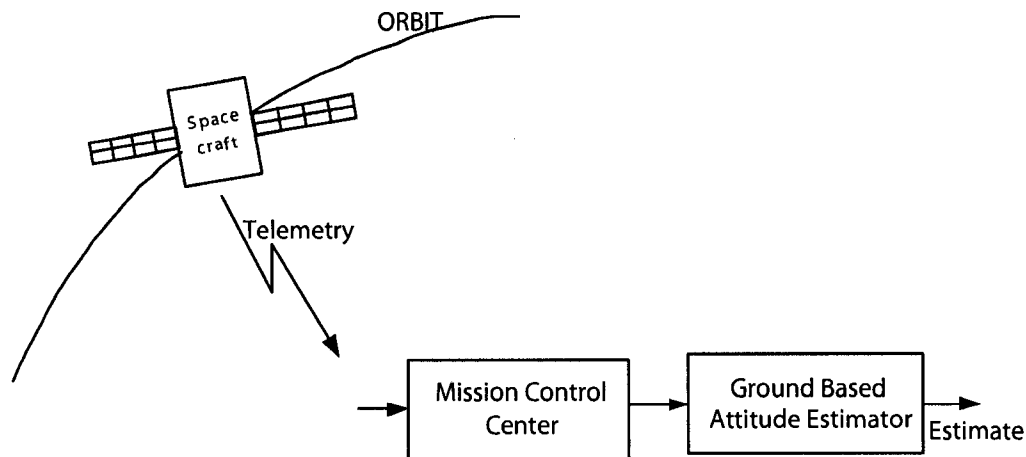
Figure 4.1: Attitude estimator

Recently, Iwata [24] and Montel [46] used an extended Kalman filter for their work on ground-based attitude estimation. Attitude sensors providing the data to the mission control center through telemetry are often involved in the closed-loop attitude control system, shown in Figure 4.2, resulting in the correlation of measurement noise and process noise. Therefore, in this section, a modified Kalman filter is proposed for processing the satellite telemetry data, that accounts for this correlation. Designing a modified Kalman filter relies on the availability of an accurate spacecraft dynamic model, which will be discussed in the next subsection
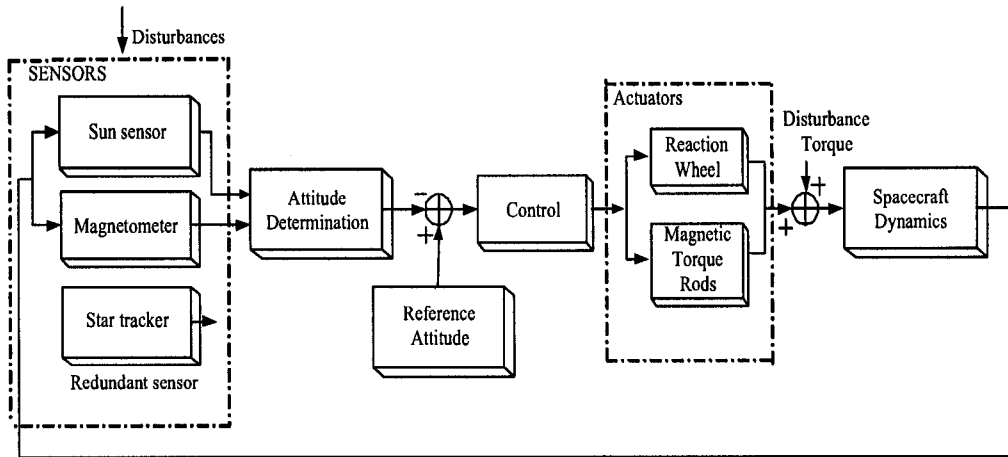
Figure 4.2: Attitude determination and control system

4.1.1 Spacecraft Angular Motion Model

In this subsection, a spacecraft attitude dynamic model will be developed. The spacecraft will be considered to be a rigid body. Although no spacecraft is perfectly rigid, considering rigid body motion is a good approximation for studying spacecraft attitude dynamics. The attitude dynamic equations are given by Newton-Euler's moment equations [30] and are written as

$$\mathbf{T} = \dot{\mathbf{H}} + \boldsymbol{\omega} \times \mathbf{H}, \tag{4.1}$$

where $\mathbf{H} = I\boldsymbol{\omega}$ is the total angular momentum, I is the inertia, $\mathbf{T}$ is the total torque acting on the body and $\boldsymbol{\omega}$ is the angular velocity of the satellite. The total torque is divided into two principal parts [74]: $\mathbf{T}_c$, the control input torques and $\mathbf{T}_d$, the torque due to environmental disturbances. Thus the total torque can be written as

$$\mathbf{T} = \mathbf{T}_c + \mathbf{T}_d. \tag{4.2}$$

Throughout this chapter, the disturbance torque is modeled as a stochastic process and is appended to the plant state model. The objective behind this is to estimate the disturbances using the obtained telemetry data from the ground. The state equation for the disturbance torque is written as

$$\dot{T}_d = w_{T_d}, \tag{4.3}$$

54

where w_{T_d} is white noise. The total angular momentum **H** in equation (4.1) is the sum of the momentum of the satellite, $\mathbf{H}_s$, and the momentum of momentum exchange devices rotating bodies inside a satellite [65] $\mathbf{H}_\omega$ and written as

$$\mathbf{H} = \mathbf{H}_s + \mathbf{H}_\omega. \tag{4.4}$$

By substituting equation (4.4) into (4.1), the spacecraft nonlinear dynamic equation with one momentum wheel aligned along each of the three axes can be written as

$$\dot{H}_x + \dot{H}_{\omega x} + \omega_y H_z - \omega_z H_y + \omega_y H_{\omega z} - \omega_z H_{\omega y} = T_x$$

$$\dot{H}_y + \dot{H}_{\omega y} + \omega_z H_x - \omega_x H_z + \omega_z H_{\omega x} - \omega_x H_{\omega z} = T_y \tag{4.5}$$

$$\dot{H}_z + \dot{H}_{\omega z} + \omega_x H_y - \omega_y H_x + \omega_x H_{\omega y} - \omega_y H_{\omega x} = T_z$$

$$\tag{4.6}$$

where $\omega_x, \omega_y, \omega_z$ are the projections of the absolute angular velocity vector of the spacecraft, H_x, H_y, H_z are the moments of inertia about the x, y, z principal axes of the coordinate system. $H_{\omega x}$, $H_{\omega y}, H_{\omega z}$ are the angular momentum of the momentum wheels, and T_x, T_y, T_z are the components of the total torque applied to the spacecraft body with respect to its center of mass. To simplify the nonlinear spacecraft model (4.5), the following assumptions are used:

1. The satellite is spinning about its x-axis which is an axis of symmetry.

2. A single momentum wheel aligned along the x-axis.

Using these assumptions, the spinning spacecraft nonlinear dynamics can be written as

$$I_x \dot{\omega}_x = -\dot{H}_{wx} + T_x$$

$$I_y \dot{\omega}_y + (I_x - I_z)\omega_x \omega_z + H_{wx}\omega_z = T_y \tag{4.7}$$

$$I_z \dot{\omega}_z + (I_y - I_x)\omega_x \omega_y - H_{wx}\omega_y = T_z.$$

The angular velocities ω_x, ω_y, ω_z may be described in relation to three Euler angles. The Euler angles are represented as ϕ, the roll angle about the x-axis , θ, the pitch

angle about the y-axis and ψ, the yaw angle about the z-axis. The angular velocities for the transformation $x - y - z$ are

$$\omega_x = \dot{\phi}\cos\theta\cos\psi + \dot{\theta}\sin\psi$$

$$\omega_y = \dot{\theta}\cos\psi - \dot{\phi}\cos\theta\sin\psi \qquad (4.8)$$

$$\omega_z = \dot{\phi}\sin\theta + \dot{\psi}.$$

Equations (4.7) and form the entire nonlinear satellite model.

The objective in this section is to consider the ground-based satellite attitude estimator in the pointing mode [65] of the mission, when attitude errors do not usually exceed a few degrees of maximum deviation from the desired orientation. Thus, it is natural and reasonable to use a set of linearized model equations for estimation purposes. Equations (4.7) and (4.8) can be linearized with respect to the undisturbed equilibrium provided at zero attitude in the Sun frame. This is the desired orientation of the body frame F_b. The Sun-pointing frame [65] is used to define the spacecraft attitude with respect to the Sun frame F_s. Figure 4.3 shows the satellite with the Sun frame X_s, Y_s, Z_s and body frame X_b, Y_b, Z_b is shown. The frames are explained explicitly in Chapter 2.
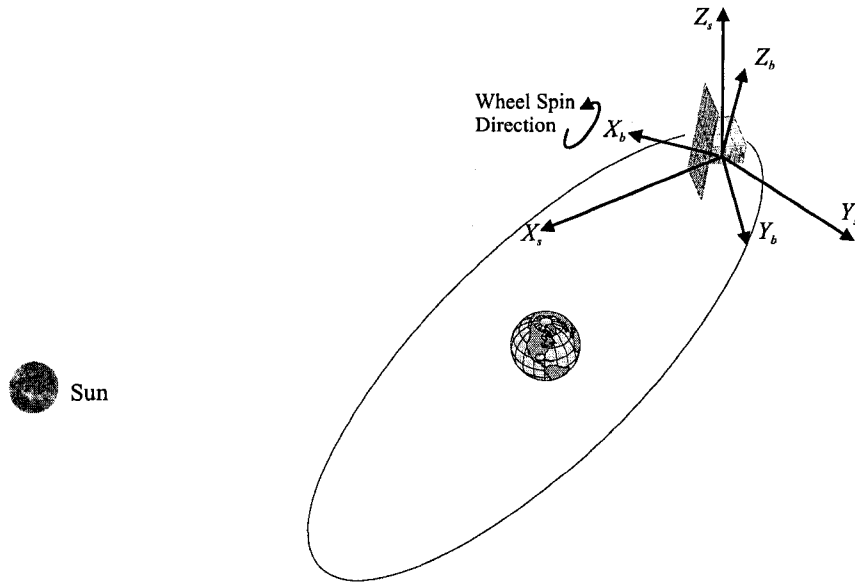
Figure 4.3: Satellite in Sun frame

The direction cosine matrix of the Sun frame relative to the body frame for small deviation angles can be written as

$$\mathbf{R}_s^b = \begin{bmatrix} 1 & \psi & -\theta \\ -\psi & 1 & \phi \\ \theta & -\phi & 1 \end{bmatrix} \tag{4.9}$$

where ϕ is the roll angle and is defined as the rotation of the spacecraft about the Sun vector and measured with respect to the direction of the ecliptic north pole. The pitch angle(θ) and yaw angle(ψ) are defined as the relative orientation of the Sun-pointing axis of the spacecraft with respect to the Sun vector. The absolute angular velocities in the body frame with respect to the Sun frame are

$$\omega_x = \dot{\phi}$$
$$\omega_y = \dot{\theta} \tag{4.10}$$
$$\omega_z = \dot{\psi} + \omega_{es}$$

where

$$\omega_{es} = \frac{2\pi}{365 \cdot 24 \cdot 3600} = 1.99 \cdot 10^{-7} \ rad/s \tag{4.11}$$

is the angular velocity of the Sun frame in its apparent annual rotation around the Earth on the celestial sphere [74]. Taking into account only small angles and performing algebraic transformations, one can get the linear differential equations of the satellite rotational dynamics as follows

$$\ddot{\phi} = -\frac{1}{I_x}\dot{H}_{wx} + \frac{T_x}{I_x}$$
$$\ddot{\theta} + \frac{H_{wx}}{I_y}\dot{\psi} = -\frac{H_{wx}}{I_y}\omega_{es} + \frac{T_y}{I_y} \tag{4.12}$$
$$\ddot{\psi} - \frac{H_{wx}}{I_z}\dot{\theta} = \frac{T_z}{I_z}.$$

The system of equations (4.12) represents the linearized spacecraft dynamical model for Sun-pointing mode. As can be seen from the first equation of (4.12), the roll equation is uncoupled from the other two equations and can be considered separately.

Before designing a ground-based attitude estimator, a linear controller is designed to ensure stability of the spacecraft. The linear control is provided by the

57

momentum wheel (neglecting saturation). Thus, the attitude control loop for the satellite roll motion can be described by

$$\ddot{\phi} = -\frac{1}{I_x}\dot{H}_{wx} + \frac{T_x}{I_x},$$ (4.13)

where T_x is the total torque and is given by the sum of the control torque, T_{cx} and the disturbance torque, T_{dx}.

$$T_x = T_{cx} + T_{dx}$$ (4.14)

The subscript x in the last two equations denotes the roll channel. The attitude control loop is shown in Figure 4.4. In this figure, T_c and T_d represent the control and disturbance torque. For the roll channel considered here, the control torque T_c is T_{cx} and the disturbance torque T_d is T_{dx}.
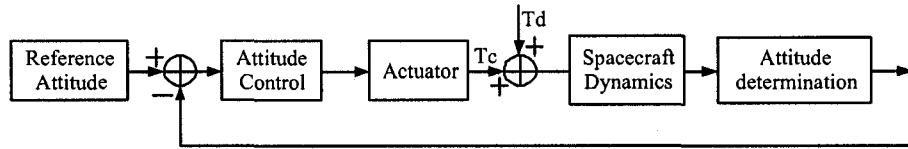
Figure 4.4: Attitude control loop

In this work, the linear control torque T_{cx} will be defined by a PD (Proportional and Differential) law in the roll angle, with actuation provided by the momentum wheel. The control torque is thus

$$T_{cx} = -\dot{H}_{wx} = k_p(\phi) + k_d(\dot{\phi}),$$ (4.15)

where k_p is the proportional gain and k_d is the derivative gain. By substituting equation (4.15) into equation(4.13), the roll dynamics with the controller is given as

$$I_x\ddot{\phi} = -k_p(\phi) - k_d(\dot{\phi}) + T_{dx}.$$ (4.16)

Equation (4.16) can be written in the form of a general second order equation as

$$\ddot{\phi} + \frac{k_d}{I_x}\dot{\phi} + \frac{k_p}{I_x}\phi = \frac{T_{dx}}{I_x}.$$ (4.17)

By taking the Laplace transformation, equation (4.17) can be written as

$$(s^2 + \frac{k_d}{I_x}s + \frac{k_p}{I_x})\phi = \frac{T_{dx}}{I_x}$$ (4.18)

Using the generalized notation of a second-order oscillator

$$s^2 + 2d\Omega s + \Omega^2$$

and comparing terms with equation (4.18), the proportional and the differential gains for the roll channel can be written as

$$k_p = I_x \Omega_x^2$$

$$k_d = 2d_x \Omega_x I_x \qquad (4.19)$$

where Ω_x is the control loop bandwidth for the roll channel and d_x is the damping coefficient for the roll channel. The control loop equation (4.15) presumes that a small angle of attitude deviation and small vector of angular velocity are measured by attitude determination methods. These attitude determination methods are involved in the control loop and provide the measured attitude. In satellites where rate gyros are not available, a first order low-pass filter is used to generate a filtered signal, which is then differentiated to obtain the angular velocities.

$$T_s = \frac{1}{\tau s + 1} \qquad (4.20)$$

where τ is the time constant of the filter.

The simplest model of the measured errors for vector measuring devices are used in the ground-based attitude determination and can be written as

$$\phi_m = \phi + \delta\phi$$

$$\theta_m = \theta + \delta\theta$$

$$\psi_m = \psi + \delta\psi \qquad (4.21)$$

where ϕ_m, θ_m, ψ_m are the measured attitude and ϕ, θ, ψ are the true attitude and $\delta\phi, \delta\theta, \delta\psi$ are the measurement errors. In a similar trend, one can write the angular velocity measurement errors, $(\delta\omega_x, \delta\omega_y, \delta\omega_z)$. To apply the modified Kalman filter estimator one can represent (4.3,4.15,4.21) in the form of a state variable vector matrix equation as

$$\dot{x} = F_x x + G_x w_x, \qquad (4.22)$$

where

$$x = \begin{bmatrix} \phi \\ \omega_x \\ T_{dx} \end{bmatrix}, F_x = \begin{bmatrix} 0 & 1 & 0 \\ -\Omega_x^2 & -2d_x\Omega_x & \frac{1}{I_x} \\ 0 & 0 & 0 \end{bmatrix}, G_x = \begin{bmatrix} 0 & 0 & 0 \\ -\Omega_x^2 & -2d_x\Omega_x & 0 \\ 0 & 0 & 1 \end{bmatrix}, w_x = \begin{bmatrix} \delta\phi \\ \delta\omega_x \\ w_{Tdx} \end{bmatrix},$$

and w_x is considered as a band limited white noise with covariance matrix

$$Q_x = \begin{bmatrix} q_{x11} & 0 & 0 \\ 0 & q_{x22} & 0 \\ 0 & 0 & q_{x33} \end{bmatrix},$$

where $q_{x11} = \frac{\sigma_{\delta\phi}^2}{\Delta t}$, $q_{x22} = \frac{\sigma_{\delta\omega_x}^2}{\Delta t}$, $q_{x33} = \frac{\sigma_{w_{Tdx}}^2}{\Delta t}$, σ_i^2 is the variance related component of w_x vector, and Δt is the measurement sampling rate. Similarly, pitch and yaw equations can be derived and written in the state form as

$$\dot{y}_z = F_{yz}y_z + G_{yz}w_{y_z} + \bar{y}_z, \tag{4.23}$$

where

$$y_z = \begin{bmatrix} \theta \\ \omega_y \\ T_{dy} \\ \psi \\ \omega_z \\ T_{dz} \end{bmatrix}, F_{yz} = \begin{bmatrix} 0 & 1 & 0 & 0 & 0 & 0 \\ \Omega_y^2 & -2d_y\Omega_y & \frac{1}{I_y} & -\frac{H_{wx}}{I_y} & -\frac{H_{wx}}{I_y} & 0 \\ 0 & 0 & 0 & 0 & 0 & 0 \\ 0 & 0 & 0 & 0 & 1 & 0 \\ 0 & \frac{H_{wx}}{I_z} & 0 & -\Omega_z^2 & -2d_z\Omega_z & \frac{1}{I_z} \\ 0 & 0 & 0 & 0 & 0 & 0 \end{bmatrix}$$

$$\bar{y}_z = \begin{bmatrix} 0 & -\frac{H_{wx}}{I_y}\omega_{es} & 0 & 0 & 0 & 0 \end{bmatrix}^T$$

$$G_{yz} = \begin{bmatrix} 0 & 0 & 0 & 0 & 0 & 0 \\ -\Omega_y^2 & -2d_y\Omega_y & 0 & 0 & 0 & 0 \\ 0 & 0 & 1 & 0 & 0 & 0 \\ 0 & 0 & 0 & 0 & 0 & 0 \\ 0 & 0 & 0 & -\Omega_z^2 & -2d_z\Omega_z & 0 \\ 0 & 0 & 0 & 0 & 0 & 1 \end{bmatrix}, w_{y_z} = \begin{bmatrix} \delta\theta \\ \delta\omega_y \\ w_{Tdy} \\ \delta\psi \\ \delta\omega_z \\ w_{Tdz} \end{bmatrix},$$

where $\bar{y}_z$ is the gyro torque due to the Earth's annual rotation around the Sun, Ω_y and Ω_z are the control loop bandwidth for pitch and yaw angles, d_y and d_z are the

60

damping coefficients for pitch and yaw angles, and w_{y_z} is considered as a band limited white noise vector with covariance matrix

$$Q_{yz} = \begin{bmatrix} q_{y11} & 0 & 0 & 0 & 0 & 0 \\ 0 & q_{y22} & 0 & 0 & 0 & 0 \\ 0 & 0 & q_{y33} & 0 & 0 & 0 \\ 0 & 0 & 0 & q_{z44} & 0 & 0 \\ 0 & 0 & 0 & 0 & q_{z55} & 0 \\ 0 & 0 & 0 & 0 & 0 & q_{z66} \end{bmatrix},$$

where $q_{y11} = \frac{\sigma^2_{\delta\theta}}{\Delta t}$, $q_{y22} = \frac{\sigma^2_{\delta\omega_y}}{\Delta t}$, $q_{y33} = \frac{\sigma^2_{\Delta w_{Tdy}}}{\Delta t}$, $q_{y44} = \frac{\sigma^2_{\delta\psi}}{\Delta t}$, $q_{y55} = \frac{\sigma^2_{\Delta\omega_z}}{\Delta t}$, and $q_{y66} = \frac{\sigma^2_{\Delta w_{Tdz}}}{\Delta t}$. Given the dynamics of the linearized spacecraft dynamical model, the next subsection addresses the application of the modified Kalman filter. The variables estimated in the ground-based attitude estimator are ϕ, ω_x and T_{dx}.

4.1.2 Stochastic Estimation

In the previous subsection, a linearized spacecraft dynamic model with controller was developed. In this subsection, a ground-based attitude estimator is developed using the modified Kalman filter. The overview of the ground based attitude estimator with the spacecraft attitude control loop is shown in the Figure 4.5. From the figure it is observed that the input to the ground-based attitude estimator is the signal from the control loop. Note that various signals are collected at mission control center through telemetry and only the attitude sensor data are extracted from the mission control center and sent to the ground-based attitude estimator.
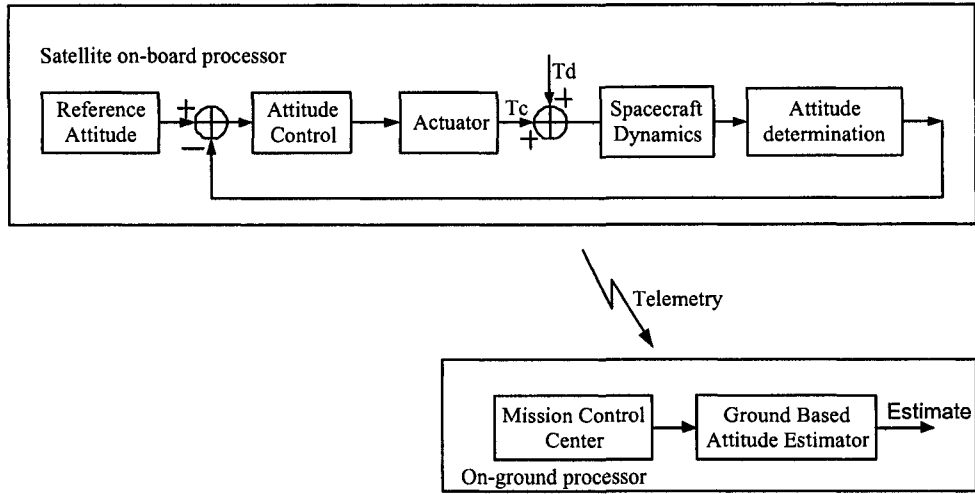
Figure 4.5: Attitude telemetry mission control

The equations of the discrete-time Kalman filter are given in [28]. In this section, equations for the discrete-time modified Kalman filter are briefly explained; more details can be found in [9]. The modification takes into consideration the correlation between measurement and process noise. The Kalman filter is designed for the case, when there is no correlation between process and measured noise in the system model. The generalized equations of the model used in the Kalman filter are given as [19]

$$x_{i+1} = \Phi_i x_i + \Gamma_i w_i$$

$$z_i = H_i x_i + v_i \tag{4.24}$$

where x_i is the process state vector at step i, $\Phi_i = I + F\Delta t$ is the system transition matrix, F is described in equation (4.22), Γ is the discrete term of G in equation (4.22), I is the identity matrix, w_i is a vector of white noise acting on the process, z_i is the measurement vector, H_i is the matrix that relates the measurement and the state vector, and v_i is the white noise acting on the measurement. The first equation of (4.24) is the model of the process to be estimated and the second describes the observation (measurement) of the process. The covariance matrices for the w_i and v_i

vectors are given by

$$E\left[w_i w_j^T\right] = Q_i \delta_i$$

$$E\left[v_i v_j^T\right] = R_i \delta_i \tag{4.25}$$

where δ_i is the kronecker constant. The model described in equation (4.24) is for open-loop systems. The derivations of the closed-loop equations of the model are given as :

$$x_{i+1} = \Phi_i x_i + u_i + \Gamma_i w_i$$

$$z_i = H_i x_i + v_i \tag{4.26}$$

where u_i is the controller, and was included in the system equation (4.15) as $T_c x$ and is written as

$$u_i = -k_c z_i, \tag{4.27}$$

where k_c is the PD controller. Substituting equation (4.27) into equation (4.26) the model for the modified Kalman filter is

$$x_{i+1} = \Phi_i x_i - k_c(H_i x_i + v_i) + \Gamma_i w_i$$

$$= (\Phi_i - k_i H_i)x - k_c v_i + \Gamma_i w_i$$

$$z_i = H_i x_i + v_i \tag{4.28}$$

Equation (4.28) is rewritten for the sake of simplicity as

$$x_{i+1} = (\Phi_i - k_c H_i)x - \eta_i. \tag{4.29}$$

where η_i is the new noise term and is equal to

$$\eta_i = k_c v_i + \Gamma_i w_i \tag{4.30}$$

From equation (4.30), it is clear that the process noises v_i and w_i are correlated. The covariance matrix for the correlation of w_i and v_i vectors is given by

$$E\left[\eta_i \eta_j^T\right] = C_i \delta_i \tag{4.31}$$

$$C_i = \begin{bmatrix} \frac{\sigma_{\delta\phi}^2}{\Delta t} & 0 & 0 \\ 0 & \frac{\sigma_{\delta\omega_x}^2}{\Delta t} & 0 \\ 0 & 0 & \frac{\sigma_{w_{Tdx}}^2}{\Delta t} \end{bmatrix}. \qquad (4.32)$$

Given the process model, measurement model and the covariance matrices for the noise, the general update equation for the modified Kalman filter is

$$\hat{x}_i = \hat{x}_i^- + K_i(z_i - H_i\hat{x}_i^-), \qquad (4.33)$$

where K_i is the Kalman gain

$$K_i = (P_i^- H_i^T + C_k)[H_i P_i^- H_i^T + R_i + H_i C_i + C_i^T H_i^T]^{-1} \qquad (4.34)$$

and P_i is the general expression for the error covariance matrix

$$P_i = (I - K_i H_i)P_i^- - K_i C_i^T. \qquad (4.35)$$

The updated estimate $\hat{x}_i$ is projected ahead via the transition matrix according to

$$\hat{x}_{i+1}^- = \Phi_i \hat{x}_i. \qquad (4.36)$$

The error covariance matrix associated with $\hat{x}_{i+1}$ is then obtained as

$$P_{i+1}^- = \Phi_i P_i \Phi_i^T + \Gamma_i C_i \Gamma_i^T. \qquad (4.37)$$

Equations (4.34), (4.35), (4.36), and (4.37) complete the set of recursive equations for the correlated process and measurement noise case. It can be seen that derivations of these equations follows the same trend as the derivations of the Standard Kalman Filter (SKF), which can be found in [9]. The differences between the standard Kalman filter and the Modified Kalman Filter(MKF) are summarized in Table 4.1.2. This estimator is validated in the next subsection using experimental telemetry data from an orbiting satellite.

4.1.3 Simulations

The modified Kalman filter estimator has been tested using telemetry data from the SCISAT-1 satellite mission. Simulation results were performed for the telemetry data

64

Table 4.1: Differences between SKF and MKF

Kalman Filter	Modified Kalman filter
$x_{i+1} = \Phi_i x_i + w_i,$ $z_i = H_i x_i + v_i$	$x_{i+1} = \Phi_i x_i + w_i + u,$ $z_i = H_i x_i + v_i$
$E\left[w_k v_i^T\right] = 0$	$E\left[w_k v_i^T\right] = C_k$
$K_i = (P_i^- H_i^T)[H_i P_i^- H_i^T + R_i]^{-1}$	$K_i = (P_i^- H_i^T + C_i)[H_i P_i^- H_i^T + R_i$ $+ H_i C_i + C_i^T H_i^T]^{-1}$

during the time period between the 30th and the 31st of January 2005. During this period, the Sun sensor and the magnetometer were active in the attitude control loop. Simulation results were obtained using the ground estimator discussed in the previous subsection. The simulation parameters used in this chapter are shown in Table 4.1.3. These values are specifically for the Canadian scientific satellite SCISAT-1. However, the theory developed is not restricted to any particular satellite.

Table 4.2: Simulation parameters

Parameters	Numerical values
Ω_x	0.015Hz
Ω_y	0.081Hz
Ω_z	0.081Hz
d_x	0.707
d_y	0.707
d_z	0.707
I_x	18.867 kgm^2
I_y	12.476 kgm^2
I_z	13.167 kgm^2
τ	1.952 s

In Figure 4.6, true roll angle is shown with time as in x-axis and degrees in

y-axis. The simulations are performed for one orbit. The true roll angle is obtained on-ground based on the vector information. In Figure 4.7, the telemetry signal for roll channel is shown. From the figure it is observed that the signal is corrupted with noise.
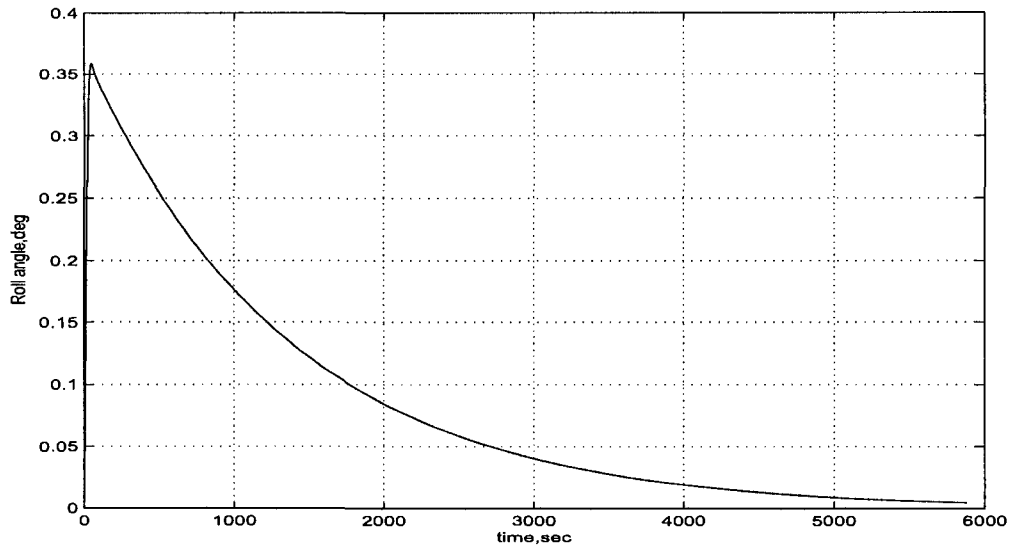
Figure 4.6: True roll angle
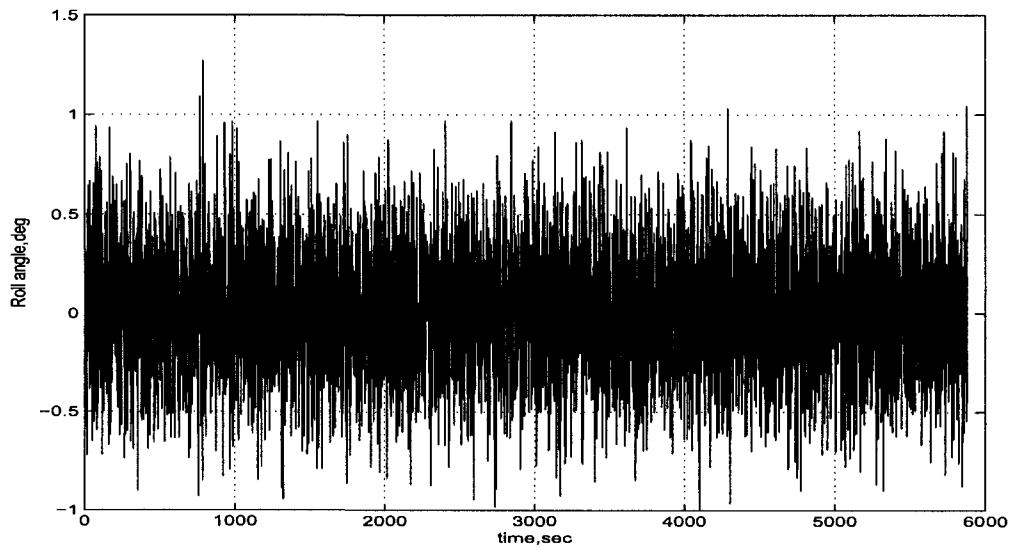
Figure 4.7: Roll angle obtained from telemetry

In Figure 4.8, the estimated roll angles are obtained from both standard and

modified Kalman filters and are compared with the true roll angle. The reason Figure 4.8 is shown because of maintaining consistency with the x-axis. For the sake of understanding, the Figure 4.8 is zoomed on the $x - axis$ and is shown in Figure 4.9. The dark solid line represents the true angle, solid line represents estimated roll angle using standard Kalman filter and the dashed line represents estimated roll angle using modified Kalman filter. As is seen, the estimated roll angle using modified Kalman filter has less transient error when compared to the standard Kalman filter.
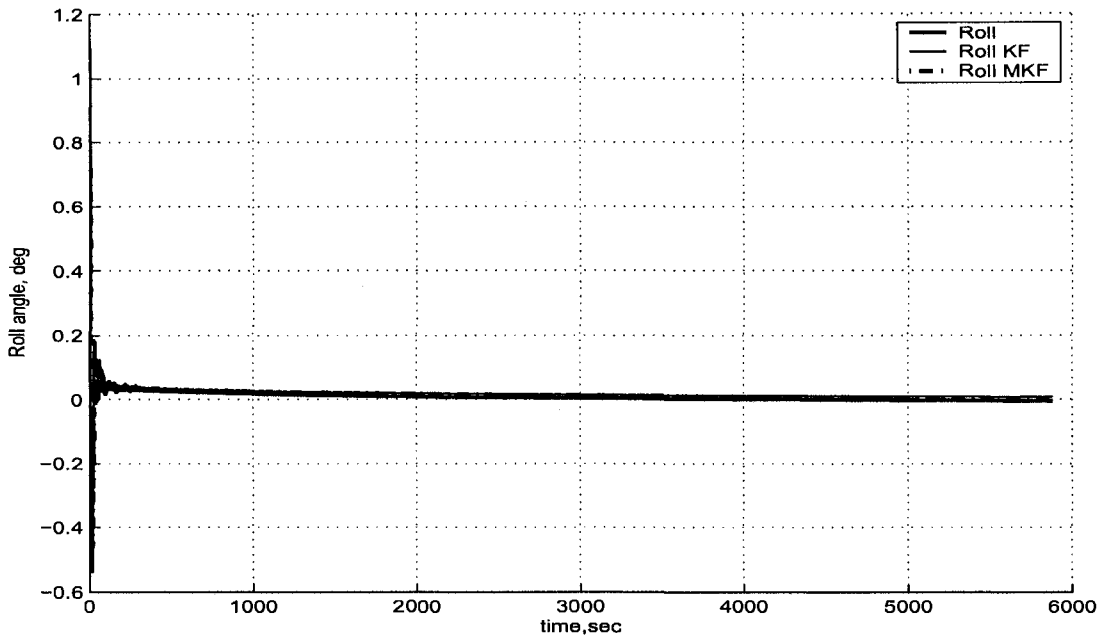
Figure 4.8: Estimation of roll angle using standard and modified Kalman filtering
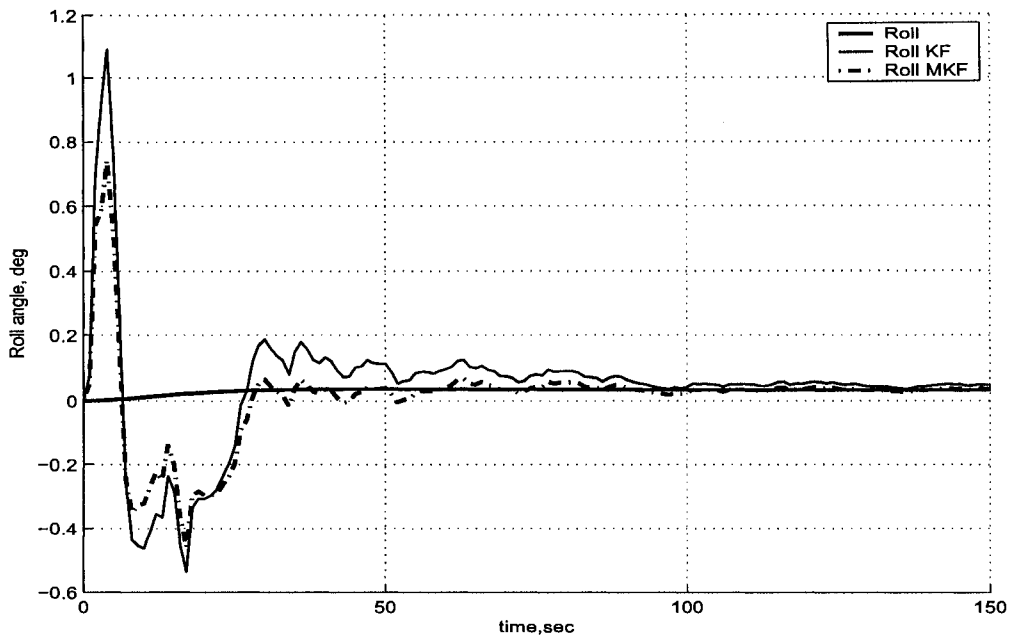
Figure 4.9: Zoom of Figure 4.8

In the following figures, absolute error between of the roll angle is given. In Figure 4.10, the absolute errors for the roll angle from both standard and modified Kalman filters are plotted. The error plotted was the difference between the true roll angle, and the estimated roll angle from the estimator. In Figure 4.11, the x-axis is zoomed so as to understand the significance of the results. From the graphs it is understood that the transient error of the standard Kalman filter exceeds 1°. For SCISAT satellite nominally at 650 km, a one deg error is equivalent to approximately 10 km in observation altitude which is significant. By implementing the modified Kalman filter the accuracy is improved, which is concluded from the results.
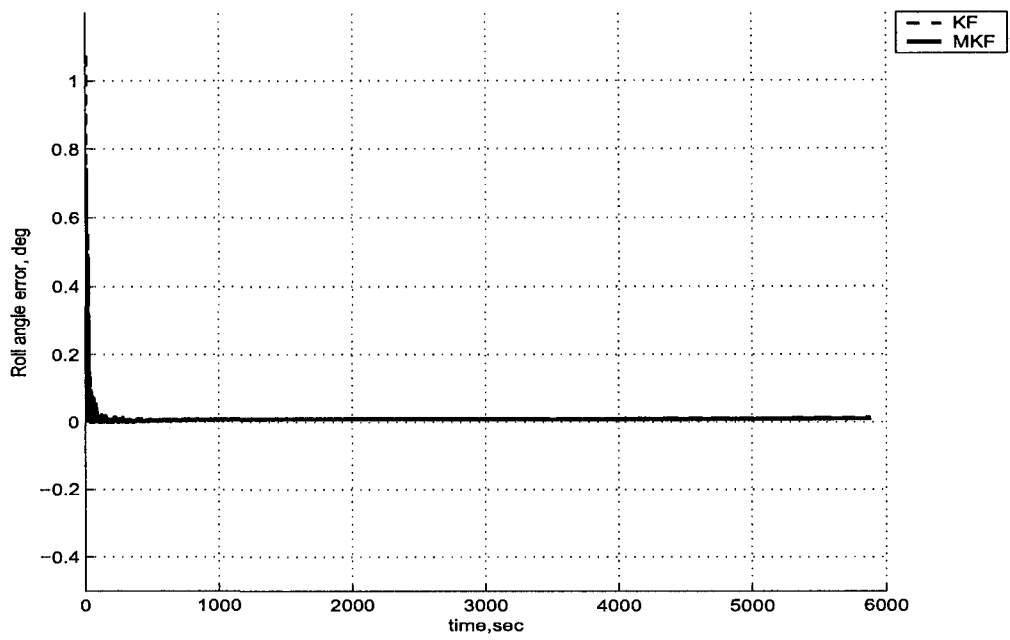
Figure 4.10: Roll error measured from standard and modified Kalman filtering
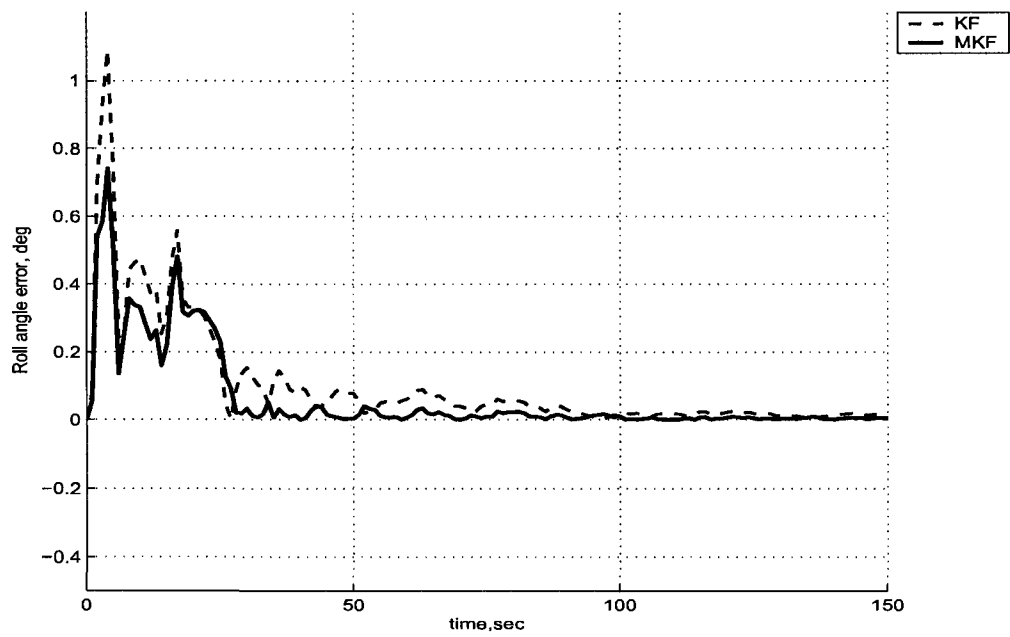
Figure 4.11: Zoom of Figure 4.10

69

4.1.4 Summary

In this section a multi-purpose ground based satellite attitude estimator is developed based on a modified Kalman filter. The standard Kalman filter cannot be used directly to develop a ground based satellite attitude estimator because the attitude sensors from which the telemetry data is obtained are in the closed-loop. However, it must be recalled that the estimator developed is only for pointing mode, where attitude errors are small and allow for linearization, and not for acquisition mode, where attitude errors can reach more than 25°. Moreover, the estimator is based on statistical information, which is often not available. Motivated by this limitation, the next section discusses estimation using the guaranteed ellipsoidal method for acquisition mode.

4.2 Attitude Estimation using Guaranteed Ellipsoidal Theory

In the previous section, attitude estimator for pointing mode was developed using the modified Kalman filtering. In this section, attitude estimation for pointing mode and acquisition mode will be developed using guaranteed ellipsoidal state estimation, where the attitude and angular velocity are bounded with ellipsoidal bounds. In acquisition mode, the attitude errors reach more than 25° degrees and therefore a nonlinear estimation procedure is necessary. The ground based attitude estimator using guaranteed ellipsoidal theory is accomplished by finding the minimum volume ellipsoid containing attitude. The center of the ellipsoidal is assumed to be the attitude estimate, while the size of the ellipsoid measures the accuracy of these estimates.

4.2.1 Introduction

The guaranteed ellipsoidal estimation method enjoys four major advantages relative to existing attitude estimation methods [15, 37, 64]. First, the estimation algorithm does not require the statistical information about the external noise and observation

errors. Second, the attitude and angular velocity measurements are bounded with sets. Third, the uncertainties are arbitrary and are not assumed to be Gaussian white noise. Fourth, this approach is formulated as a convex optimization technique. The most recent work on satellite attitude estimation using guaranteed ellipsoidal estimation is given by Sanyal *et al.* [55]. In Sanyal's work, Lie algebra theory is used to describe the attitude kinematics.

There are two contributions in this section with regards to ellipsoidal state estimation for satellites. The first is to propose the method of analytic centers to minimize the volume of the uncertainty ellipsoid containing the state of the satellite for the case of pointing mode, where the spacecraft dynamic model is linear. The method of analytic centers first computes the analytic center of the feasibility set and then fits an ellipsoid centered at this point that contains the feasible set. Thus, the method computes a point estimate with certain properties and then estimates the set. Algorithms to compute analytic centers have been widely studied in [7,8,22] and are used in the thesis for ellipsoidal state estimation. Note that the contribution in the thesis is not about how to find the analytic center, but how to use the analytic centers concept in the theory of state estimation. Bai *et al.* [2] used analytic centers in the case of parameter estimation. To the best of the author's knowledge, the method of analytic centers to minimize the volume of an uncertainty ellipsoid, where the state lies, has not been used in state estimation. The second contribution of this section is to extend the work of Polyak *et al* [50], which concentrates on uncertain linear systems to nonlinear systems. The most recent work on ellipsoidal state estimation for nonlinear systems is published by Scholte and Campbell [59]. The algorithm proposed in [59] is called Extended Set Membership Filter (ESMF). The main difference between the proposed algorithm in this section to that of Scholte and Campbell [59] is that this thesis proposes including the linearization error in the system. The difference between the two methods are shown in Figure 4.12. The primary distinction between these methods is in blocks B and C, which are discussed in the subsection 4.2.3.
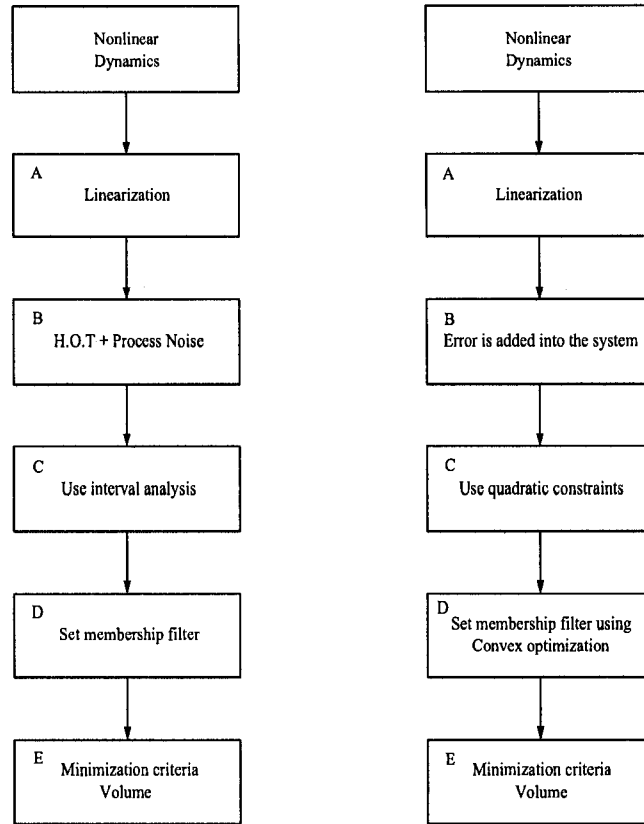
Figure 4.12: Simplified graphical representation of ESMF(left) and proposed set membership filter(right) at each time step

4.2.2 Mathematical Preliminaries

Four preliminary mathematical results are now stated for convenience.

1. **Ellipsoids**: Ellipsoids in this work will be described in the following forms [8,10]

$$E_1 = \left\{x : x^T A x + 2x^T b + c \leq 0\right\}, \tag{4.38}$$

such that $A = A^T > 0, \quad b^T A^{-1} b - c > 0$, and

$$E_2 = \left\{x : (x - x_c)^T P^{-1} (x - x_c) \leq 1\right\}, \tag{4.39}$$

where $P = P^T > 0$. The positive definite matrix P is related to the shape of the ellipsoid and the vector x_c is the center of the ellipsoid E_2. The two ellipsoids

72

E_1 and E_2 can be related according to

$$A = P^{-1}, \quad b = -P^{-1}x_c, \quad c = x_c^T P^{-1} x_c - 1. \tag{4.40}$$

2. **Linear Matrix Inequality(LMI)** [8]: An LMI is of the form

$$F(x) = F_0 + \sum_i^n x_i F_i > 0 \tag{4.41}$$

where $x \in \Re^n$ and $F_i = F_i^T \in \Re^{m \times m}, i = 0, \ldots, n$.

3. **Schur's complement** [8] : Given an LMI

$$\begin{bmatrix} A & B \\ C & D \end{bmatrix} > 0, \tag{4.42}$$

where $A = A^T$ and $D = D^T$. Then equation (4.42) is equivalent to $D > 0$ and $A - BD^{-1}C > 0$.

4. **S-procedure** [8]: Given ellipsoids of the form

$$S_i = \{x | x^T A_i x + 2b_i^T x + c_i \leq 0\}, \tag{4.43}$$

where,$i = 0, 1$. Then sufficient condition for $S_1 \subseteq S_0$ is if there exists $\tau \geq 0$ such that

$$\begin{bmatrix} x \\ 1 \end{bmatrix}^T \begin{bmatrix} A_0 & b_0 \\ b_0^T & c_0 \end{bmatrix} \begin{bmatrix} x \\ 1 \end{bmatrix} \leq \tau \begin{bmatrix} x \\ 1 \end{bmatrix}^T \begin{bmatrix} A_1 & b_1 \\ b_1^T & c_1 \end{bmatrix} \begin{bmatrix} x \\ 1 \end{bmatrix}. \tag{4.44}$$

4.2.3   Problem Formulation

Attitude Estimation for Pointing Mode

During the pointing mode, the attitude errors are small and therefore a linear spacecraft dynamical model is used. The dynamical system under consideration is represented by a linear discrete-time state equation

$$x_{i+1} = \Phi_i x_i + \Gamma_i w_i$$
$$z_i = H_i x_i + v_i \tag{4.45}$$

where $x_i \in \mathbb{R}^n$ is the state vector, $w_i \in \mathbb{R}^n$ is the disturbance, z_i is the measurement and v_i is the sensor noise. The matrices Φ_i, G_i and H_i are given in equation (4.24). The initial state x_0 of the system is known to be in the ellipsoidal set

$$E_0(\hat{x}_0, P) = \{x_0 : (x_0 - \hat{x}_0)^T P^{-1}(x_0 - \hat{x}_0) \leq 1\}, \qquad (4.46)$$

where $\hat{x}_0$ is the center of the ellipsoid and positive definite matrix P defines its shape. The disturbance w_i and sensor noise v_i are also bounded at each time step i by

$$W_i(0, Q_i) = \{w_i : w_i^T Q_i^{-1} w_i \leq 1\} \qquad (4.47)$$

$$V_i(0, R_i) = \{v_i : v_i^T R_i^{-1} v_i \leq 1\} \qquad (4.48)$$

where positive definite matrices Q_i and R_i define the shape of these ellipsoids. Since no other information is required for these bounds, many types of noise are included within this framework, including random and biased signals.

Remark 4.1. *Note that the equation (4.45) describing the spacecraft dynamics is the same as the model (4.24) used for the modified Kalman filter. However, the assumptions on noise are different. In equation (4.47) the noise is bounded but in equation (4.25) the statistical information is given.*

Problem 1 (Linear Filter) : Given the system dynamics (4.45), initial conditions (4.46) and noise assumptions (4.47), find the minimum volume ellipsoid which contains all the state vectors.

Attitude Estimation for Acquisition Mode

During the acquisition mode, attitude errors can exceed 25 ° and therefore a nonlinear spacecraft dynamical model is used. The nonlinear discrete-time spacecraft model is given as

$$x_{i+1} = f(x_i) + w_i,$$
$$z_i = h(x_i) + v_i, \qquad (4.49)$$

where f and h are nonlinear functions, w_i and v_i are disturbances (unknown but bounded) as described in equation (4.47), x_i is the unknown state vector, and y_i is

the measured output. It is assumed that the initial state x_0 is known to be bounded by an ellipsoid (4.46).

Linearization

First the nonlinear system (4.49) is linearized and assumptions are discussed before proceeding to the problem formulation. Linearizing equation (4.49) about the *current estimate* $\hat{x}_i$ yields

$$x_{i+1} = f(x_i)|_{x_i=\hat{x}_i} + \frac{\partial f(x_i)}{\partial x}|_{x_i=\hat{x}_i}(x_i - \hat{x}_i) + H.O.T. + w_i \qquad (4.50)$$

$$z_i = h(x_i)|_{x_i=\hat{x}_{i+1}} + \frac{\partial h(x_i)}{\partial x}|_{x_i=\hat{x}_{i+1}}(x_i - \hat{x}_{i+1|i}) + H.O.T. + v_i \qquad (4.51)$$

where H.O.T. stands for Higher-Order Terms or the remainder from the linearization.

Error Bounds

The traditional ESMF combines the H.O.T. and process noise into one bound [59]. The approach here is to combine the linearization error into the system uncertainties such that equation (4.50) can be written as

$$\delta x_{i+1} = (A_i + \Delta A_i(x_i))\delta x_i + f_0 + w_i$$

$$\delta z_i = (C_i + \Delta C_i(x_i))\delta x_i + c_0 + v_i \qquad (4.52)$$

where

$$f_0 = f(x_i)|_{x_i=\hat{x}_i}; \qquad c_0 = h(x_i)|_{x_i=\hat{x}_{i+1}}$$

$$A_i = \frac{\partial f(x_i)}{\partial x}|_{x_i=\hat{x}_i}(x_i - \hat{x}_i); \quad C_i = \frac{\partial h(x_i)}{\partial x}|_{x_i=\hat{x}_{i+1}}$$

$$\Delta A_k(x_k)\delta x_k = H.O.T.; \qquad \Delta C_i(x_i)\delta x_i = H.O.T \qquad (4.53)$$

Remark 4.2. *This method is an extension to the work of Polyak et al. [50], in the sense that the uncertainty is included in the system, where the uncertainty is the linearization error.*

It is assumed that the model uncertainties are combined with those due to linearization errors and measurement noise in the following ellipsoidal constraints

$$\frac{||\Delta A_i(x_i)||^2}{\delta_A^2} + \frac{||w_i||^2}{\delta_w^2} \leq 1, \qquad (4.54)$$

$$\frac{||\Delta C_i(x_i)||^2}{\delta_C^2} + \frac{||v_i||^2}{\delta_v^2} \leq 1, \qquad (4.55)$$

where δ_A, δ_C, δ_w, δ_v are prespecified constants.

Problem 2 (Nonlinear Filter) : Given the system dynamics (4.49), initial conditions (4.46) and noise assumptions (4.47), find the minimum volume ellipsoid which contains all state vectors.

4.2.4 Guaranteed Ellipsoidal State Estimation

As in conventional state estimation, recursive guaranteed ellipsoidal bounding with known bounds on the process and measurement contains both time and measurement updates. The time and measurement updates produce the vector sum and intersection of two ellipsoids respectively. Neither the sum nor the intersection is generally ellipsoidal, so both sets are approximated by ellipsoidal sets containing the original set. Hereafter, superscript m denotes variables related to the measurement update, superscript s denotes variables related to time update, superscript i denotes the predicted uncertainty ellipsoid in which the state lies, and $(i+1|i)$ indicates information about state x_{i+1} based on observations at times up to and including i. The ellipsoidal state estimation procedure of a two -dimensional system is illustrated in Figures 4.13 and 4.14. Figure 4.13 shows the time update of the feasible ellipsoid E^s and Figure 4.14 shows the observation update.
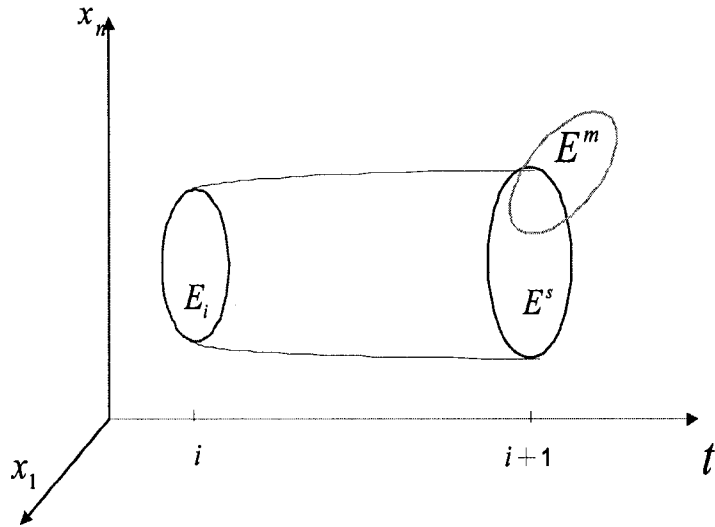
Figure 4.13: Time update of states bounded by ellipsoids

Suppose that the time interval between two sets of measurements is divided into l equal time steps for discrete integration, and the subscript i denotes the ith discrete integration time step. At the ith step, the state is bounded by an uncertainty ellipsoid E_i centered at $\hat{x}_i$. The initial ellipsoid evolves over time and at the $(i+1)^{th}$ time step, the ellipsoid E_i transforms to E_{i+1}^s with center $\hat{x}_{i+1}^s$. At the same instant of time, a measurement update is available through on-board sensors, and another ellipsoidal bound on the state is obtained, denoted by E^m, with center at $\hat{x}_{i+1}^m$. The state estimate to be determined is in the intersection of the ellipsoids E^m and E^s. Note that the intersection of two ellipsoids is not necessarily an ellipsoid. Thus, the intersection set has to be approximated as an ellipsoid, resulting in E^i, and is shown in Figure 4.14.
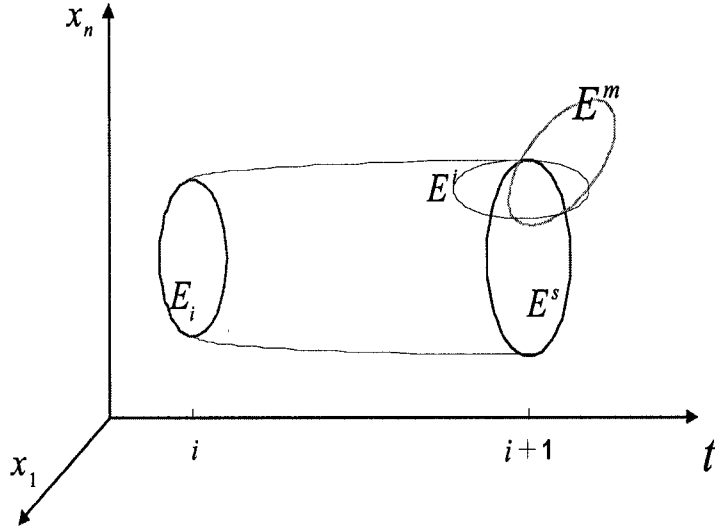
Figure 4.14: Observation update of states bounded by ellipsoids

The center of the new ellipsoid E^i, $\hat{x}_{i+1}$, is considered as a point estimate at time step $(i + 1)$, and the magnitude of the new uncertainty ellipsoid measures the accuracy of the estimation. The objective is to find the minimum volume ellipsoid using convex optimization techniques. In the next subsections, the time update and the observation update are described mathematically.

4.2.5 Attitude Estimation for Pointing Mode

In this subsection, attitude estimation for pointing mode is discussed. The time update is discussed first and is based semi-definite programming [8]. Then, the measurement update is discussed.

Time Update

The discrete model considered for the time update is given as

$$x_{i+1} = \Phi_i x_i + \Gamma_i w_i$$
$$z_i = H_i x_i + v_i \tag{4.56}$$

Given an ellipsoid E_i containing the state of the system at time i, the objective is to determine an ellipsoid that contains the set of states of the system at time $(i+1)$, subject to model uncertainty. The set of all values of x_{i+1} consistent with the information available at time $(i+1)$ are approximated recursively by the minimum volume ellipsoid denoted by $E_{i+1|i} = E(\hat{x}_{i+1|i}; P_{i+1|i})$. The ellipsoid that contains the feasible set of the state vector values at time $(i+1)$ is given by

$$E(\hat{x}_{i+1|i}, P_{i+1|i}) = \left\{ \hat{x}_{i+1} : (x_{i+1} - \hat{x}_{i+1|i})^T P_{i+1|i}^{-1} (x_{i+1} - \hat{x}_{i+1|i}) \leq 1 \right\}. \qquad (4.57)$$

The center $\hat{x}_{i+1|i}$ and the matrix $P_{(i+1)|i}$ defining its shape are obtained using semi-definite programming [8]. The advantage of using semi-definite programming to that of support functions, widely used in the literature [42,59], is that no scalar parameter is needed to obtain the minimum volume ellipsoid. The condition for the minimum volume ellipsoid is given as

$$E(\hat{x}_{i+1|i}, P_{i+1|i}) \supseteq E_0(\hat{x}_0, P) + W_i(0, Q_i) \qquad (4.58)$$

Before proving the condition (4.58), first a linear transformation is considered for the discrete linear system described in (4.56). Assuming that $y_i = \Phi_i x_i$, where x_i belongs to the ellipsoid $E_0(\hat{x}_0, P)$, the linear transformation is given as

$$E_0(\hat{y}_0, P) = \{y_0 : (y_0 - \Phi_i \hat{x}_0)^T (\Phi_i P \Phi_i)^{-1} (y_0 - \Phi_i \hat{x}_0) \leq 1\}$$

Similarly, by assuming the noise equation to be $l_i = \Gamma_i w_i$, the linear transformation is

$$E_w(0, Q_i) = \{l_0 : l_0 (\Gamma_i Q_i \Gamma_i)^{-1} (l_0) \leq 1\}$$

Given these linear transformations, the condition (4.58) becomes

$$E(\hat{x}_{i+1|i}, P_{i+1|i}) \supseteq E_0(\hat{y}_0, P) + E_w(0, Q_i). \qquad (4.59)$$

The ellipsoids $E_0(\hat{y}_0, P)$ and $E_w(0, Q_i)$ are described as

$$E_0(\hat{y}_0, P) = \{\hat{y}_0 | T_1(\hat{y}_0) \leq 0\}, \quad T_1(\hat{y}_0) = (\hat{y}_0)^T A_1(\hat{y}_0) + 2(\hat{y}_0)^T b_1 + c_1,$$
$$E_w(0, Q_i) = \{\hat{l}_i | T_2 \hat{l}_i \leq 0\}, \quad T_2 \hat{l}_i = \hat{l}_i^T A_2 \hat{x}_i + 2 \hat{l}_i^T b_2 + c_2, \qquad (4.60)$$

79

where

$$A_1 = (\Phi_i P \Phi_i^T)^{-1}, \quad b_1 = -(\Phi_i P \Phi_i^T)^{-1} \Phi_i x_c$$

$$c_1 = (\Phi_i x_c)^T (\Phi_i P \Phi_i^T)^{-1} \Phi_i x_c - 1$$

$$A_2 = (\Gamma_i Q \Gamma_i)^{-1}, \quad b_2 = 0, \quad c_2 = -1$$

The summation of two ellipsoids is defined as

$$E(\hat{x}_{i+1|i}, P_{i+1|i}) = \{\hat{y}_0 + l_i | \hat{y}_0 \in E_0(\hat{y}_0, P), l_i \in E_w\}.$$

The above condition can be proven by using the S-procedure discussed in subsection 4.2.2 if there exists $t_1 \geq 0$ and $t_2 \geq 0$, such that

$$T_{x_{i+1}} - t_1 T_1(\hat{y}_0) + t_2 T_2(l_i) \leq 0.$$

where $T_{x_{i+1}}$ is the ellipsoid $E(\hat{x}_{i+1|i}, P_{i+1|i})$, then

$$\begin{bmatrix} A_{x_{i+1}} & b_{x_{i+1}} & 0 \\ b_{x_{i+1}}^T & -1 & b_{x_{i+1}}^T \\ 0 & b_{x_{i+1}} & -A_{x_{i+1}} \end{bmatrix} - \sum_{i=1}^{2} t_i \begin{bmatrix} A_i & b_i & 0 \\ b_i^T & c_i & 0 \\ 0 & 0 & 0 \end{bmatrix} \leq 0 \quad (4.61)$$

To find the minimum volume ellipsoid $T_{x_{i+1}}$ that contains all the state vectors, equation (4.61) is solved using the optimization problem discussed below. Since the determinant of the shape matrix is directly proportional to the volume of the ellipsoid, the determinant is used as the objective function in the convex optimization problem, which is now stated.

Definition 4.2.1. *The minimum volume ellipsoid optimization problem is:*

$$minimize \; logdet \; A_{x_{i+1}}^{-1}$$

$$subject \; to \; A_{x_{i+1}} > 0, \; t_i >= 0,$$

$$T_{x_{i+1}} - (t_1 T_1(\hat{x}_0) + t_2 T_2(\hat{x}_i)) \leq 0,$$

where *logdet* defines the logarithm of the determinant. The optimization problem defined in Definition 4.2.1 can be solved using the available software YALMIP [40]. The center and the size of the ellipsoid $E(\hat{x}_{i+1|i}, P_{i+1|i})$ can be obtained as

$$\hat{x}_{i+1|i} = -A_{x_{i+1}} b_{x_{i+1}}$$

$$P_{i+1|i} = (b_{x_{i+1}}^T A_{x_{i+1}} b_{x_{i+1}} - c_{x_{i+1}}) A_{x_{i+1}}^{-1}$$

80

Measurement Update

Given the state of the system after the time update, it is now necessary to find the measurement update ellipsoid $E(\hat{x}_{i+1|i+1}, P_{i+1|i+1})$. The measurement update is the intersection of two ellipsoids, the time update ellipsoid (4.57) and the measurement equation (4.49), is confined to the ellipsoid

$$R_i = \left\{ x_i : (z_i - H_i \hat{x}_{i+1})^T \hat{R}_i^{-1} (z_i - H_i \hat{x}_{i+1}) \leq 1 \right\}. \tag{4.62}$$

The intersection ellipsoid which contains the state estimate is obtained using the analytic center approach [8]:

$$E(\hat{x}_{i+1|i+1}, P_{i+1|i+1}) = E(\hat{x}_{i+1|i}, P_{i+1|i}) \bigcap R_i \tag{4.63}$$

The ellipsoids (4.62) and (4.57) can be written in the form of an LMI by using Schur's complement as

$$F(\hat{x}_{i+1|i}) = diag \left(\begin{bmatrix} 1 & a^T \\ a & b \end{bmatrix}, \begin{bmatrix} 1 & c^T \\ c & R^{-1} \end{bmatrix} \right) \tag{4.64}$$

where

$$a = (x - \hat{x}_{i+1|i})^T, \quad b = P_{i+1|i}^{-1}, \quad c = (z_{i+1|i} - H\hat{x}_{i+1|i}).$$

Associated with $F(\hat{x}_{i+1|i})$ is the function

$$L(\hat{x}_{i+1|i}) = \begin{cases} logdet F(\hat{x}_{i+1|i})^{-1} & \hat{x}_{i+1|i} \in int\, E(\hat{x}_{i+1|i+1}, P_{i+1|i+1}) \\ \infty & elsewhere \end{cases}$$

The function $L(\hat{x}_{i+1|i})$ is finite if and only if $\hat{x}_{i+1|i} \in E(\hat{x}_{i+1|i+1}, P_{i+1|i+1})$ and becomes infinite as $\hat{x}_{i+1|i}$ approaches the boundary of S. It is called a barrier function for $E(\hat{x}_{i+1|i+1}, P_{i+1|i+1})$. It can be shown that when $\hat{x}_{i+1|i} \in E(\hat{x}_{i+1|i+1}, P_{i+1|i+1})$, $L(\hat{x}_{i+1|i})$ is analytic and strictly convex. The unique minimizer of $L(\hat{x}_{i+1|i})$, denoted by x^*, is referred to as the analytic center of the LMI $F(\hat{x}_{i+1|i}) > 0$. The center x^* is obtained from

$$x^* = \begin{cases} argmin\ logdet & F(\hat{x}_{i+1|i})^{-1} \\ such\ that & F(\hat{x}_{i+1|i}) > 0. \end{cases}$$

The shape of the ellipsoid $P_{i+1|i+1}$ is the Hessian of

$$log\, det\, F(\hat{x}_{i+1|i})^{-1} \tag{4.65}$$

at x^*. The analytic center x^* is the state $\hat{x}_{i+1}$ of the system and the minimum volume ellipsoid $P_{i+1|i+1}$ is the Hessian $H(x^*)$.

Summary of the algorithm :

Equations for the attitude estimation in pointing mode

- Time update

$$\hat{x}_{i+1|i} = -A_{x_{i+1}} b_{x_{i+1}}$$

$$P_{i+1|i} = (b_{x_{i+1}}^T A_{x_{i+1}} b_{x_{i+1}} - c_{x_{i+1}}) A_{x_{i+1}}^{-1}$$

- Measurement update

$$\hat{x}_{i+1|i+1} = x^*$$

$$P_{i+1|i+1} = H(x^*) = \nabla^2 L(\hat{x}_{i+1|i}) \tag{4.66}$$

4.2.6   Attitude Estimation for Acquisition Mode

The dynamic model considered for the attitude estimation for acquisition mode is given as

$$\delta x_{i+1} = (A_i + \Delta A_i(x_i))\delta x_i + f_0 + w_i$$

$$\delta z_i = (C_i + \Delta C_i(x_i))\delta x_i + c_0 + v_i \tag{4.67}$$

where A_i, $\Delta A_i(x_i)$, f_0, C_i, $\Delta C_i(x_i)$, and c_0 are given in (4.53). Given the system (4.67), the approach to be followed here is to recursively compute the minimum volume ellipsoid guaranteed to contain δx_i. It is assumed that the model uncertainties are combined with those due to linearization errors and measurement noise in the following ellipsoidal constraints

$$\frac{||\Delta A_i(x_i)||^2}{\delta_A^2} + \frac{||w_i||^2}{\delta_w^2} \leq 1, \tag{4.68}$$

$$\frac{||\Delta C_i(x_i)||^2}{\delta_C^2} + \frac{||v_i||^2}{\delta_v^2} \leq 1, \tag{4.69}$$

Time Update

The time update of the system (4.67) is as follows. Given an ellipsoid $E_{i|i}$ containing the state of the system at time step i, an ellipsoid that contains the set of states that the system can achieve at time $(i+1)$, under model uncertainty is to be determined. The set of all values of δx_{i+1} consistent with the information available at time $(i+1)$ are approximated recursively by the minimum volume ellipsoid denoted by $E_{i+1|i} = E(\hat{x}_{i+1|i}; P_{i+1|i})$. Therefore, the objective is to find the smallest ellipsoid $E_{i+1|i}$ containing the set

$$S_{i+1} = \{\delta x_{i+1} \mid \delta x_{i+1} = (A_i + \Delta A_i(x_i))\delta x_i + f_0 + w_i \, \delta x_i \in E_{i|i}, \frac{||\Delta A_i(x)||^2}{\delta_A^2} + \frac{||w_i||^2}{\delta_w^2} \leq 1\}$$

$$(4.70)$$

The dynamic equation (4.70) is written as two equations to separate the dynamics from the noise terms. This last set of equations can be written as

$$\delta x_{i+1} = A_i \delta x_i + f_0 + d_i$$

$$d_i = \Delta A_i(x_i)\delta x_i + w_i$$

The ellipsoid $E_{i|i}$, which contains the state δx_i is described as

$$E_{i|i} = \{\hat{x}_i | (x_i - \delta \hat{x}_{i|i})^T P_i^{-1}(x_i - \delta \hat{x}_{i|i})\}$$

$$(4.71)$$

To transform the problem into convex one, the ellipsoid (4.71) is rewritten in the form

$$E_{i|i} = \{\delta x_i | (\delta x_i^T Q_i \delta x_i + 2\delta x^T q_i + r_i) \leq 0\}$$

$$(4.72)$$

where

$$Q_i = P_i^{-1}, \quad q_i = -P_i^{-1}\delta \hat{x}_{i|i}, \quad r_i = \delta \hat{x}_{i|i}^T P_i^{-1} \delta \hat{x}_{i|i}.$$

Using Lemma 1 from [50], it can be shown that the quadratic constraints on the uncertainties is transformed into

$$d_i = \Delta A_i(x)\delta x_i + w_i|$$

$$|d_i||^2 \leq \delta_A^2 ||\delta x_i||^2 + \delta_w^2.$$

$$(4.73)$$

The two variables δx_i and d_i are grouped in a vector form and written as

$$s_i = \begin{bmatrix} \delta x_i \\ d_i \end{bmatrix} \qquad (4.74)$$

The ellipsoid $E_{i|i}$ written in s_i is

$$\Sigma_{i|i} = \{s_i | (s_i^T Q_{si} s_i + 2 s_i^T q_{si} + r_{si}) \leq 0\} \qquad (4.75)$$

with

$$Q_{si} = \begin{bmatrix} Q_i & 0 \\ 0 & 0 \end{bmatrix}, \qquad q_{si} = \begin{bmatrix} q_i \\ 0 \end{bmatrix}, \qquad r_{si} = r_i. \qquad (4.76)$$

The ellipsoid for the quadratic constraint (4.73) in s_i is

$$\Sigma_w = \{s_i | (s_i^T Q_w s_i + r_w) \leq 0\} \qquad (4.77)$$

where

$$Q_w = \begin{bmatrix} \delta_A^2 & 0 \\ 0 & 1 \end{bmatrix}, \qquad r_w = -\delta_w^2. \qquad (4.78)$$

Using the S-procedure, the objective is to find the ellipsoid $\Sigma_{i+1|i}$ which contains $\Sigma_{i|i}$ and Σ_w. Thus

$$\Sigma_{i+1|i} = \{s_i | (s_i^T Q_{s(i+1)} s_i + 2 s_i^T q_{s(i+1)} + r_{s(i+1)}) \leq 0\} \qquad (4.79)$$

provided

$$[I - A_i^T] q_{s(i+1)} = 0$$
$$[I - A_i^T] Q_{s(i+1)} = [0 \quad 0]. \qquad (4.80)$$

The derivations of the convex problem (4.79) are the same as described explicitly in the time update of the attitude estimation for pointing mode in subsection 4.2.5. The conditions described in (4.80) are obtained using the following mathematical derivations. First let us rewrite the equation

$$\delta x_{i+1} = A_i \delta x_i + d_i + f_0 \qquad (4.81)$$

as

$$\delta x_{i+1} = y_{i+1} + f_0 \qquad (4.82)$$

84

where

$$y_{i+1} = A_i \delta x_i + d_i. \tag{4.83}$$

The motivation behind rewriting equation (4.81) is to remove the affine term f_0 for converting the problem as described in subsection 4.2.5. Now, writing the time update ellipsoid $E(\hat{x}_{i+1|i}, P_{i+1|i})$ to be found in the new variable y_{i+1}, the ellipsoid is

$$E_{i+1|i} = \{y_{i+1} | (y_{i+1}^T Q_{i+1} y_{i+1} + 2y_{i+1}^T q_{i+1} + r_{i+1}) \le 0\} \tag{4.84}$$

By substituting y_{i+1} in (4.84), the ellipsoid $E_{i+1|i}$ is written as

$$E_{i+1|i} = \{y_{i+1} | ((A_i \delta x_i + d_i)^T Q_{i+1} (A_i \delta x_i + d_i) + 2(A_i \delta x_i + d_i)^T q_{i+1} + r_{i+1}) \le 0\}.$$

Expanding the equations and writing in the matrix notation yields

$$s_i^T \begin{bmatrix} A_i^T Q_{i+1} A_i & A_i^T Q_{i+1} \\ Q_{i+1} A_i & Q_{i+1} \end{bmatrix} s_i + 2s_i^T \begin{bmatrix} A_i^T q_{i+1} \\ q_{i+1} \end{bmatrix} + r_{i+1} \le 0 \tag{4.85}$$

In order for the ellipsoid $\Sigma_{i+1|i}$ to contain the ellipsoids $\Sigma_{i|i}$ and Σ_w, the following conditions have to be satisfied.

$$[I - A_i^T] q_{s(i+1)} = 0$$
$$[I - A_i^T] Q_{s(i+1)} = [0 \quad 0]. \tag{4.86}$$

The conditions (4.86) are obtained by equating equation (4.85) with the ellipsoid (4.79). Finally, the update ellipsoid is given as

$$E_{i+1|i} = \{y_{i+1} | (y_{i+1} - \hat{y}_{i+1|i})^T P_{i+1}^{-1} (y_{i+1} - \hat{y}_{i+1|i})\} \tag{4.87}$$

with

$$P_{i+1} = Q_{i+1}^{-1}, \quad \hat{y}_{i+1|i} = -Q_{i+1}^{-1} q_{i+1}, \quad r_{i+1} = q_{i+1}^T P_{i+1} q_{i+1} - 1 \tag{4.88}$$

Substituting y_{i+1} in equation (4.82) the update equations can be written as

$$\delta \hat{x}_{i+1|i} = -Q_{i+1}^{-1} q_{i+1} + f_0 \tag{4.89}$$

$$P_{i+1} = Q_{i+1}^{-1} \tag{4.90}$$

Measurement Update

Given $E_{i+1|i}$, the aim is for the minimum volume ellipsoid $E_{i+1|i+1}$ containing

$$I_{k+1} = \begin{cases} \delta x_{i+1} | \delta z_i = (C_i + \Delta C_i(x))\delta x_i + c_0 + v_i \ \delta x_i \in E_{i+1|i} \\ \frac{\|\Delta_{C_i}(x)\|^2}{\delta_C^2} + \frac{\|v_i\|^2}{\delta_v^2} \leq 1, \end{cases} \tag{4.91}$$

The minimum volume ellipsoid that contains the state update is given as

$$E_{i+1|i+1} = \{\delta x_{i+1|i+1} | (x_i - \hat{x}_{i+1|i+1})^T P_{i+1|i+1}^{-1}(x_i - \hat{x}_{i+1|i+1})^T \leq 1\} \tag{4.92}$$

The measurement equation (4.91) is written as two equations to separate the dynamics from the noise terms. These can also be written as

$$\delta zi = C_i \delta x_i + c_0 + e_i$$

$$e_i = \Delta C_i(x_i)\delta x_i + v_i.$$

The ellipsoid $E_{i+1|i}$, which contains the state δx_i, is described as

$$E_{i+1|i} = \{\hat{x}_i | (x_i - \delta \hat{x}_{i+1|i})^T P_{i+1|1}^{-1}(x_i - \delta \hat{x}_{i+1|i}) \leq 0\}. \tag{4.93}$$

To transform the problem into a convex problem, the ellipsoid (4.93) is rewritten in the form

$$E_{i+1|i} = \{((\delta \hat{x}_{i+1|i})^T Q_{i+1}(\delta \hat{x}_{i+1|i}) + 2(\delta \hat{x}_{i+1|i})^T q_{i+1|i} + r_{i+1|i}) \leq 0\} \tag{4.94}$$

where

$$Q_{i+1} = P_{i+1}^{-1}, \quad q_{i+1} = -P_{i+1}^{-1}\delta \hat{x}_{i+1|i}, \quad r_{i+1} = \delta \hat{x}_{i+1|i}^T P_{i+1}^{-1}\delta \hat{x}_{i+1|i}$$

Using Lemma 1 from [50], it can be shown that the quadratic constraints on the uncertainties is transformed into the equation

$$e_i = \Delta C_i(x)\delta x_i + v_i$$

$$|e_i\|^2 \leq \delta_C^2 \|\delta x_i\|^2 + \delta_v^2. \tag{4.95}$$

The two variables δx_{i+1} and e_i are grouped in a vector form and written as

$$s_{i+1} = \begin{bmatrix} \delta x_{i+1} \\ e_i \end{bmatrix} \tag{4.96}$$

The ellipsoid $E_{i+1|i}$ written in s_i is

$$\Sigma_{i+1|i} = \{s_i | (s_i^T Q_{s(i+1)} s_i + 2 s_i^T q_{s(i+1)} + r_{s(i+1)}) \leq 0\} \tag{4.97}$$

with

$$Q_{s(i+1)} = \begin{bmatrix} Q_{i+1} & 0 \\ 0 & 0 \end{bmatrix}, \quad q_{s(i+1)} = \begin{bmatrix} q(i+1) \\ 0 \end{bmatrix}, r_{s(i+1)} = r_{i+1}. \tag{4.98}$$

The ellipsoid for the quadratic constraint (4.73) in s_{i+1} is

$$\Sigma_v = \{s_i | (s_i^T R_v s_i + r_w) \leq 0\} \tag{4.99}$$

$$R_v = \begin{bmatrix} \delta_C^2 & 0 \\ 0 & 1 \end{bmatrix}, r_v = -\delta_v^2. \tag{4.100}$$

Using the s-procedure the objective is to find the ellipsoid $\Sigma_{i+1|i+1}$ which is the intersection of $\Sigma_{i+1|i}$ and Σ_v

$$\Sigma_{i+1|i+1} \supset \Sigma_{i+1|i} \bigcap \Sigma_v \tag{4.101}$$

provided

$$[I - A_i^T] Q_{s(i+1|i+1)} = [0 \quad 0]$$

$$[I - C_i^T] q_{s(i+1|i+1)} = 0. \tag{4.102}$$

The derivation of the convex problem (4.79) are the same as described explicitly in the time update of attitude estimation for acquisition mode of subsection 4.2.6. The conditions described in (4.102) can be obtained in a similar way as in the time update. By solving the optimization problem, the update ellipsoid which contains the state estimate is given as

$$\delta \hat{x}_{i+1|i+1} = -Q_{i+1|i+1}^{-1} q_{i+1|i+1} + c_0 \tag{4.103}$$

$$P_{i+1|i=1} = Q_{i+1|i+1}^{-1} \tag{4.104}$$

Summary of the algorithm: Equations for the attitude estimation for acquisition mode

- Time update

$$\delta \hat{x}_{i+1|i} = -Q_{i+1}^{-1} q_{i+1} + f_0$$

$$P_{i+1} = Q_{i+1}^{-1}$$

- Measurement update

$$\delta\hat{x}_{i+1|i+1} = -Q^{-1}_{i+1|i+1}q_{i+1|i+1} + c_0$$

$$P_{i+1|i=1} = Q^{-1}_{i+1|i+1}$$

4.2.7 Simulations

The algorithms discussed above are applied to the roll channel discussed in the subsection 4.1.2. The parameters used in the simulation are $I = 18.83 kgm^2$; $k_p = 0.15762$; $k_d = 2.51$. Additionally x_1 is the roll angle, ϕ and x_2 is the angular velocity ω_x. The initial ellipsoid in which the state lies is assumed to be $x_0 = [0.15,\ 0.4]^T$ and $P = 0.1I$, where I is the identity matrix of size 2×2. The bounds on noise W_i and V_i are $0.001I$, and $0.002I$ respectively. The simulation results for the roll channel are shown below. Figure (4.15) the phase-plane of the estimated roll angle and angular velocity ω_x using convex optimization technique is shown. Note that the simulations are only partial and does not include all the data points of an orbit. The time period for one orbit is almost 6000 seconds. For simplicity and to understand the concept, the phase-plane of fist 6 time steps is shown. From the figure it is observed that the state lies inside the ellipsoid, and as time increases, the volume of the ellipsoid decreases. In Figure (4.16) the true roll angle is compared with the estimated roll angle. The true roll angle is obtained on the ground. The true roll angle obtained in Figure 4.6 is used for comparison in this section. It is observed that the estimated roll angle (dashed line) follows the true angle (thick line).
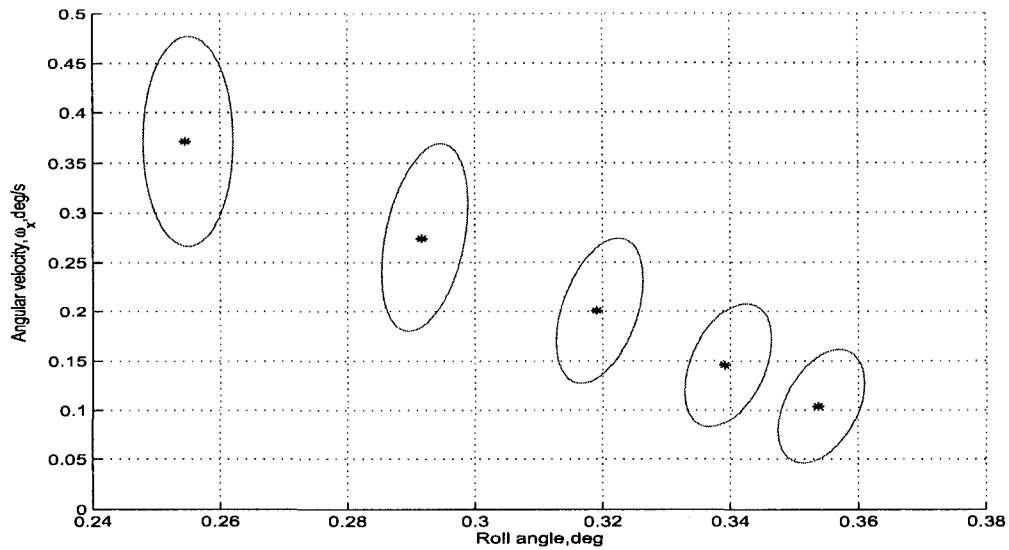
Figure 4.15: Phase-plane estimation of the roll channel
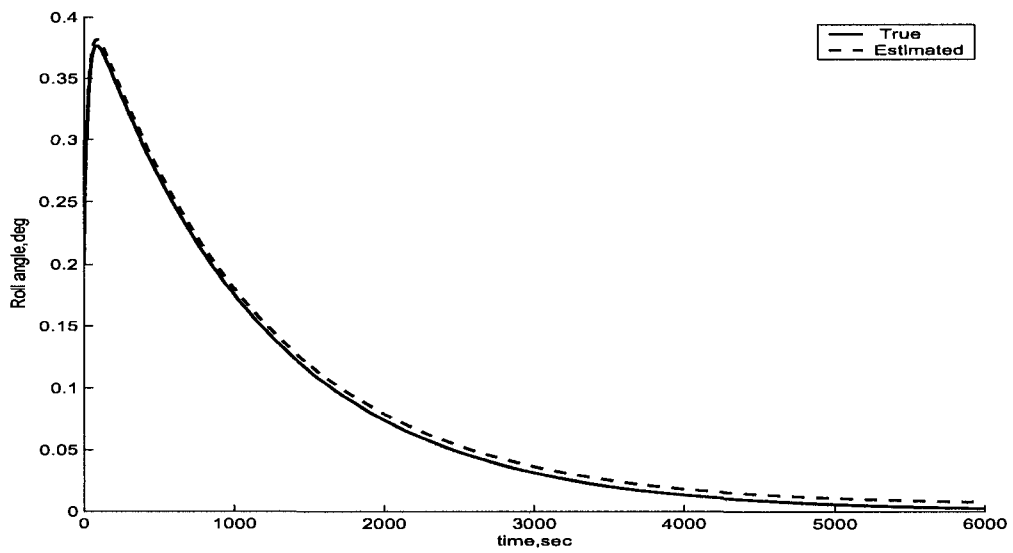
Figure 4.16: Roll angle using ellipsoidal estimation

4.3 Chapter Summary

In this chapter, three methods were proposed for attitude estimation. First, an attitude estimation problem for pointing mode is solved using modified Kalman filtering

for pointing mode. Secondly, the same attitude estimation problem is solved using guaranteed ellipsoidal estimation techniques. Depending on the available data, either method can be used. Thirdly, the attitude estimation problem for acquisition mode is solved using the guaranteed ellipsoidal estimation technique. The three principal contributions in this chapter are:

- Applying the modified Kalman filter to the satellite attitude estimation problem.

- Developing an estimation algorithm using analytic centers for the spacecraft attitude estimation problem in pointing mode.

- Developing an ellipsoidal estimation algorithm for acquisition mode, where the dynamic model is nonlinear. This nonlinear estimation algorithm was based on a convex optimization technique.

The work on attitude estimation discussed in this chapter will be included in the development of new approaches to the attitude control problem, discussed in the next chapter.

Chapter 5

ATTITUDE CONTROL

For any spacecraft attitude control system, a successful choice of an appropriate attitude determination method is very important to meet mission requirements, which was the discussion in the previous chapters. In this chapter, spacecraft attitude control synthesis is addressed. The main contribution in this chapter is the development of a two-step switched approach for satellite attitude control in the acquisition mode (convergence of attitude and body rates from an arbitrary motion to zero). In this case attitude errors cannot be considered as small angles and, strictly speaking, linear control theory and linear controller are not applicable because satellite angular dynamics are nonlinear for an arbitrary motion and can be considered linear only under small angle errors. The proposed method guarantees both global stabilization and local performance. The first step consists of parameterizing the attitude dynamics of the satellite by Modified Rodrigues Parameters (MRP) and searching for a stabilizing controller using Sum of Squares (SOS). In the second step, when the rigid body is close to its desired attitude set point, the control switches to a linear optimal controller. This approach can guarantee local performance and global performance by using less computational operations in a microprocessor when implemented. The effectiveness of the proposed control technique is shown in simulations for a large-angle acquisition maneuver.

The chapter is divided into five parts and is organized as follows. In section 1 an introduction to the considered satellite attitude control is discussed. The previous

work related to the satellite attitude control problem is addressed in section 2. Section 3 briefly describes attitude kinematics and dynamics. Section 4 formulates stabilizing controller synthesis as an SOS feasibility problem and controller synthesis as a linear quadratic regulator problem. Section 5 presents the switching law. Finally, Section 6 presents a numerical example.

5.1 Introduction

Satellite attitude control is one of the most widely studied problems largely because of its importance in many practical applications of satellite Attitude Control System (ACS) design. The objective of satellite ACS is to maintain desired attitude despite disturbances. For various satellite missions it is required to acquire desired attitude as soon as possible to start desired mission activity or to have safe Sun lighting conditions for satellite power generation. For this purpose satellite ACS usually has specially dedicated mode called acquisition mode. Very often this is just a conventional linear PD controller [65] with a wide bandwidth (that can provide a short decaying time). However, the linear controller works effectively within a narrow range of small Euler angles (less than 20 deg), during which, satellite angular dynamic equations can be considered as linear. To prevent any unexpected effects when the angles are large a saturation zone is used. Such a controller within the linear zone can be considered as a linear one and outside of this zone as a bang-bang controller [65]. This is the most common approach implemented by engineers for years in many satellite ACS designs [36]. It should be noted that acquisition mode has not been widely discussed in publications and the intent of this chapter is to contribute beneficial results providing with application of optimal control theory. Unlike the formal approach of using a global optimal non-linear controller throughout the mission, this chapter considers switching the global controller and linear controller using optimization techniques. The proposed technique is more computationally economical and can be easily implemented in practical satellite ACS design which is illustrated in section 5.6.

92

5.2 Previous Work

Crouch [17] extended the work of Meyer's [45] and provided necessary and sufficient conditions for the controllability of a rigid body in the case of one, two or three independent torques. Wie and Barba [75] derived nonlinear feedback control schemes using quaternions and angular velocity feedback and proved asymptotic stability using Lyapunov functions. Tsiotras [69–71] extended these results using a Lyapunov function that involved the sum of a quadratic term in the angular velocities and a logarithmic term in the kinematic parameters leading to the design of linear controllers. Singh and Bossart [66] derived a feedback control law for prescribed pitch attitude tracking based on dynamic feedback linearization for spacecraft using a control moment gyro. Singh and Iyer [67] used sliding modes for attitude control of an orbiting spacecraft using reaction jets in the presence of uncertainty. A nonlinear H_∞ control methodology had been developed by Kang [29] to control rigid spacecraft with three torques in the presence of disturbances. This methodology involves the solution of the Hamilton-Jacobi-Isaacs inequalities. Crassidis $et\ al.$ [16] were the first to consider the problem of controlling a spacecraft without full state feedback. The controller is designed by minimizing the norm-squared local errors between the predicted and desired quantities. A Lyapunov-based adaptive controller that estimates external torques has been developed by Schaub $et\ al.$ [57]. Lim [39] developed a linear parameter-varying controller, in which a single quadratic Lyapunov function for each frozen Linear Time-Invariant (LTI) system was used in a parameter variation set. Raymond and Johan [53] used integrator backstepping design for satellite attitude control based on quaternions. In the authors' previous work [20], a two step integrated and systematic approach for modelling and control of large angle attitude maneuvers of a rigid body was developed. The difference in the types of maneuvers that are usually performed during these two modes (acquisition and pointing) naturally leads to the consideration of a switching control law in which a nonlinear controller can be used during the acquisition mode and a linear controller is used during the pointing mode. In such a mission, nonlinear control is only needed during the

acquisition mode. While the problem of attitude control and stabilization has been a subject of much research, the problem of switching between a nonlinear controller and a linear controller has not been explicitly considered for spacecraft. In fact, much of the switching work in the literature is between linear models. The linear models are obtained by linearizing around multiple equilibrium points and then designing local controllers for each model. This kind of control strategy is called gain scheduling, and is treated in [31]. A recent work by Hamada *et al.* [21] applied the gain scheduling technique to the problem of satellite attitude control problem. Switching between a nonlinear controller and a local linear controller was considered previously to implement anti-windup controllers [3]. In [48], a fuzzy controller was used for swinging up a pendulum and a linear state feedback controller was used for balancing the pendulum in the upper position.

The aforementioned techniques use mainly Lyapunov and storage functions for analysis, and control Lyapunov functions for synthesis. However, these approaches suffer from one drawback: constructing such functions is far from obvious and not systematic. In particular, no general systematic and efficient computational method has been suggested in previous research to obtain the Lyapunov function. Further the global stability is proved by using quaternions. However quaternions have one redundant parameter.

Based on the above limitations, the main contribution of this chapter is the development of a two-step switched approach for large-angle attitude maneuvers of satellites. The method guarantees both global stabilization and local performance. The first step consists of parameterizing the attitude dynamics of the satellite by Modified Rodrigues Parameters (MRP) and searching for a stabilizing controller using Sum of Squares (SOS). From a computational perspective, the method relaxes the search for positive definite stability certificate functions (eg. Lyapunov functions) to a search for SOS certificate functions (of appropriate polynomials). In the second step, when the rigid body is close to its desired attitude set point, the control switches to a linear controller that can guarantee local performance and that uses less computational operations in a microprocessor when implemented.

5.3 Attitude Kinematics and Dynamics

This section presents a brief review of the kinematic and dynamic equations of motion for a three-axis stabilized spacecraft using MRP.

5.3.1 Attitude Kinematics

The MRP are a recent addition to the family of attitude representations and are particularly well suited for describing very large attitudes [56]. The MRP are able to describe an orientation with only three parameters, instead of the four parameters required by quaternions.

The MRP vector $\boldsymbol{\sigma}$ can be expressed in terms of the principal rotation elements $(\hat{\mathbf{e}}, \boldsymbol{\Phi})$ as

$$\boldsymbol{\sigma} = \hat{\mathbf{e}} \tan \frac{\boldsymbol{\Phi}}{4} \tag{5.1}$$

or in terms of the four quaternion elements (q_1, q_2, q_3, q_4) as

$$\boldsymbol{\sigma} = \begin{bmatrix} q_1/(1+q_4) \\ q_2/(1+q_4) \\ q_3/(1+q_4) \end{bmatrix}. \tag{5.2}$$

It can be seen from these equations that the MRP representation has a geometric singularity at $\boldsymbol{\Phi} = \pm 360°$, which corresponds to $q_4 = -1$ in (5.2). Thus, any rotation less than a complete revolution can be expressed using these parameters. Note however that complete revolutions are generally not encountered in most attitude maneuvers as the spacecraft would end in the same orientation as it started.

The kinematic differential equation can be written in terms of the MRP [62] as

$$\dot{\boldsymbol{\sigma}} = \Omega(\boldsymbol{\sigma})\boldsymbol{\omega}, \tag{5.3}$$

where $\boldsymbol{\omega} = [\omega_x \ \omega_y \ \omega_z]^T$ are the angular velocities of the satellite about each of the principal body axes,

$$\Omega(\boldsymbol{\sigma}) = \frac{1}{4} \begin{bmatrix} 1 - \sigma^2 + 2\sigma_1^2 & 2(\sigma_1\sigma_2 - \sigma_3) & 2(\sigma_1\sigma_3 - \sigma_2) \\ 2(\sigma_2\sigma_1 - \sigma_3) & 1 - \sigma^2 + 2\sigma_2^2 & 2(\sigma_2\sigma_3 - \sigma_1) \\ 2(\sigma_3\sigma_1 - \sigma_2) & 2(\sigma_3\sigma_2 - \sigma_1) & 1 - \sigma^2 + 2\sigma_3^2 \end{bmatrix}$$

and $\sigma^2 = \sigma_1^2 + \sigma_2^2 + \sigma_3^2$. The next subsection describes the attitude dynamic equations.

5.3.2 Attitude Dynamics

The attitude dynamics are given by the Newton-Euler's moment equations [65] and are expressed in satellite principal inertia axes frame as

$$
\begin{aligned}
I_x \dot{\omega}_x + (I_z - I_y)\omega_y \omega_z &= T_x \\
I_y \dot{\omega}_y + (I_x - I_z)\omega_z \omega_x &= T_y \\
I_z \dot{\omega}_z + (I_y - I_x)\omega_x \omega_y &= T_z
\end{aligned}
\tag{5.4}
$$

which can also be written as

$$
\begin{bmatrix} \dot{\omega}_x \\ \dot{\omega}_y \\ \dot{\omega}_z \end{bmatrix} = \begin{bmatrix} \frac{I_y - I_z}{I_x}\omega_y \omega_z \\ \frac{I_z - I_x}{I_y}\omega_z \omega_x \\ \frac{I_x - I_y}{I_z}\omega_x \omega_y \end{bmatrix} + \begin{bmatrix} \frac{1}{I_x} & 0 & 0 \\ 0 & \frac{1}{I_y} & 0 \\ 0 & 0 & \frac{1}{I_z} \end{bmatrix} \begin{bmatrix} T_x \\ T_y \\ T_z \end{bmatrix}
\tag{5.5}
$$

or

$$
\dot{\boldsymbol{\omega}} = -\mathbf{I}^{-1}(\boldsymbol{\omega} \times \mathbf{I}\boldsymbol{\omega}) + \mathbf{I}^{-1}\mathbf{u}
\tag{5.6}
$$

where $\mathbf{u} = [T_x \; T_y \; T_z]^T$ are the external torques acting on the satellite, and the principal moments of inertia I_x, I_y and I_z are the components of the inertia tensor $\mathbf{I}$ given by

$$
\mathbf{I} = \begin{bmatrix} I_x & 0 & 0 \\ 0 & I_y & 0 \\ 0 & 0 & I_z \end{bmatrix}.
\tag{5.7}
$$

Throughout this chapter it is assumed that there are no disturbance torques and only 3-axis control torques are applied to satellite $T = T_c$. The state variable equations are obtained by combining equations (5.3) and (5.5) and can be written in the form

$$
\begin{bmatrix} \dot{\omega}_x \\ \dot{\omega}_y \\ \dot{\omega}_z \\ \dot{\sigma}_1 \\ \dot{\sigma}_2 \\ \dot{\sigma}_3 \end{bmatrix} = \begin{bmatrix} f_1 \\ f_2 \\ f_3 \\ f_4 \\ f_5 \\ f_6 \end{bmatrix} + \begin{bmatrix} 1/I_x & 0 & 0 \\ 0 & 1/I_y & 0 \\ 0 & 0 & 1/I_z \\ 0 & 0 & 0 \\ 0 & 0 & 0 \\ 0 & 0 & 0 \end{bmatrix} \begin{bmatrix} T_x \\ T_y \\ T_z \end{bmatrix}
\tag{5.8}
$$

where

$$f_1 = [(I_y - I_z)/I_x]\omega_y\omega_z,$$

$$f_2 = [(I_z - I_x)/I_y]\omega_z\omega_x$$

$$f_3 = [(I_x - I_y)/I_z]\omega_x\omega_y$$

$$f_4 = \tfrac{1}{4}[1 - \sigma^2 + 2\sigma_1^2]\omega_x + \tfrac{1}{4}[2(\sigma_1\sigma_2 - \sigma_3)]\omega_y + \tfrac{1}{4}[2(\sigma_1\sigma_3 - \sigma_2)]\omega_z \qquad (5.9)$$

$$f_5 = \tfrac{1}{4}[2(\sigma_2\sigma_1 - \sigma_3)]\omega_x + \tfrac{1}{4}[1 - \sigma^2 + 2\sigma_2^2]\omega_y + \tfrac{1}{4}[2(\sigma_2\sigma_3 - \sigma_1)]\omega_z$$

$$f_6 = \tfrac{1}{4}[2(\sigma_3\sigma_1 - \sigma_2)]\omega_x + \tfrac{1}{4}[2(\sigma_3\sigma_2 - \sigma_1)]\omega_y + \tfrac{1}{4}[1 - \sigma^2 + 2\sigma_3^2]\omega_z$$

Using the state vector $\mathbf{x} = [\omega_x \ \omega_y \ \omega_z \ \sigma_1 \ \sigma_2 \ \sigma_3]^T$, containing the angular velocities and the MRP, and the input torque vector $\mathbf{u} = [T_x \ T_y \ T_z]^T$, the dynamic equations become

$$\dot{\mathbf{x}} = \mathbf{f}(\mathbf{x}) + \mathbf{B}\mathbf{u}, \qquad (5.10)$$

where

$$\mathbf{f}(\mathbf{x}) = \begin{bmatrix} f_1 \\ f_2 \\ f_3 \\ f_4 \\ f_5 \\ f_6 \end{bmatrix}, \quad \mathbf{B} = \begin{bmatrix} 1/I_x & 0 & 0 \\ 0 & 1/I_y & 0 \\ 0 & 0 & 1/I_z \\ 0 & 0 & 0 \\ 0 & 0 & 0 \\ 0 & 0 & 0 \end{bmatrix}.$$

The next subsection reviews the linearized attitude dynamics, which will be used for designing the local linear controller.

5.3.3   Linearized Attitude Dynamics

To derive a linearized model of the satellite attitude, the nonlinear model in (5.10) has to be differentiated with respect to the total state vector, which is chosen as $\mathbf{x} = [\omega_x \ \omega_y \ \omega_z \ \sigma_1 \ \sigma_2 \ \sigma_3]^T$. The linearized system can then be written as

$$\Delta\dot{\mathbf{x}} = \mathbf{A}_l\Delta\mathbf{x} + \mathbf{B}\mathbf{u} \qquad (5.11)$$

where the matrix $\mathbf{A}_l$ is of the form

$$\mathbf{A}_l = \begin{bmatrix} \frac{\partial f_1}{\partial x_1} & \cdots & \frac{\partial f_1}{\partial x_6} \\ \frac{\partial f_2}{\partial x_1} & \cdots & \frac{\partial f_2}{\partial x_6} \\ \vdots & \cdots & \vdots \\ \frac{\partial f_6}{\partial x_1} & \cdots & \frac{\partial f_6}{\partial x_6} \end{bmatrix}_{x_p} \tag{5.12}$$

Linearizing the nonlinear system (5.10) around an equilibrium point p,
$\mathbf{x}_p = \begin{bmatrix} 0 & 0 & 0 & 0 & 0 & 0 \end{bmatrix}^T$ yields a linear state space model

$$\dot{\mathbf{x}} = \mathbf{A}_l \mathbf{x} + \mathbf{B} \mathbf{u} \tag{5.13}$$

where $\mathbf{A}_l = \begin{bmatrix} O_{3\times3} & O_{3\times3} \\ 1/4I & O_{3\times3} \end{bmatrix}$, $I = \begin{bmatrix} 1 & 0 & 0 \\ 0 & 1 & 0 \\ 0 & 0 & 1 \end{bmatrix}$, $O = \begin{bmatrix} 0 & 0 & 0 \\ 0 & 0 & 0 \\ 0 & 0 & 0 \end{bmatrix}$.

5.3.4 Problem Statement

Given attitude dynamics (5.10), the problem is to design an attitude controller for large-angle attitude maneuvers, a linear controller for local performance, and a stabilizing switching rule that switches between the global nonlinear controller and the local linear controller. The following steps are used in solving the problem:

1. Design a nonlinear controller for the nonlinear system (5.10) using SOS.

2. Design a linear controller for the linearized model (5.13) using LQR.

3. Using the control Lyapunov function obtained in step 1, and the linear controller obtained in step 2, find the largest region of attraction.

4. Propose a switching strategy between the nonlinear controller and the linear controller that switches controllers once this region of attraction is reached.

5.4 Satellite Attitude Control

Attitude control system consists of two steps namely, attitude maneuver and attitude stabilization. Attitude maneuvering is the process of controlling the reorientation of

98

the spacecraft from one attitude to another. Attitude stabilization is the process of maintaining an existing orientation. The controller design approach proposed here is broken up into two steps. The first part involves the design of a controller that performs the large-angle attitude maneuver. The second part involves the design of an optimal state feedback controller for the linearized model that will stabilize the satellite around the equilibrium position and guarantees that a performance measure is achieved.

5.4.1 Attitude Maneuver

After release from the launch vehicle, a satellite tumbles freely but with known bounds on the initial angular velocity. The objectives of the attitude control are to first damp the high angular velocity, then to stabilize the satellite in three axes with respect to the orbit. Linearized equations of motion cannot be applied, since a control strategy satisfying global stability of the satellite motion is necessary. Thus, a nonlinear controller is designed in this section. The nonlinear controller design will now be formulated as an optimization program. The formulation consists of the two steps described next.

Model Parameterization

The model parameterization consists of rewriting the equations (5.10) in the form

$$\dot{\mathbf{x}} = \mathbf{A}(\mathbf{x})\mathbf{x} + \mathbf{B}\mathbf{u}, \qquad (5.14)$$

with

$$\mathbf{x} = \begin{bmatrix} \omega_x \\ \omega_y \\ \omega_z \\ \sigma_1 \\ \sigma_2 \\ \sigma_3 \end{bmatrix}, \quad \mathbf{A}(\mathbf{x}) = \begin{bmatrix} 0 & a_{12} & 0 & 0 & 0 & 0 \\ 0 & 0 & a_{23} & 0 & 0 & 0 \\ a_{31} & 0 & 0 & 0 & 0 & 0 \\ a_{41} & a_{42} & a_{43} & 0 & 0 & 0 \\ a_{51} & a_{52} & a_{53} & 0 & 0 & 0 \\ a_{61} & a_{62} & a_{63} & 0 & 0 & 0 \end{bmatrix}, \quad \mathbf{B} = \begin{bmatrix} 1/I_x & 0 & 0 \\ 0 & 1/I_y & 0 \\ 0 & 0 & 1/I_z \\ 0 & 0 & 0 \\ 0 & 0 & 0 \\ 0 & 0 & 0 \end{bmatrix},$$

99

where

$$a_{12} = [(I_y - I_z)/I_x]\omega_z, \qquad a_{23} = [(I_y - I_z)/I_x]\omega_z, \qquad a_{31} = [(I_x - I_y)/I_z]\omega_y,$$

$$a_{41} = \tfrac{1}{4}[1 - \sigma^2 + 2\sigma_1^2], \qquad a_{42} = \tfrac{1}{4}[2(\sigma_1\sigma_2 - \sigma_3)], \qquad a_{43} = \tfrac{1}{4}[2(\sigma_1\sigma_3 - \sigma_2)],$$

$$a_{51} = \tfrac{1}{4}[2(\sigma_1\sigma_3 - \sigma_2)], \qquad a_{52} = \tfrac{1}{4}[1 - \sigma^2 + 2\sigma_2^2], \qquad a_{53} = \tfrac{1}{4}[1 - \sigma^2 + 2\sigma_2^2],$$

$$a_{61} = \tfrac{1}{4}[2(\sigma_3\sigma_1 - \sigma_2)], \qquad a_{62} = \tfrac{1}{4}[2(\sigma_3\sigma_2 - \sigma_1)], \qquad a_{63} = \tfrac{1}{4}[1 - \sigma^2 + 2\sigma_3^2].$$

For this model parameterization, a quadratic control Lyapunov function is proposed to perform the controller synthesis using SOS technique.

SOS Controller Design

This step involves designing a Lyapunov-based controller using SOS. However, first a brief description of Sum of Squares is addressed. For $\mathbf{x} \in \mathbb{R}^n$, a multivariate polynomial $p(\mathbf{x})$ is a sum of squares if there exist some polynomials $f_i(\mathbf{x})$, $i = 1, \ldots, M$, such that [51]

$$p(\mathbf{x}) = \sum_{i=1}^{M} f_i^2(\mathbf{x}). \tag{5.15}$$

A polynomial $p(\mathbf{x})$ of degree $2d$ is a sum of squares if and only if there exists a positive semidefinite matrix Q and a vector of monomials $Z(\mathbf{x})$, which contains monomials in $\mathbf{x}$ of degree less than d, such that [51]

$$p(\mathbf{x}) = Z(\mathbf{x})^T Q Z(\mathbf{x}). \tag{5.16}$$

It should be noted that $p(\mathbf{x})$ being a sum of squares implies that $p(\mathbf{x}) \geq 0$, but the converse is generally not true. Consider a candidate Lyapunov function

$$V(\mathbf{x}) = \mathbf{x}^T Q \mathbf{x}, \tag{5.17}$$

where $Q = Q > 0$. Differentiating the Lyapunov function (5.17) along the trajectories of (5.14)

$$\dot{V} = (\mathbf{A}(\mathbf{x})\mathbf{x} + \mathbf{B}\mathbf{u})^T Q \mathbf{x} + \mathbf{x}^T Q (\mathbf{A}(\mathbf{x})\mathbf{x} + \mathbf{B}\mathbf{u}) \tag{5.18}$$

Assuming a control input $\mathbf{u}$ of the form

$$\mathbf{u}(\mathbf{x}) = K(\mathbf{x})\mathbf{z}, \tag{5.19}$$

with $\mathbf{z} = Q\mathbf{x}$ and substituting into equation (5.18) yields

$$\dot{V} = \mathbf{x}^T(\mathbf{A(x)} + \mathbf{B}K(\mathbf{x})Q)^T Q\mathbf{x} + \mathbf{x}^T Q[\mathbf{A(x)} + \mathbf{B}K(\mathbf{x})Q]\mathbf{x} \qquad (5.20)$$

Using $\mathbf{x} = P\mathbf{z}$, where $P = Q^{-1}$ equation (5.20) can be rewritten as

$$\dot{V} = \mathbf{z}^T[P\mathbf{A(x)}^T + \mathbf{A(x)}P + (\mathbf{B}K(\mathbf{x}))^T + \mathbf{B}K(\mathbf{x})]\mathbf{z} \qquad (5.21)$$

Note that $\dot{V}$ is a polynomial function and the condition that must be imposed to this polynomial for asymptotic stability of the closed-loop system is $\dot{V} < 0$. However, it is well known that verifying a given polynomial is non-negative is in general a Nondeterministic Polynomial-time ($\mathcal{NP}$) hard problem [49]. Therefore, a relaxation of the non-positive condition proposed by Parrilo [49] is to limit the use of polynomials to a special form that is known to be positive semi-definite: sums of squares (SOS).

A simplified version of a Theorem from [52] is stated that will be useful to prove that condition (5.21) is asymptotic stability.

Theorem 5.4.1. *[52] For the system (5.14), suppose there exists $P = P^T > 0$, a polynomial matrix $K(\boldsymbol{x})$, and a sum of squares $\epsilon(\boldsymbol{x})$, such that the following expression*

$$-v^T(P\boldsymbol{A}^T(\boldsymbol{x}) + \boldsymbol{A}(\boldsymbol{x})P + K^T(\boldsymbol{x})\boldsymbol{B}^T(\boldsymbol{x}) + \boldsymbol{B}(\boldsymbol{x})K(\boldsymbol{x}) + \epsilon(\boldsymbol{x})I)v, \qquad (5.22)$$

is SOS, where $v \in \mathbb{R}^n$. Then the state feedback stabilization problem is solvable, and a controller that stabilizes the system is given by

$$\boldsymbol{u}(\boldsymbol{x}) = K(\boldsymbol{x})P^{-1}\boldsymbol{x}. \qquad (5.23)$$

Furthermore, if equation (5.22) holds with $\epsilon(x) > 0$ for $x \neq 0$, then the zero equilibrium is globally asymptotically stable.

Proof: It follows from the proof of [52] with $P(\tilde{x}) = P$, $Z(\mathbf{x}) = \mathbf{x}$ and $M = I$.

Based on Theorem 5.4.1 and the relaxations using sum of squares techniques, the following control optimization problem is defined.

101

Definition 5.4.1. *The attitude control design optimization problem is:*

$$find \quad P, \ K(\boldsymbol{x})$$

$$s.t. \quad (P - \epsilon_1 I) > 0, \ \epsilon_1 > 0, \ \epsilon_2(x) \ \text{is} \ \text{SOS}$$

$$-z^T[P\boldsymbol{A}^T + \boldsymbol{A}P + (\boldsymbol{B}\boldsymbol{K})^T + \boldsymbol{B}\boldsymbol{K}]z - \epsilon_2||\boldsymbol{x}||^2 \ \text{is} \ \text{SOS}$$

where I is an identity matrix. The next section will present the linear controller design.

5.4.2 Attitude Stabilization

The state feedback controller responsible for maintaining the satellite in a given attitude is based on a Linear Quadratic Regulator (LQR) [26] design using the linearized system (5.13). The LQR is an optimal control problem where the state equation of the plant is linear, the cost function is quadratic, and the test conditions consist of initial conditions on the state and no disturbance inputs. For a linear time-invariant system

$$\dot{\mathbf{x}} = \mathbf{A}\mathbf{x} + \mathbf{B}\mathbf{u}, \tag{5.24}$$

where $\mathbf{x}(0) = \mathbf{x}_0$, $\mathbf{x} \in \mathbb{R}^n$ is the state vector and $\mathbf{u} \in \mathbb{R}^m$ is the vector of control variables. It is desired to minimize the quadratic function of the form

$$J = \int_0^\infty [\mathbf{x}(t)^T Q \mathbf{x}(t) + \mathbf{u}(t)^T R \mathbf{u}(t)]dt \tag{5.25}$$

subject to the system dynamical equation (5.24), where Q and R are weighting parameters that penalize the energy on the states and control inputs, respectively. To control the state and actuator usage the system must fulfill the controllability condition according to [31].

Definition 5.4.2. *[26] (Controllability) The state and input matrices $(\boldsymbol{A}, \boldsymbol{B})$ must satisfy the controllability condition to ensure that there exists a control $\boldsymbol{u}$ which can drive any arbitrary state $\boldsymbol{x}$. The controllability condition requires that the matrix*

$$C = \begin{bmatrix} \boldsymbol{B} & \boldsymbol{A}\boldsymbol{B} & \dots \boldsymbol{A}^{n-1}\boldsymbol{B} \end{bmatrix} \tag{5.26}$$

must be of full row rank.

102

The optimal control law that solves the LQR problem is given by [26]

$$\mathbf{u}_l = \mathbf{k}_l \mathbf{x} \tag{5.27}$$

where

$$\mathbf{k}_l = -R^{-1} B^T P^* \tag{5.28}$$

is the optimal feedback gain and P^* is the unique, positive semidefinite solution to the algebraic Riccati equation [26]

$$\mathbf{A}^T P^* + P^* \mathbf{A} - P^* \mathbf{B} R^{-1} \mathbf{B}^T P^* + Q = 0. \tag{5.29}$$

Thus the problem of finding the optimal gain matrix $\mathbf{k}_l$ reduces to the problem of solving an algebraic Riccati equation for P^*. This matrix can then be substituted into equation (5.27), which stabilizes the system around the linearized point and guarantees the required performance. Since this control law is based on the linearized system, the state feedback optimal controller is only effective when the system is close to the linearizing point, i.e., when the satellite is in the pointing mode.

5.5 Switching between Global and Local Controller

The objective of this section is to formulate a switching strategy to switch from the globally stabilizing controller in acquisition mode to the local performance controller in pointing mode as shown in Figure 5.1. The theory proposed here is, that the switching occurs when the satellite approaches the maximum attractive region for the linear controller that can be estimated using the quadratic Lyapunov function (5.17). Given this Lyapunov function and the linear controller (5.27), the objective is therefore to find the largest invariant set

$$\Omega_\alpha = \{\mathbf{x} \in \mathbb{R}^n | V(\mathbf{x}) < \alpha\} \tag{5.30}$$

for the nonlinear closed-loop system which is obtained by substituting the linear controller (5.27) into equation: (5.14)

$$\dot{\mathbf{x}} = \mathbf{A}(\mathbf{x})\mathbf{x} + \mathbf{B} \mathbf{k}_l \mathbf{x}. \tag{5.31}$$
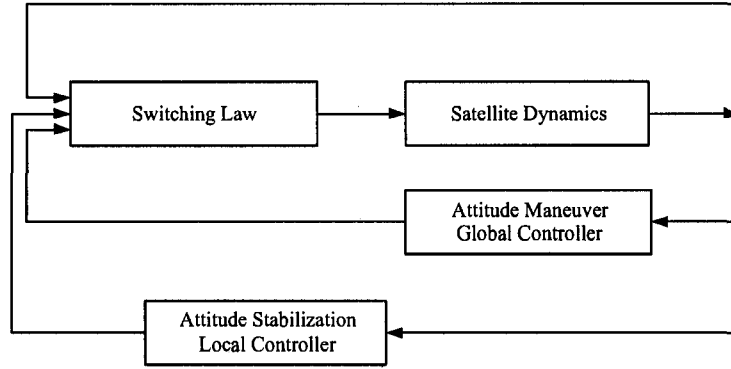
Figure 5.1: Switching between global and local controller

Based on Khalil ([31], pp. 122), if there is a Lyapunov function that satisfies the conditions of asymptotic stability over a bounded domain $\mathcal{D}$ and if Ω_α is contained in $\mathcal{D}$, then every trajectory starting in Ω_α remains in Ω_α and approaches the origin as $t \to \infty$. Using the dynamics (5.31), the derivative of the candidate Lyapunov function (5.17) along the trajectories of the system is

$$\dot{V}_c = \mathbf{x}^T[(\mathbf{A}(\mathbf{x}) + (\mathbf{Bk}_l))^T Q + Q(\mathbf{A}(\mathbf{x}) + (\mathbf{Bk}_l))]\mathbf{x}. \qquad (5.32)$$

A sufficient condition for estimating the largest region of attraction can now be formulated as the following optimization problem.

Definition 5.5.1. *Given* $Q,\ k_l$

$$max \quad \alpha$$
$$s.t. \quad \epsilon_3 > 0, s(x) \ is \ SOS$$
$$\quad - s(x)(V(x) - \alpha) \, is \ SOS$$
$$\quad -\dot{V}_c - \epsilon_3||x||^2 + s(x)(V(x) - \alpha) \ is \ SOS$$

The above optimization problem 5.5.1 is biconvex. With the recent introduction of YALMIP [40] and PENBMI [34], which allows to solve locally biconvex optimization problem, the above optimization problem is solved, resulting in a region

$$\Omega_{\alpha^*} = \{\mathbf{x} \in \mathbb{R}^n | V(\mathbf{x}) < \alpha^*\} \qquad (5.33)$$

where Ω_{α^*} is the largest region of attraction that can be found numerically.

104

Given a nonlinear controller (5.23) for the system (5.14), a linear controller (5.27) designed for the linearized system (5.13), and the largest region of attraction (5.33) for the nonlinear closed-loop system (5.31), the switching between the controllers happens when the states enter the largest region of attraction. The linear controller is used when the states are inside the region of attraction and the nonlinear controller is used when the states are outside the region of attraction:

$$\mathbf{U} = \begin{cases} \mathbf{k}_l \mathbf{x} & \text{if } \mathbf{x} \in \Omega_{\alpha^*}; \\ K(\mathbf{x})Q\mathbf{x} & \text{otherwise.} \end{cases} \tag{5.34}$$

Now, the system dynamics can be written as

$$\dot{\mathbf{x}} = f_l(\mathbf{x}) = \mathbf{Ax} + \mathbf{Bk}_l\mathbf{x}, \tag{5.35}$$

$$\dot{\mathbf{x}} = f_{nl}(\mathbf{x}) = \mathbf{A}(\mathbf{x})\mathbf{x} + \mathbf{B}K(\mathbf{x})Q\mathbf{x}, \tag{5.36}$$

Theorem 5.5.1. *For system (5.14), let there exist a global control Lyapunov function of the form (5.17), a nonlinear controller (5.23), and a linear controller (5.27) for the linearized system (5.13), then the system (5.14) is asymptotically stable when using the switching law (5.34).*

Proof

The proof of this theorem is divided into three parts.

1. *If the states start outside the region of attraction, the states will reach this region in a finite time of T. To prove that the trajectories of the closed loop system converge to a region Ω_{α^*}, the comparison lemma [31] is used. From the conditions in definition 5.4.1,*

$$-\nabla V^T f_{nl}(\boldsymbol{x}) - \epsilon_2 ||\boldsymbol{x}||^2 \text{ is SOS}$$

   which implies

$$\nabla V^T f_{nl}(\boldsymbol{x}) \leq -\epsilon_2 ||\boldsymbol{x}||^2.$$

   Given that $V(\boldsymbol{x}) = \boldsymbol{x}^T Q \boldsymbol{x} < \lambda_{max}(Q)||\boldsymbol{x}||^2$, it follows that

$$\nabla V^T f_{nl}(\boldsymbol{x}) < -\beta V(\boldsymbol{x}),$$

105

where $\beta = \frac{\epsilon_2}{\lambda_{max}(Q)}$ is the decay rate and $\lambda_{max}(Q)$ is the maximum eigenvalue of Q. Using the comparison lemma, the statement $V(t) < V(0)e^{-\beta t}$ can be proven. However from definition 5.5.1, $V(t) = \alpha^*$, which implies

$$\alpha^* = V(0)e^{-\beta t}$$

$$t < -\frac{1}{\beta}ln\frac{\alpha^*}{V(0)} \tag{5.37}$$

From equation (5.37) it can be concluded that the system trajectories converge to the region within a finite time $t = T$.

2. *If the states start inside the region of attraction, by the definition of the region of attraction, they remain in the region. Given the definition of region of attraction in (5.30), one can conclude that $V(x) - \alpha < 0$. Using the definition 5.5.1, it can be shown that the equation*

$$-\nabla V^T f_l(x) - \epsilon_3||x||^2 + s(x)(V(x) - \alpha)$$

is SOS, where $s(x)$ is a sum of squares polynomial.

3. *If the states start at the boundary of the region of attraction, then the states will enter into the region of attraction, because of the properties of the Lyapunov theory.*

$$\frac{\partial V}{\partial x}\dot{x} = \nabla V^T f_{nl}(x) < -\epsilon_2||x||^2 < 0 \tag{5.38}$$

$$\frac{\partial V}{\partial x}\dot{x} = \nabla V^T f_l(x) < -\epsilon_3||x||^2 < 0 \tag{5.39}$$

The system dynamics at the boundary is the convex combination of the nonlinear system vector (5.36) and the linear system vector (5.35) for $0 \leq l_1 \leq 1$ and written as

$$f_B(x) = l_1 f_{nl}(x) + (1 - l_1)f_l(x). \tag{5.40}$$

Therefore using the condition,

$$\dot{V} = \nabla V^T f_B(x)$$

$$= l_1 \nabla V^T f_{nl}(x) + (1 - l_1)\nabla V^T f_l(x) < -l_1\epsilon_2||x||^2 - (1 - l_1)\epsilon_3||x||^2 < 0 \tag{5.41}$$

it is concluded that there will be no sliding modes or chattering.

5.6 Simulation Results

The preceding theoretical results are now applied to a numerical example. The objective is to bring a rigid spacecraft with an initial nonzero attitude to rest at a zero attitude vector. A rigid spacecraft with inertia parameters $I = diag(140, 100, 80)$ $kg \cdot m^2$ is considered for simulation purposes. The initial angular velocities are zero and the initial Euler angles of the satellite are $\Theta_0 = [166° \; -43.5° \; 298°]^T$. The desired Euler angles of the satellite are $\Theta_d = [0° \; 0° \; 0°]^T$. Using MRP, Θ_0 corresponds to $\sigma(0) = [0.6936, -0.4, 0.2]^T$ and Θ_d to $\sigma(d) = (0, 0, 0)^T$. Substituting the inertial parameters into equation (5.14), $\mathbf{A}(\mathbf{x})$ and $\mathbf{B}$ become

$$\mathbf{A}(\mathbf{x}) = \begin{bmatrix} 0 & 0.14\omega_z & 0 & 0 & 0 & 0 \\ 0 & 0 & -0.6\omega_x & 0 & 0 & 0 \\ -0.5\omega_y & 0 & 0 & 0 & 0 & 0 \\ a_{41} & a_{42} & a_{43} & 0 & 0 & 0 \\ a_{51} & a_{52} & a_{53} & 0 & 0 & 0 \\ a_{61} & a_{62} & a_{63} & 0 & 0 & 0 \end{bmatrix} \tag{5.42}$$

$$\mathbf{B} = \begin{bmatrix} 0.0070 & 0 & 0 \\ 0 & -0.0100 & 0 \\ 0 & 0 & -0.0125 \\ 0 & 0 & 0 \\ 0 & 0 & 0 \\ 0 & 0 & 0 \end{bmatrix} \tag{5.43}$$

where a_{41}, a_{42}, a_{43}, a_{51}, a_{52}, a_{53}, a_{61}, a_{62}, a_{63} are defined in equation (5.14). Given the matrices $\mathbf{A}(\mathbf{x})$, $\mathbf{B}$ and the values

$$\epsilon_1 = 1,$$
$$\epsilon_2 = 1, \tag{5.44}$$

the software package SOStools [51] is used to solve the feasibility problem in Definition 5.4.1.

The following controller and the symmetric matrix P are obtained

$$P = \begin{bmatrix} 16.8274 & 0.0000 & 0.0000 & -29.8773 & -0.0000 & 0.0000 \\ 0.0000 & 26.4409 & -0.0000 & 0.0000 & -46.3713 & 0.0000 \\ 0.0000 & -0.0000 & 17.8282 & 0.0000 & 0.0000 & -22.2516 \\ -29.8773 & 0.0000 & 0.0000 & 96.4584 & -0.0000 & -0.0000 \\ -0.0000 & -46.3713 & 0.0000 & -0.0000 & 124.5621 & -0.0000 \\ 0.0000 & 0.0000 & -22.2516 & -0.0000 & -0.0000 & 69.0296 \end{bmatrix}$$

$$T_x = -34.1x_1^3 - 13.5x_1^2x_4 - 18.2x_1x_2^2 - 6.8x_1x_2x_5 - 10.7x_1x_3^2 - 4.1x_1x_3x_6 - 6.3x_1x_4^2$$

$$- 4.1x_1x_5^2 - 7.9x_1x_6^2 - 41.1x_1 - 4x_2^2x_4 - 1.5x_2x_3 - 1.3x_2x_4x_5 - 6.3x_2x_6 - 2.1x_3^2x_4$$

$$- 0.1x_3x_4x_6 + 0.6x_3x_5 - 1.6x_4^3 - 1.1x_4x_5^2 - 2.1x_4x_6^2 - 1.9x_5x_6$$

$$T_y = -29.7x_1^2x_2 - 7.3x_1^2x_5 - 9.6x_1x_2x_4 - 1.4x_1x_3 - 2.1x_1x_4x_5 - 9.9x_1x_6 - 32.3x_2^3$$

$$- 15.4x_2^2x_5 - 15.3x_2x_3^2 - 5.8x_2x_3x_6 - 7.4x_2x_4^2 - 5.5x_2x_5^2 - 9.0x_2x_6^2 - 43.4x_2$$

$$- 3.9x_3^2x_5 + 3.5x_3x_4 - 1x_3x_5x_6 - 2.6x_4^2x_5 - 1.6x_4x_6 - 1.5x_5^3 - 3.1x_5x_6^2 - 16.4x_5$$

$$T_z = 22.4x_1^2x_3 - 4.2x_1^2x_6 + 0.8x_1x_2 - 7.1x_1x_3x_4 - 0.1x_1x_4x_6 + 2.4x_1x_5 - 21x_2^2x_3$$

$$- 4.4x_2^2x_6 - 7.8x_2x_3x_5 + 6.4x_2x_4 - 1x_2x_5x_6 - 21.2x_3^3 - 9.2x_3^2x_6 - 5.8x_3x_4^2$$

$$- 3.9x_3x_5^2 - 7x_3x_6^2 - 23x_3 + 3x_4x_5 - 0.9x_5^2x_6 - 2x_6^3 - 7.6x_6$$

Now, the linearized system (5.13) where $\mathbf{A}_l$ and $\mathbf{B}$ are

$$\mathbf{A}_l = \begin{bmatrix} O_{3\times3} & O_{3\times3} \\ 1/4I & O_{3\times3} \end{bmatrix}, \quad \mathbf{B} = \begin{bmatrix} 0.0070 & 0 & 0 \\ 0 & -0.0100 & 0 \\ 0 & 0 & -0.0125 \\ 0 & 0 & 0 \\ 0 & 0 & 0 \\ 0 & 0 & 0 \end{bmatrix} \tag{5.45}$$

where O and I are given in equation (5.13) is simulated. For

$$Q = \begin{bmatrix} 10 & 0 & 0 & 0 & 0 & 0 \\ 0 & 10 & 0 & 0 & 0 & 0 \\ 0 & 0 & 10 & 0 & 0 & 0 \\ 0 & 0 & 0 & 10 & 0 & 0 \\ 0 & 0 & 0 & 0 & 10 & 0 \\ 0 & 0 & 0 & 0 & 0 & 10 \end{bmatrix}, \quad R = \begin{bmatrix} 10 & 0 & 0 \\ 0 & 10 & 0 \\ 0 & 0 & 10 \end{bmatrix}, \quad (5.46)$$

the linear controller gain k_l is given as

$$\mathbf{k}_l = \begin{bmatrix} 8.4261 & 0 & 0 & 1.0000 & 0 & 0 \\ 0 & 7.1414 & 0 & 0 & 1.0000 & 0 \\ 0 & 0 & 6.4031 & 0 & 0 & 1.0000 \end{bmatrix}.$$

Given the nonlinear controller gains and linear controller gains, the comparison of linear controller and nonlinear controller for nonlinear system in Figure 5.2 with time in x-axis and attitude parameters in y-axis is shown. From Figure 5.2, it is observed that the linear controller on its own performs poorly when compared to the nonlinear controller. The comparison of the time response of angular velocities between global and local controller is shown in Figure 5.3.
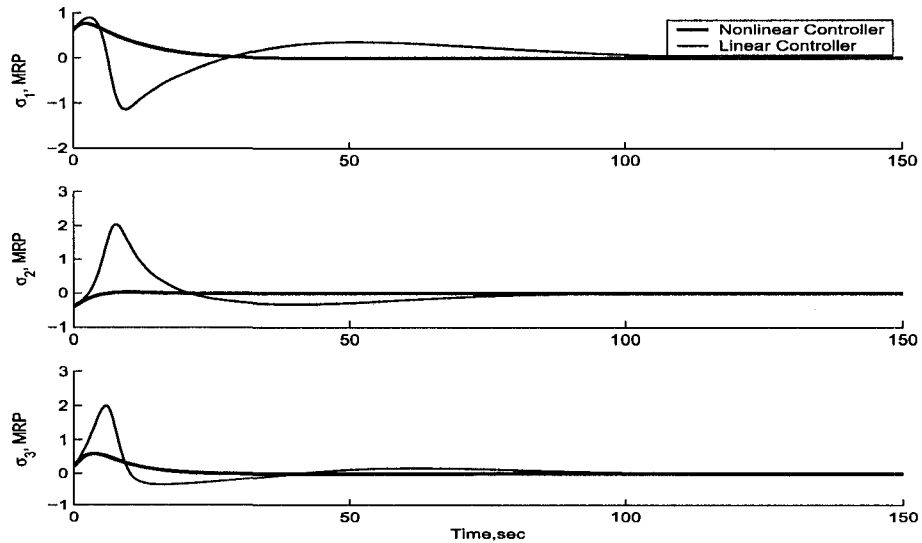
Figure 5.2: Comparison of time response of attitude parameters (σ) between nonlinear and linear system
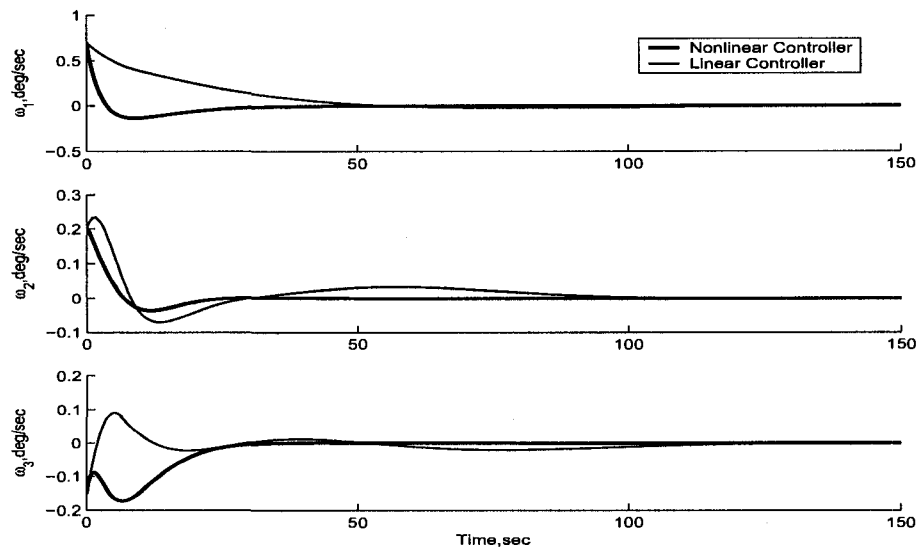
Figure 5.3: Comparison of time response of angular velocities (ω) between nonlinear and linear system
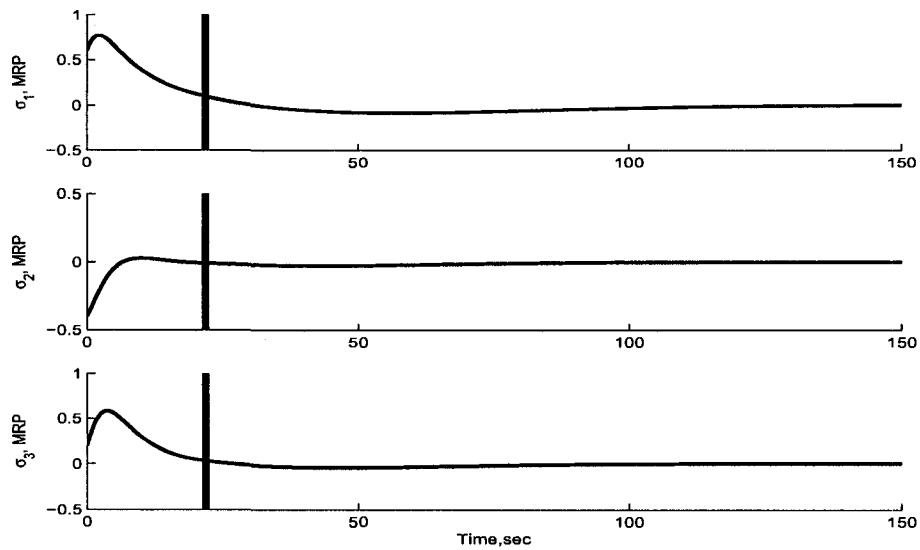
Figure 5.4: Time response of attitude parameters(σ) using switching law

110
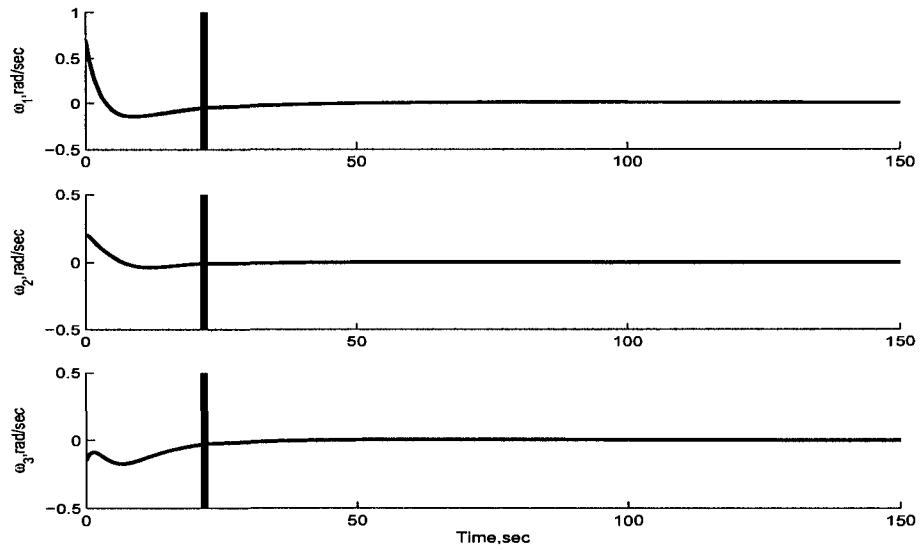
Figure 5.5: Time response of angular velocities (ω) using switching law
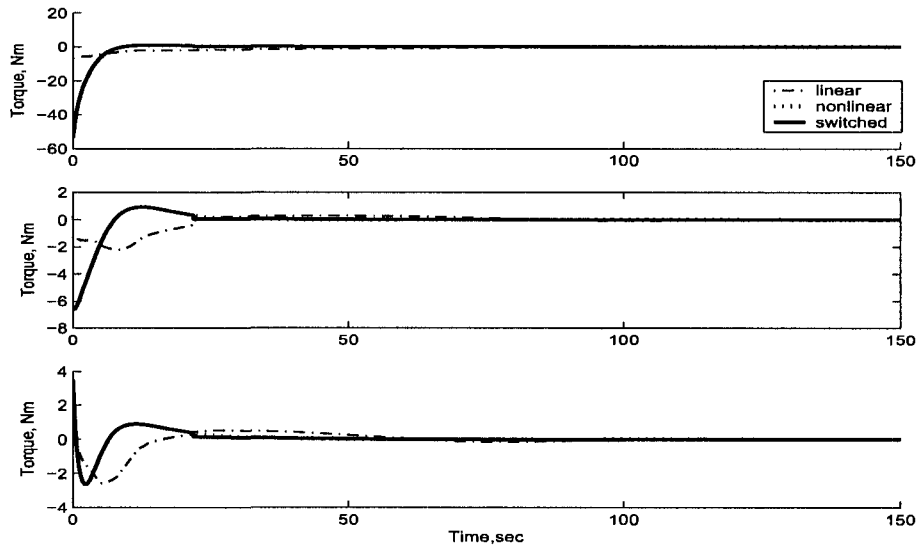
Figure 5.6: Control inputs

In Figure 5.4, the time response for attitude parameters is plotted using the switching law (5.34), where $\alpha^* = 1.3$. The value of α^* is obtained by solving the optimization problem 5.5.1. It is observed that the switching happens after 21.8 seconds and the attitude parameters converge to the desired points. The time response of angular velocities using the switching law is shown in Figure 5.5. In Figure 5.6

111

the control signal is plotted with time on the x-axis and torque (Nm) on the y-axis. In Figure 5.6 the control signal for three different controllers were compared: the nonlinear controller, linear controller and the switched controller. It is observed from the figure that the switched controller used less torque when compared to the global controller right after the switching, which occurs at 21.8 seconds.

5.7   Chapter Summary

In this chapter, a two-step switched approach for control of large-angle attitude maneuvers of a spacecraft guaranteeing local performance close to the desired point was developed. In the first step, the attitude dynamics of the rigid body are represented by modified Rodrigues parameters and a controller is designed based on the sum of squares technique. Further, a linear optimal steady state controller is designed for pointing mode and the region of attraction for the nonlinear closed-loop system using the linear controller is obtained. In the second step, a switching strategy is proposed to switch between acquisition mode and pointing mode that can guarantee local performance and uses less computational operations to be implemented in a microprocessor when compared to just a global controller.

Chapter 6

CONCLUSIONS AND FUTUREWORK

In this chapter the principal contributions of this thesis are summarized. Further, potential extensions of the developed methods are then discussed. The focus of this thesis has been to develop *novel attitude determination and control algorithms* to improve attitude estimation accuracy. In the following, the limitations raised in Chapter 1 are revisited considering the contributions of this work.

- The greatest drawback of current deterministic methods is that they can only be used when two vector measurements are simultaneously available.

  Chapter 3 addresses the problem by developing a novel attitude determination method, called the dyad method, where partial Euler angles can be determined using only one sensor information. It was shown through numerical simulation and verified with experimental data that the dyad method is very effective. During the loss of sensor information the TRIAD method is not valid whereas dyad method at least gives two angles. Further the advantage of this method is that it is ideally suitable to attitude group support software systems when the attitude must be computed very frequently. This method is therefore recommended for implementation in modern satellite ACS design to determine single-frame (i.e. non-sequential) attitude estimates.

- The attitude estimation algorithms using stochastic theory in the literature are based on the statistical information of the system, which is often not available. Moreover, all the existing approaches assume that the correlation between the process noise and the measurement noise is zero.

There are two contributions to address the problem described above. A modified Kalman filtering technique is implemented in the ground-based attitude determination. Secondly, a guaranteed ellipsoidal estimation technique is developed using convex theory.

  - In Chapter 4, section 4.1 addresses the problem when the process noise and measurement noise are correlated. A modified Kalman filter is implemented in the ground-based attitude estimator, where correlation between process noise and measurement noise is considered. Note that the filter states are not used in place of noisy measurements as the estimator is on-ground and not in the control-loop. However, the input to the attitude estimator is signal from the attitude control-loop on-board.

  - The above method is valid provided the statistical information is available. In the same Chapter, section 4.2 addresses the problem when statistical information about the noise is not available. A guaranteed ellipsoidal estimation technique is developed using convex theory. This technique has been developed for both pointing mode, where the attitude errors are less than 20 ° and for acquisition mode where the errors are larger. One of the main advantages of the guaranteed ellipsoidal estimator is, it is formulated using convex optimization method.

- While the problem of attitude control and stabilization has been the subject of much research, the problem of switching between a global controller and a local controller has not been explicitly considered for spacecraft.

In Chapter 5, a two-step switched approach for control of large-angle attitude maneuvers of a spacecraft guaranteeing local performance close to the desired point is developed. In the first step, the attitude dynamics of the rigid body are

represented by modified Rodrigues parameters (MRP) and a Lyapunov-based controller is designed based on the Sum of Squares (SOS) technique. Further, a linear controller is designed for pointing mode and the region of attraction for the nonlinear closed-loop system using the linear controller is obtained. In the second step, a switching strategy is proposed to switch between acquisition mode and pointing mode, which can guarantee local performance and is less computationally intensive for implementation in an on-board microprocessor when compared to just the global controller.

Despite the outcomes of the thesis, there are some limitations to the methods proposed in this thesis. Therefore, the following topics are proposed for future work:

- Extend the dyad method for different sensor configuration.

- Apply the estimator developed including the modified Kalman filter and the guaranteed ellipsoidal estimation in a real flight environment.

- Validate the proposed switching controller synthesis method through hardware experiments. The use of proper sensors is always an issue that must be considered when developing hardware testbeds.

Bibliography

[1] T. Alamo, J. M. Bravo, and E. F. Camacho. Recursive state bounding by parallelotopes. *Automatica*, 32(7):1049–1055, 1996.

[2] E.W. Bai, Y. Ye, and R. Temop. Bounded error parameter estimation, a sequential anayltic center approach. *IEEE Transactions on Automatic Control*, 44(6), 1999.

[3] C. Barbu, S. Galeani, A. R. Teel, and L. Zaccarian. Non-linear anti-windup for manual flight control. *International Journal of Control*, 78(14):1111–1129, 2005.

[4] A. Bargiela, W. Pedrycz, and M. Tanaka. A study of uncertain state estimation. *IEEE Transactions on Systems, Man and Cybernetics*, 33(3):288–301, 2003.

[5] D. P. Bertsekas and I. B. Rhodes. Recursive state estimation for a set-membership description of uncertainty. *IEEE Transactions on Automatic Control*, 16(2):117–128, 1971.

[6] R.G. Bland, D. Goldfard, and M.J. Todd. The ellipsoid method: A survey. *Operation Research*, 29:1039–1091, 1981.

[7] S. Boyd and L. El Ghaoui. Method of centers for minimizing generalized eigenvalues. *Systems and Control*, 188:63–111, 1993.

[8] S. Boyd, L. El Ghaoui, E. Feron, and V. Balakrishnan. *Linear Matrix Inequalities in System and Control Theory*, volume 15 of *Studies in Applied Mathematics*. SIAM, Philadelphia, PA, 1994.

[9] R. G. Brown and P. Y. C. Hwang. *Introduction to Random Signals and Applied Kalman Filtering.* John Wiley, 1997.

[10] F. L. Chernousko. *State Estimation for Dynamic Systems.* CRC Press, Boca Raton, FL, 1994.

[11] L. Chisci, A. Garulli, and G. Zappa. Recursive state bounding by parallelotopes. *Automatica,* 32(7):1049–1055, 1996.

[12] J. L. Crassidis and F. L. Markley. A minimum model error approach for attitude estimation. *AIAA Journal of Guidance Control and Dynamics,* 20(6):1241–1247, 1997.

[13] J. L. Crassidis and F. L. Markley. A new algorithm for attitude determination using global positioning sysmtes. *Proceeding of AIAA Guidance, Navigation and Control Conference,* 1997.

[14] J. L. Crassidis and F. L. Markley. Predictive filtering for attitude estimation. *AIAA Journal of Guidance Control and Dynamics,* 20(6):552–557, 1997.

[15] J. L. Crassidis and F. L. Markley. Unscented filtering for attitude estimation. *AIAA Journal of Guidance Control and Dynamics,* 26(4), 2003.

[16] J. L. Crassidis, F. L. Markley, T. C. Anthony, and S. F. Andrews. Nonlinear predictive control of spacecraft. *35th Aerospace Sciences Meeting and Exhibit,* 1997.

[17] P. E. Crouch. Spacecraft attitude control and stabilization: Application of geometric control theory to rigid body models. *IEEE Transactions on Automatic Control,* 29:321–331, 1984.

[18] E. Fogel and Y. F. Huang. On the value of information in system identification - bounded noise case. *Automatica,* 18(2):229–238, 1982.

[19] A. Gelb. *Applied Optimal Estimation.* MIT Press, Cambridge, MA, 1974.

[20] N. Gollu and L. Rodrigues. Control of large angle attitude maneuvers for rigid bodies using sum of squares. *IEEE Proceedings American Control Conference*, 2006.

[21] Y. Hamada, T. Ohtani, T. Kida, and T. Nagashio. A new gain scheduling controller synthesis and its application to attitude control systems of a large flexible satellite. *IEEE Proceedings of CCA/CACSD/ISIC*, 2006.

[22] D. Henrion, S. Tarbouriech, and D. Arzelier. Linear matrix inequalities approximations for the radius of the intersection of ellipsoids. *IEEE Proceedings Conference on Decision and Control*, 1998.

[23] P. C. Hughes. *Spacecraft Attitude Dynamics*. John Wiley and Sons, New York, 1986.

[24] T. Iwata. Ground based precision attitude determination for the advanced land observing satellite. *25th International Symposium on Space Technology and Science*, 2006.

[25] L. Jaulin and E. Walter. *Bounding Approaches to System Identification*. Plenum, 1996.

[26] T. Kailath. *Linear Systems*. Prentice Hall, 1989.

[27] T. Kailath, A. H. Sayed, and B. Hassibi. *State Space Estimation*. Prentice Hall, 1999.

[28] R. E. Kalman. A new approach to linear filtering and prediction problems. *Transactions of the AMSE, Part D, Journal of Basic Engineering*, 82:35–45, 1960.

[29] W. Kang. Nonlinear H_∞ control and its application to rigid spacecraft. *IEEE Transactions on Automatic Control*, 40(7):1281–1285, 1995.

[30] M. H. Kaplan. *Modern Spacecraft Dynamics and Control*. John-Wiley and Sons, 1976.

[31] H. Khalil. *Nonlinear Systems*. Prentice Hall, 1996.

[32] Y. Kim and A. Ng. Satellite sensor fusion system, inherent informational redundancy in vector measurement attitude determination methods. Technical report, Canadian Space Agency, Montreal, 2003.

[33] Y. V. Kim, N. Gollu, and A. Ng. On inherent informational redundancy in vector measuring attitude determination methods. *56th International Astronautical Congress Conference*, 2005.

[34] M. Kocvara, F. Leibfritz, M. Stingl, and D. Henrion. A nonlinear SDP algorithm for static output feedback problems in $COMPl_eib$. Technical report, University of Trier, Germany, 2004.

[35] A. Kurzhanski and I. Valyi. Guaranteed state estimation for dynamic systems: Beyond the overviews. *Proceedings of 9th IFAC/IFORS Symposium on Identification and System Parameter EStimation*, pages 1033–1037, 1991.

[36] W. L. Larson and J. R. Wertz. *Space Mission Analysis and Design*. Microcosm Inc., 1995.

[37] E.J. Lefferts, F.L. Markley, and M.D. Shuster. Kalman filtering for spacecraft attitude estimation. *AIAA Journal of Guidance Control and Dynamics*, 5(5):417–429, 1982.

[38] Q. Li and W. Tian. Sensor fusion in remote sensing satellites using a modified kalman filter. *Measurement Science and Techonolgy*, 14:356–367, 2003.

[39] S. Lim and K. Chan. Quaternion controller design using switching linear parameter varying framework. *AIAA Journal of Guidance Control and Dynamics*, 26(3), 2003.

[40] J. Löfberg. YALMIP : A toolbox for modeling and optimization in MATLAB. In *Proceedings of the CACSD Conference*, Taipei, Taiwan, 2004.

[41] Lerner G. M. *Spacecraft Attitude Determination and Control, Chapter 12.* Reidel, Dordrecht, 1978.

[42] D. Maksarov and J. P. Norton. Computationally efficient algorithms for state estimation with ellipsoidal approximations. *International Journal of Adaptive Control and Signal Processing*, 16:411–434, 2002.

[43] F. L. Markley. Attitude determination from vector observations: A fast optimal matrix algorithm. *The Journal of the Astronautical Sciences*, 41(2):261–280, 1993.

[44] F.L. Markley. Attitude determination using vector observations and the singular value decomposition. *The Journal of the Astronautical Sciences*, 41:261–280, 1993.

[45] G. Meyer. Design and global analysis of spacecraft attitude control. Technical report, NASA TR R-361, 1971.

[46] J. Montel. Pleades hr : On-ground attitude estimation. *25th International Symposium on Space Technology and Science*, 2006.

[47] R. E. Moore. *Interval Analysis.* Prentice Hall, 1966.

[48] N. Muskinja and B. Tovornik. Adaptive state controller for inverted pendulum. *9th Mediterranean Conference on Control and Automation*, 2001.

[49] P. A. Parrilo. *Structured Semidefinite Programs and Semialgebraic Geometry Methods in Robustness and Optimization.* PhD thesis, Massachusetts Institute of Technology, Boston, 2000.

[50] B. Polyak, S. Nazin, C. Durieu, and E. Walter. Ellipsoidal parameter or state estimation under model uncertainty. *Automatica*, 40:1171–1179, 2004.

[51] S. Prajna, A. Papachristodoulou, P. Seiler, and P. A. Parrilo. Sostools: Sum of squares optimization toolbox for matlab. Technical report, California Institude of Technology, Pasadena, California, 2004.

[52] S. Prajna, A. Papachristodoulou, and F. Wu. Nonlinear control synthesis by sum of squares optimization: A Lyapunov-based approach. *Proceedings of the ASCC*, 2004.

[53] K. Raymond and N. P. Johan. Satellite attitude control by quaternion-based backstepping. *IEEE Proceedings American Control Conference*, 2005.

[54] A. H. J. Ruiter and C. J. Damaren. Extended Kalman filtering and nonlinear predictive filtering for spacecraft attitude determination. *Canadian Aeronautics and Space Journal*, 48(1), 2002.

[55] A. K. Sanyal, T. Lee, M. Leok, and N. H. McClamroch. Global optimal attitude estimation using uncertainty ellipsoids. *Systems and Control Letters*, 57:236–245, 2008.

[56] H. Schaub and J. L. Junkins. *Analytical Mechanics of Aerospace Systems*. AIAA, 2003.

[57] H. Schaub, J. L. Junkins, and R. D. Robinett. Adaptive external torque estimation by means of tracking a lyapunov function. *AAS/AIAA Space Flight Mechanics Meeting*, 1996.

[58] F. M. Schlaepfer and F. Schweppe. Continous time state estimation under disturbances bounded by convex sets. *IEEE Transactions on Automatic Control*, 17(2):197–205, 1972.

[59] E. Scholte and M. Campbell. A nonlinear set-membership filter for on-line applications. *International Journal of Robust Nonlinear Control*, 13(15):1337–1358, 2003.

[60] F. C. Schweppe. Recursive state estimation: unknown but bounded errors and system inputs. *IEEE Transactions on Automatic Control*, 13(1):22–28, 1968.

[61] J. S. Shamma and K.-Y. Tu. Approximate set-valued observers for nonlinear systems. *IEEE Transactions on Automatic Control*, 42(5):648–658, 1997.

121

[62] M. D. Shuster. A survey of attitude representations. *The Journal of the Astronautical Sciences*, 41(4):439–517, 1993.

[63] M. D. Shuster and S. D. Oh. Three axis attitude determination from vector observations. *AIAA Journal of Guidance Control and Dynamics*, 4(1):70–77, 1981.

[64] M.D. Shuster. The quest for better attitudes. *The Journal of the Astronautical Sciences*, 54:657–683, 2006.

[65] M. J. Sidi. *Spacecraft Dynamics and Control.* Cambridge University Press, New York, 1997.

[66] S. N. Singh and T. C. Bossart. Exact feedback linearization and control of space station using cmg. *IEEE Transactions on Automatic Control*, 38(1):184–187, 1993.

[67] S. N. Singh and A. Iyer. Nonlinear decoupling sliding mode control and attitude control of spacecraft. *IEEE Transactions on Aerospace and Electronics System*, 25(5):621–633, 1989.

[68] H. W. Sorenson. *Kalman Filtering: Theory and Application.* IEEE Press, 1993.

[69] P. Tsiotras. New control laws for the attitude stabilization of rigid bodies. *13th IFAC Symposium on Automatic Control in Aerospace*, pages 316–321, 1994.

[70] P. Tsiotras. Stabilization and optimality results for the attitude control problem. *AIAA Journal of Guidance Control and Dynamics*, 19(4):772–779, 1996.

[71] P. Tsiotras. Further passivity results for the attitude control problem. *IEEE Transactions on Automatic Control*, 43(11):1597–1600, 1998.

[72] D. A. Vallado. *Fundamentals of Astrodynamics and Applications.* Microcosm Press, 2007.

[73] G. Wahba. A least-squares estimate of satellite attitude. *SIAM Review*, 7(3):409, 1965.

[74] J. Wertz. *Satellite Attitude Determination and Control.* D. Reidel Publication Co., 1984.

[75] B. Wie and P. M. Barba. Quaternion feedback for spacecraft large angle maneuvers. *AIAA Journal of Guidance Control and Dynamics*, 8(3):360–365, 1985.

Appendix A

Chapter 1 Definitions

In this appendix, definitions for Chapter 1 are presented.

A.1 Definitions

Definition A.1.1. *Attitude: Attitude is described as the orientation of the space-craft relative to either an inertial reference frame or some specific object of interest such as the Earth.*

Definition A.1.2. *Deterministic methods: Three axis point by point solutions, that utilize only the vector measurements obtained at a single point of time.*

Definition A.1.3. *Estimation methods:Estimation algorithms use a dynamic and/or a kinematic model of the spacecraft's motion to determine its attitude.*

Definition A.1.4. *arc-second: one arc-second is equal to $1/3,600$ of a degree.*

Definition A.1.5. *LEO: Low Earth Orbit includes orbits having apogees (high points) and perigees (low points) between 100km and 1500 km*

Definition A.1.6. *GEO: Geostationary orbit includes orbits having the apogees and perigees equal to 35,786 km*

Definition A.1.7. *MEO: An orbit that is between LEO and GEO in altitude.*

Appendix B

Chapter 2 Definitions

In this appendix, definitions for Chapter 2 is presented.

B.1 Definitions

Definition B.1.1. *Euler angles: Roll (ϕ) angle is defined as the rotation of the spacecraft about the Sun vector and measured with respect to the direction of the ecliptic north pole. The pitch angle(θ) and yaw angle(ψ) are defined as the relative orientation of the Sun-pointing axis of the spacecraft with respect to the Sun vector.*

Definition B.1.2. *Vernal Equinox: The Vernal Equinox is the line from the center of the Earth to a point where the ecliptic crosses the Earth's equator going from south to north.*

Appendix C

Attitude Determination Simulator

In this appendix, some definitions and the attitude determination simulator used in Chapter 3 are presented.

C.1 Definitions

Definition C.1.1. *Vector: A vector is a mathematical quantity with two properties, magnitude and direction. In this thesis, vectors are denoted in bold, lower case and have a hat if they are unit vectors. For example, $\hat{s}$ is a unit vector.*

Definition C.1.2. *Longitude: Longitude is the angular distance measured along the Earth's equator from the Greenwich meridian to the meridian of a satellite's location.*

Definition C.1.3. *Latitude: Latitude is the angular distance on the Earth measured north or south of the equator along the meridian of a satellite's location.*

C.2 Attitude Determination Simulator

The attitude determination simulator is divided into four parts:

1. Initial conditions

2. Attitude sensors

3. Telemetry data processing

4. Attitude determination methods

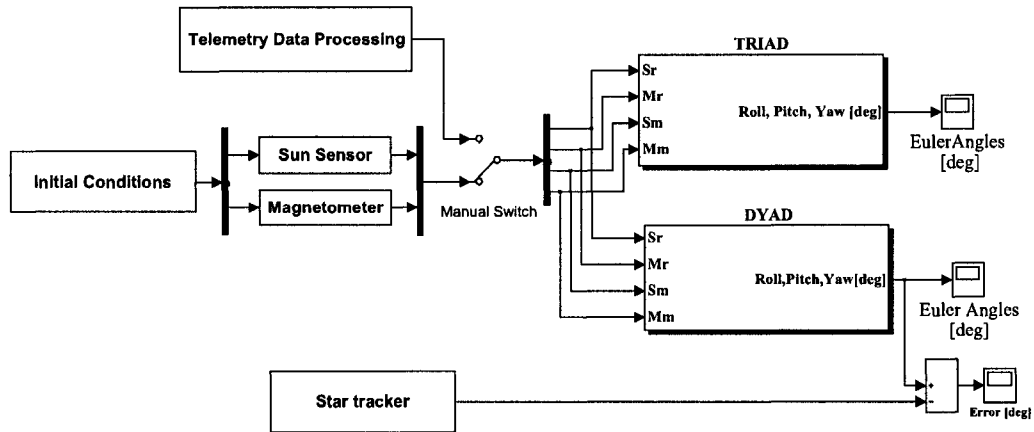These are explained briefly in the following subsections.

Figure C.1: Attitude determination simulator

C.2.1 Initial Conditions

To attain the reference vectors, satellite's position and time expressed in Julian date are required. Below, the Julian date calculator from the time represented in year, date and time is given.

$$
JD = 367Y - INT \left\{ \frac{7[Y + INT(\frac{M+9}{12})]}{4} \right\} + INT \left(\frac{275M}{9} + D \right)
$$
$$
+ 1721013.5 + \frac{H}{24} + \frac{M}{1440} + \frac{S}{86400},
$$

(C.1)

where Y is the year, INT represents an integer conversion, M is the month, D is the day, and S is the seconds. For example, the Julian date of March 1, 2008, 11:45 PM is 2454526.989.

C.2.2 Attitude Sensors

In this subsection three attitude sensors are discussed. Simple mathematical models for a Sun sensor and a magnetometer are explained.

127

Sun Sensor: To obtain the reference Sun vector and the measured Sun vector, an algorithm is developed in [72] and is presented below. Given the Julian date (C.1), the reference Sun vector in the inertial frame can be found using the formula

$$
\mathbf{s}_i = \begin{bmatrix} \cos \lambda_{ecliptic} \\ \cos \epsilon \sin \lambda_{ecliptic} \\ \sin \epsilon \sin \lambda_{ecliptic} \end{bmatrix} , \tag{C.2}
$$

where $\lambda_{ecliptic}$ is the ecliptic longitude of the Sun, while ϵ is the obliquity of the ecliptic [72] and is assumed to be $23.439°$. The derivation of the formulae in (C.2) can be found in [pp. 281, [72]]. Using the reference Sun vector and knowing the rotation matrix R_r^b, one can find the measured Sun vector using the formula (3.1). However, during an eclipse period, when the Sun vector is not available, it is assumed that the reference Sun vector is equal to the measured Sun vector $(\hat{\mathbf{s}}_r = \hat{\mathbf{s}}_m)$ as is shown in Figure C.2. From the figure, it is observed that a switch is used to bypass the measured Sun vector with the reference vector during the eclipse event. The logic behind the switch is such that when the threshold of the signal from the measured Sun vector is less than 0.5, the reference Sun vector is considered.
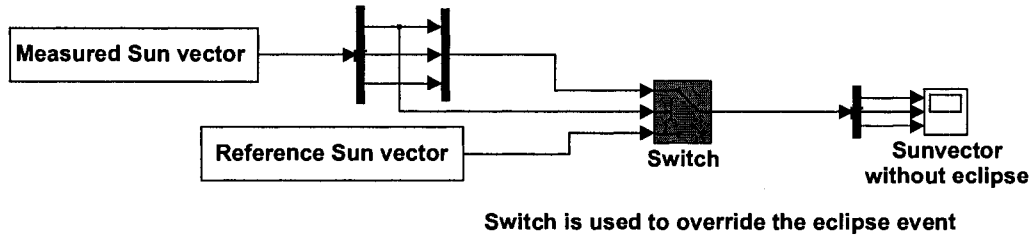

Switch is used to override the eclipse event

Figure C.2: Sun vector during eclipse

Magnetometer: Magnetic field components in a geocentric inertial frame for a simple tilted dipole model of the Earth's magnetic field are given below. The derivations of the formulae presented below can be found in [74]:

$$
\mathbf{m}_i = \frac{R_e^3 H_0}{r^3} \begin{bmatrix} 3(\hat{\mathbf{m}} \cdot \hat{\mathbf{r}})r_x - \sin \theta_m' \cos \alpha_m \\ 3(\hat{\mathbf{m}} \cdot \hat{\mathbf{r}})r_y - \sin \theta_m' \cos \alpha_m \\ 3(\hat{\mathbf{m}} \cdot \hat{\mathbf{r}})r_z - \sin \theta_m' \cos \alpha_m \end{bmatrix} \tag{C.3}
$$

where R_e is the radius of the Earth, H_0 is the Earth's magnetic field and $\alpha_m = \theta_{g0} + \omega_e t + \phi'_m$, where θ_{g0} is the Greenwich sidereal time at epoch, ω_e is the average rotation rate of the Earth, t is the time since *epoch*, and θ'_m and ϕ'_m are the coelevation and East longitude of the dipole. Using the orientation of the magnetometer frame with respect to the spacecraft body frame, the measurements of the magnetic field in the body frame, $\hat{m}_b$ can be obtained. Note that the most accurate magnetic field reference vector measurements can be obtained using the IGRF model [6] of 10-th order.

Star Tracker: Star tracker data has been used as the true roll angle in this work. It is assumed that the roll angle obtained using the star tracker is more accurate. The roll angle error compared in Figure 3.16 between the DYAD and the TRIAD is obtained by taking the difference between the roll angle obtained using star tracker and TRIAD/DYAD method. In Figure C.1 it is observed that a summator is used to find the difference between the signal from star tracker and the DYAD method.

C.2.3   Telemetry Data Processing

The telemetry data obtained for validating the attitude determination methods is from the period November 9, 2004 to November 10,2004. With an orbital period of 98 minutes, SCISAT completed four orbits in that time. Of the enormous amount of data received by mission control center, only measured magnetic vector, reference magnetic vector, measured Sun vector, reference Sun vector, star tracker, and attitude errors on all three axes are extracted.

C.2.4   Attitude Determination Methods

In Figure C.1, the two right-hand side blocks are meant for the attitude determination. The top block is used for determining the attitude using the TRIAD method, while the bottom block is used for attitude computation using the DYAD method. The mathematical formulations of the TRIAD and DYAD methods are given in sections 3.3.2 and 3.4, respectively. Two simple examples are shown to demonstrate the idea

of the attitude computations.

Example C.1. *Suppose a spacecraft has two attitude sensors that provide the follow-ing measurements of the vectors $\hat{s}$ and $\hat{m}$:*

$$s_b = \begin{bmatrix} 0.3808 & 0.3077 & 0.8720 \end{bmatrix}^T, \tag{C.4}$$

$$m_b = \begin{bmatrix} 0.5 & 0.01 & 0.866 \end{bmatrix}^T. \tag{C.5}$$

These vectors have known reference frame components of

$$s_r = \begin{bmatrix} 1 & 0 & 0 \end{bmatrix}^T, \tag{C.6}$$

$$m_r = \begin{bmatrix} 0.99 & 0 & 0.1411 \end{bmatrix}^T. \tag{C.7}$$

Applying the TRIAD algorithm, we construct the components of the vector $\hat{q}$, $\hat{r}$, $\hat{t}$ in both the body and reference frames

$$q_b = \begin{bmatrix} 0.3808 & 0.3077 & 0.8720 \end{bmatrix}^T, \tag{C.8}$$

$$r_b = \begin{bmatrix} 0.8141 & 0.3355 & -0.4739 \end{bmatrix}^T, \tag{C.9}$$

$$t_b = \begin{bmatrix} -0.4384 & 0.8904 & -0.1227 \end{bmatrix}^T, \tag{C.10}$$

and

$$q_r = \begin{bmatrix} 1 & 0 & 0 \end{bmatrix}^T, \tag{C.11}$$

$$r_r = \begin{bmatrix} 0 & -1 & 0 \end{bmatrix}^T, \tag{C.12}$$

$$t_r = \begin{bmatrix} 0 & 0 & -1 \end{bmatrix}^T. \tag{C.13}$$

Using these results, we obtain the appropriate rotation matrix (3.12)

$$R_r^b = \begin{bmatrix} 0.3808 & -0.8141 & 0.4384 \\ 0.3707 & -0.3355 & -08904 \\ 0.8720 & 0.4739 & 0.1227 \end{bmatrix}. \tag{C.14}$$

Given the rotation matrix (C.14), Euler angles can be obtained using the formulae

(3.14), yielding

$$\phi = -75.4806°$$

$$\theta = 60° \qquad\qquad (C.15)$$

$$\psi = -38.9394°$$

Example C.2. *Suppose a spacecraft has two attitude sensors that provide the follow-ing measurements of the two vectors* $\hat{s}$ *and* $\hat{m}$.

$$s_b = \begin{bmatrix} 0.3808 & 0.3077 & 0.8720 \end{bmatrix}^T \qquad\qquad (C.16)$$

$$m_b = \begin{bmatrix} 0.5 & 0.01 & 0.866 \end{bmatrix}^T m_r \qquad = \begin{bmatrix} 0.99 & 0 & 0.1411 \end{bmatrix}^T. \qquad (C.17)$$

Applying the DYAD algorithm, we first obtain two angles based on equation (3.18)

$$s_b = \begin{bmatrix} 0.3808 \\ 0.3077 \\ 0.8720 \end{bmatrix} = \begin{bmatrix} \cos\theta\cos\psi \\ -\cos\theta\sin\psi \\ \sin\theta \end{bmatrix}, \qquad\qquad (C.18)$$

$$\theta = 60.69°, \qquad\qquad (C.19)$$

$$\psi = -38.93°. \qquad\qquad (C.20)$$

Given the two angles in (C.18), obtained from one vector measurement, the objec-tive now is to use these angles to obtain the third angle with respect to the vector measurement which coincides with the first rotation axes using equation (3.27)

$$\tan\phi_{sm} = \frac{m_{r_z} m_{b_y} - m_{r_y} m_{b_z}}{m_{b_y} m_{r_y} + m_{b_z} m_{r_z}}. \qquad\qquad (C.21)$$

Substituting the values given in equation (C.16), ϕ_{sm} *is given as*

$$\phi_{sm} = 0.66°. \qquad\qquad (C.22)$$